EXOTIC INTEREST RATE OPTIONS IN QUANTUM FINANCE

TANG PAN
(B.Sc., Soochow University)

A thesis submitted for the
Degree of Doctor of Philosophy

Supervisor
Professor Belal E Baaquie

DEPARTMENT OF PHYSICS
NATIONAL UNIVERSITY OF SINGAPORE

2011

Acknowledgements

I would like to thank all people who have helped and inspired me through my thesis.

First and foremost I would like to express the deepest appreciation and sincerest gratitude to my supervisor, Professor Belal E Baaquie, who has supported me during my doctoral study with his patience and knowledge. Without his guidance, encouragement and persistent help, this dissertation would not have been possible. I am grateful to be his student, and his perpetual energy and enthusiasm in research enabled me to develop an good understanding of research.

I would like to thank Cao Yang and Jiten Bhanap for their useful discussion and collaboration. I thank National University of Singapore and Department of Physics for the financial support.

Lastly, I would like to thank my parents for giving my life in the first place, for educating me with aspects from both academic education and mind characteristics, for unconditional support and for their love.

Contents

Summary

The modern mathematical finance refers to the use of applied mathematics in analyzing and studying financial markets. The history of mathematical finance starts with evaluating stock options by using Brownian motion, which is discussed in *The Theory of Speculation* [1]. The bedrock of the modern mathematical finance is the stochastic calculus, based on which most interest rate models are developed. However, after the 2008 economic crisis, the credibility of most stochastic interest rate models and derivative pricing strategies is doubted and questioned. Quantum Finance is firstly proposed by Baaquie (2004) [2]. The quantum field theory has, in principle, the advanced theoretical and mathematical tool in studying random evolution compared to stochastic calculus. This new theoretical framework may offer a better way for modeling and pricing the financial instruments.

A major subject matter of this thesis is focused on studying the generalized forward interest rate model and the Libor Market Model in Quantum Finance. Compared to the stochastic interest rate models, the imperfectly correlated interest rates are modeling as a Gaussian field. The feature of the Gaussian field is that it contains much more information than the one-dimensional stochastic processes, which drive the entire evolution of interest rates in traditional financial theory. The simulation algorithm for modeling interest rates is extensively studied. Due to the complex structure of interest rate instruments, the approximate price only can be derived based on the perturbation expansion for small value of volatility. The comparison between simulation results and analytical formula is studied for many instruments and shows the flexible and potential of simulation method in pricing interest rate derivatives. In particular, it is shown that the simulation method provides a powerful tool in studying any kind of interest rate instruments without limitation.

Another part of this thesis is studying the Constant Elasticity of Variance (CEV) process. A recursion equation of CEV process is developed and used to calibrate the value of β, which is the key term in CEV model. The value of β for market observed Equity Default Swaps (EDS) spreads is obtained and agrees with the recent studies. However, the results for Credit

Default Swaps (CDS) show that the market observed CDS spreads have no sensitivity to the implied volatility, which cannot be explained by CEV process. It is suggested that the EDS spreads with low barriers are more attractive to the market compared to CDS spreads.

In the third part, an unequal time Gaussian model is developed to calibrate the stock market data. The nontrivial Lagrangian is defined and the unequal time propagator is studied for fitting the correlation of different stocks on different time. Compared to modern portfolio theory, Gaussian model is more powerful in describing the behavior of unequal time correlation. Based on the nontrivial Lagrangian, Gaussian model is generally applicable to other liquid markets which have strong unequal time correlation.

Publication List

[1] B.E. Baaquie and Tang Pan*. Simulation of Coupon Bond European and Barrier Options in Quantum Finance. *Physica A: Statistical Mechanics and its Applications*, 390(2), 263-289, 2011.

[2] B.E. Baaquie, Tang Pan* and J. D. Bhanap. Empirical analysis and calibration of the CEV process for pricing equity default swaps. *Quantitative Finance*, 1469-7696, 2010.

[3] B.E. Baaquie and Tang Pan*. Simulation of Nonlinear Interest Rates in Quantum Finance: Libor Market Model. *Submitted for publication.*

[4] B.E. Baaquie, Ada Lau, Cao Yang* and Tang Pan. Path Integral for Equities: Dynamic Correlation and Empirical Analysis. *Submitted for publication.*

* Corresponding author

List of Tables

List of Figures

Symbol

Symbol	Definition
r	spot rate
$B(t,T)$	zero coupon bond
$\mathcal{B}(t,T)$	coupon bond
$f(t;T_1,T_2)$	forward interest rate, at calendar time t, for a deposit from future time T_1 to T_2
$f(t,x)$	forward interest rate, at calendar time t, for an instantaneous deposit at future time x
$f_L(t,x)$	Libor forward interest rate
$F(t,T_1,T_2)$	forward price, at calendar time $t < T_1$, of a zero coupon bond $B(T_1,T_2)$
ℓ	Libor tenor, taken to be 90 days in this thesis
$L(t,T_n)$	Libor rate, at calendar time t, for a deposit from future time T_n to $T_n+\ell$
$\Theta(t)$	Heaviside function
$M(t,t_*)$	money market numeraire
$\mathcal{P}_*$	option payoff function
$\alpha_*(t,x)$	drift for forward bond numeraire $B(t,t_*)$
$\sigma(t,x)$	forward interest rate's volatility
$\chi_n(t)$	martingale instruments for Libor Market Model
$\xi(t,x)$	Libor Market Model drift
$\gamma(t,x)$	Libor Market Model deterministic volatility
$R(t)$	Gaussian white noise
$A(t,x)$	Gaussian quantum field
$f_{m,n}, A_{m,n}$	lattice of forward interest rates and $A(t,x)$
$\delta_{mn}(t,x)$	Libor Market Model correlator
$\mathcal{L}[A], S[A]$	Lagrangian and action for $A(t,x)$
$Z[h]$	generating function for $A(t,x)$

Symbol	Definition
$D(t;x,x')$	forward interest rate propagator
$E[...]$	expectation value of interest rate instruments
$\phi(t,x)$	logarithmic Libor rate
$\rho(t,x)$	drift of logarithmic Libor rate
$\mathcal{L}[\phi], S[\phi]$	Lagrangian and action for $\phi(t,x)$
$u(0,1)$	uniform distribution
$N(0,1)$	normal distribution
ϵ	updating step size in calendar time, taken to be 1 day
$\sigma_M(t,x), \gamma_M(t,x)$	market volatility for forward interest rates and Libor
$N(x)$	cumulative normal distribution function
$I(X)$	function derived from $N(x)$
$C(t_0,t_*,T,K)$	call price of instruments, at present time t_0, issued at t_* and matures at future time T with strike price K
$\tilde{C}(t_0,t_*,T,K)$	call price obtained using simulation
$C_B(t_0,t_*,T,K)$	call price of barrier options
$\tilde{C}_B(t_0,t_*,T,K)$	call price of barrier options obtained using simulation
$Caplet(t_0,t_*,T,K)$	caplet price
$\tilde{C}aplet(t_0,t_*,T,K)$	caplet price obtained using simulation
$\mathcal{S}_U, \mathcal{S}_L, \mathcal{S}_D$	scaling function for up, down and double barrier
$\mathcal{Q}$	barrier function
S_t	stock price at time t
$x = \ln S$	logarithmic stock price
$dW(t)$	Wiener process
β	parameter of elasticity in CEV model
p	cumulative n-year default probability
$P_{BS}(x,\tau;x')$	pricing kernel for Black-Scholes model
$P_D(x,\tau;x')$	normalized Black-Scholes pricing kernel
Π	portfolio
$X_I(t)$	rate of return of single stock $S_I(t)$
d_I	deterministic drift of $X_I(t)$
$\varphi_I(t)$	Gaussian field for rate of return
$G_{IJ}(t,t')$	non-equal time propagator of rate of return
$\mathcal{L}[\varphi], S[\varphi]$	Lagrangian and action for $\varphi(t)$

Chapter 1

Interest Rates and Interest Rate Derivatives

The debt market has shown its grown importance in the global financial market in the recent years. The three main instruments, known as interest rates, coupon bonds and their derivatives, have strong liquidity and can be interpreted in the way of mathematics. Hence, the complex dynamics of interest rates and option pricing theory have been attractive to the researchers in the fields of mathematics and theoretical physics. The concepts of interest rates, especially forward interest rates, are briefly discussed. The Libor and Euribor, which are two main daily quoted rates and widely used in the interbank market, are introduced and discussed. Following with the introduction of arbitrage pricing theory-*martingale measure*, a diversity of interest rate instruments are discussed.

§ 1.1 Introduction

Finance is the science of fund management. The general aspects of finance are saving, borrowing, lending, and investing of money. Finance is also the practical application of economics by means of allocating money to its highest value, thus leading to economic growth. And, in economics, a financial market is a market for purchase and sale of financial securities (e.g. stocks and bonds), commodities, futures and options, and other fungible items. A very important subtype of the financial market is the capital market - a market for securities, where business enterprises and governments can raise long-term funds. Capital markets consist of the stock market (equity securities) and the debt market.

The debt market, also known as a bond market, is a financial market which allows people to buy and sell debt securities. Amounts outstanding on the global debt market in 2008 became twice of the asset of the global debt market in 2004. In 2008, the global debt market was worth nearly US $67.0 trillion-accounting for 60% of the capital market. The US debt market had a total worth of US $33.5 trillion and the rest of world accounts for a half of total value of global debt market. The debt market has increasingly played an important role in the global world's financial market over the past two decades, especially the recent several years. Along with the increase of total assets and size of debt market, much more attention has been paid to the research of debt market. A diversity of instruments can be traded in the debt market, which prompts the development of the debt market. Interest rates, coupon bonds and their derivatives are the main instruments in the debt market. Interest rates often refer to the rate of return that the lender receives for permitting the borrower to use the borrowed money for a specified term. Interest rates reflect the movement of the stock market, and the overall trend of interest rates can have a major effect on investors. Thus, the research of interest rates is extremely important in finance. Furthermore, interest rates also can be used to determine the price of bonds, another fundamental instrument of debt markets. Thus, developing models for simulating interest rates is extremely important in the research of debt market.

So far, many models have been established to simulate interest rates. The earliest studies attempted to model the bond price dynamics and interest rates by term structure. However, these studies did not give a good understanding of the term structure. Many interest rate models were then developed based on stochastic evolution. These models gave a better description of the evolution of forward interest rates (forward rates) by introducing the stochastic process, which is also known as stochastic calculus, into the models. The most famous model for forward interest rates is the HJM (Heath, Jarrow and Morton) model, which is now the industry standard interest rate model. Such models based on stochastic process are widely used in finance. However, the main limitation of these models is that the forward rates are simulated as one-dimensional stochastic process, and hence all the forward rates between different maturities are exactly correlated. In recent years, the concepts from physics (especially statistical mechanics and quantum field theory) have shown great potential of application of physics in both theoretical and applied finance. Compared to stochastic calculus, some ideas from quantum field theory are much more appropriate to describe the fluctuations of interest rates.

Quantum finance refers to the application of the theoretical and mathematical formalism of quantum mechanics and quantum field theory to problems arising in finance [2]. Models

based on quantum finance are able to incorporate subtle correlations of interest rates between different maturities. For example, based on a two-dimensional Gaussian field model, forward rates in quantum finance can contain much more information than models based on stochastic processes. Quantum field theory has great potential in the theory of finance. Improving the accuracy by capturing more information from data and simulating interest rates by using powerful tool of quantum field theory are the main motivations for establishing interest rate models based on quantum finance.

§ 1.2 Interest rates

§ 1.2.1 Definition of interest rates

Interest rates are the factor used to define the amount of money paid by the borrower for the use of the money borrowed from the lender. Interest rates are the key tool in the valuation of all derivatives, which constitute the main part of financial market. There are three different ways to define interest rates.

Simple interest rates: Propose a principal is M at present time t (today), and a simple interest rate r earned per year. r remains constant for each year. The amount of capital will increase to $M[1 + r(T - t)]$ at future time T.

Discrete compounding and discounting: If the interest earned for one year is compounded to the principal, the amount will be $M[1 + r]$ at the end of one year. This new principal is reinvested at the beginning of second year, the amount will increase to $M[1 + r]^2$ at the end of second year. Thus, the amount of capital at future time T will be $M[1 + r]^{T-t}$.

Continuous compounding and discounting: continuous compounding is the extreme case of the discrete compounding where the discrete time interval is taken to be infinitesimal. In discrete compounding, the interest rate r is constant for one year. If an infinitesimal period ϵ is used instead of one year, the principal M will increase to $M(1+\epsilon r)$ at time $t+\epsilon$. Following the same procedure of discrete compounding for infinitesimal interval ϵ, the total amount of capital at future time T will be

$$\lim_{\epsilon \to 0} M(1 + \epsilon r)^{(T-t)/\epsilon} = Me^{r(T-t)}. \tag{1.1}$$

These three ways of defining interest rates are, in principle, equivalent in pricing any financial instrument.

§ 1.2.2 Forward rates

The forward rate is the future yield on a bond, and is calculated using the interest yield curve. The continuous compounding and discounting is used for studying the interest rates through all Chapters, and the forward rates are discussed in the way of continuous compounding in the following.

Consider a fixed deposit that has a value of \$1 at time t, the deposit will increase to $\{\exp(T-t)r\}$ at time T in the future, where r is the spot rate. Therefore, the present value of zero coupon bond, which yields a value of \$1 at future time T, is given by

$$B(t,T) \quad = \quad e^{-(T-t)r}. \tag{1.2}$$

In practice, the interest rate is not always constant from time t to T. Instead, the continuous interest rate $r(t,T)$ should be used to describe the term structure of interest rates, which is well known as the *interest yield curve*. The interest rate $r(t,T)$ can be calculated from the zero coupon bond by using

$$r(t,T) \quad = \quad -\frac{1}{T-t}\ln B(t,T). \tag{1.3}$$

Forward interest rates are similar with the continuous interest rate $r(t,T)$, except that the forward interest rates $f(t;T_1,T_2)$, at present time t , are defined on the period of future time from T_1 to T_2. The forward interest rates $f(t;T_1,T_2)$ can be calculated from two bonds with different maturity times T_1 and T_2.

$$e^{-(T_2-T_1)f(t;T_1,T_2)} \quad = \quad \frac{B(t,T_1)}{B(t,T_2)}. \tag{1.4}$$

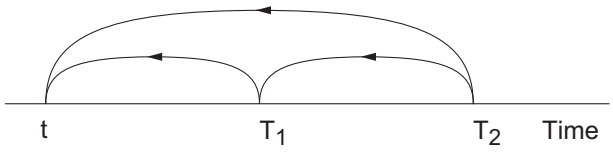

Figure 1.1: The discounting of bond from T_2 to t or first from T_2 to T_1, and then from T_1 to t.

As shown in Figure 1.1, the interest rate, which is discounted from T_2 to present time t directly, should be equivalent to being discounted from T_2 to T_1 and then from T_1 to t. Thus,

the forward rates $f(t; T_1, T_2)$ is given by

$$f(t; T_1, T_2) = -\frac{1}{T_2 - T_1} \ln[\frac{B(t, T_1)}{B(t, T_2)}]. \tag{1.5}$$

More precisely, the *instantaneous forward interest rates* can be obtained by taking $T_2 = T_1 + \epsilon$, which is the following

$$B(t, T + \epsilon) = B(t, T) \times e^{-\epsilon f(t,T,T+\epsilon)}, \tag{1.6}$$

$$\frac{\partial B(t, T)}{\partial T} = -f(t, T)B(t, T). \tag{1.7}$$

If the bond price is \$1 when the bond matures at future time T, the value of bond at present time t can be obtained by taking infinitesimal backward time step ϵ from future time T to present time t, which is

$$B(t, T) = e^{-\epsilon f(t,t+\epsilon)} e^{-\epsilon f(t,t+2\epsilon)} \cdots e^{-\epsilon f(t,x)} \cdots e^{-\epsilon f(t,T)}. \tag{1.8}$$

Simply, $B(t, T)$ is given by

$$B(t, T) = \exp\{-\int_t^T dx f(t, x)\}, \tag{1.9}$$

where $f(t, x)$ is defined as forward interest rates. At every instant calendar t, $f(t, x)$ constitutes an entire curve as a function of future time x. $f(t, x)$ is defined on a two-dimensional semi-infinite plane with $t \geq t_0$ and $x \geq t$, shown as the shaded domain in Figure 1.2.

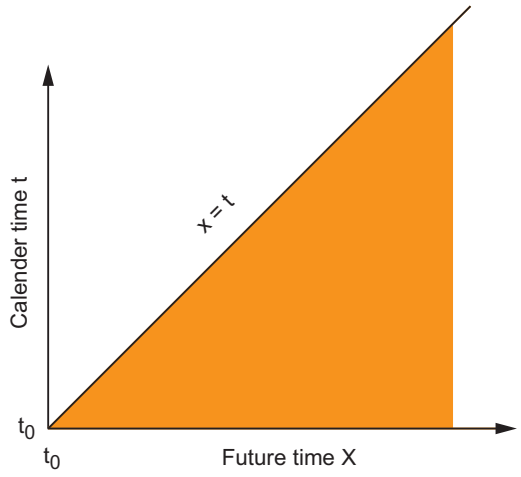

Figure 1.2: Two-dimensional forward interest rates $f(t,x)$ which is shown in shaded domain.

Suppose the zero coupon bond $B(t_*,T)$ will be issued at a future time t_* ($t_* > t_0$,) and expire at time T; the forward price of $B(t_*,T)$, at earlier time t_0 denoted by $F(t_0,t_*,T)$, is given by

$$F(t_0,t_*,T) \;=\; \exp\Big\{-\int_{t_*}^{T} dx f(t_0,x)\Big\}. \tag{1.10}$$

Figure 1.3 shows the plot of bond price $B(t_*,T)$ and forward bond price $F(t_0,t_*,T)$. The difference between $B(t_*,T)$ and $F(t_0,t_*,T)$ is that $F(t_0,t_*,T)$ is defined on present time t_0 while $B(t_*,T)$ is issued at future t_*.

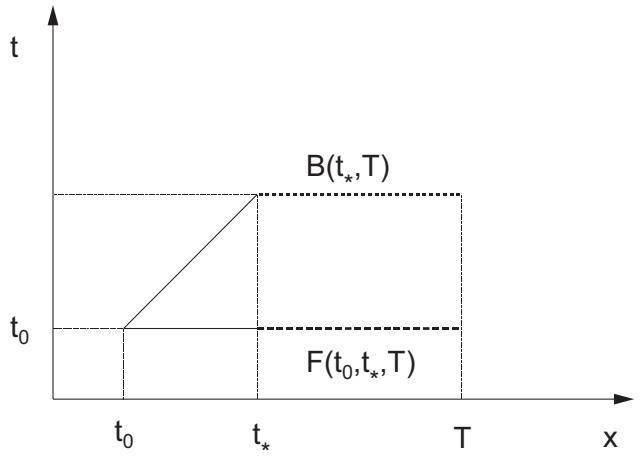

Figure 1.3: Bond price $B(t_*,T)$ and its forward price $F(t_0,t_*,T)$.

§ 1.2.3 Libor and Euribor

The London Interbank Offered Rate (**LIBOR**) is a daily quoted rate based on the interest rates at which banks are prepared to make a large deposit with other banks in the London wholesale money market (or interbank market) [3]. Libor is one of main interest instruments in the debt market. Libor was commenced officially by British Bankers' Association from 1 January 1986. The duration of daily quoted Libor can be different, and overnight, 1-week, 2-weeks, 1-month, 3-month, 6-month and 12-month are often quoted by large commercial banks and financial institutions. Libor rates can have a duration of 30 years, and Libor with long duration can be obtained from the interest swap market.

The 3-month Libor is the mainly quoted rate in the Libor derivative market. All Libor caps, floors, swaps and swaptions are all based on 3-month Libor. The Libor rate $L(t, T_n)$ is the forward interest rate, fixed at time t, for a cash deposit from future time T_n to $T_n + \ell$. Libor time is defined as $T_n = n\ell$ and ℓ is called the tenor of Libor rates. Figure 1.4 shows the Libor rates on the Libor calendar and future time lattice.

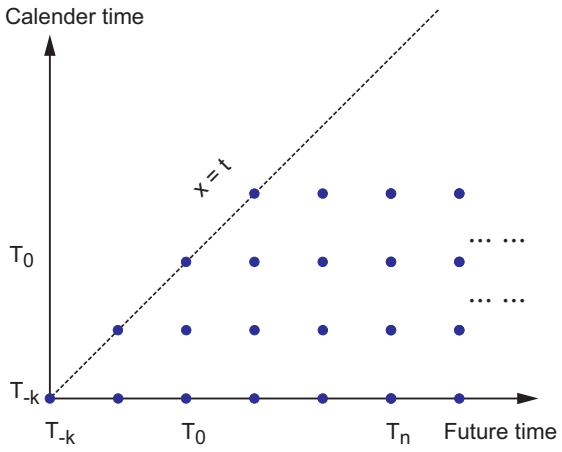

Figure 1.4: Libor rates defined on the time lattice with tenor ℓ.

Euro Interbank Offered Rate (**Euribor**) is a daily quoted rate based on the interest rates at which the huge deposits are offered by one bank to another in the Euro interbank market. Euribor was sponsored by the Financial Markets Association and the European Banking Federation (FBE). Euribor was firstly announced on 30 December 1998 and commenced from 1 January 1999. Euribor and Libor are comparable base rates and all the features of Libor are also applicable for Euribor. Hence, the models developed for Libor also can be used to simulate the dynamic of Euribor directly.

§ 1.3 Zero coupon bond and coupon bonds

Bonds are the debt securities, in which the authorized seller (borrower) is obliged to pay the prefixed principal to the holders (lender) at a later date, which is called the maturity of the bonds. A coupon bond is a formal contract to repay borrowed money with interest at fixed intervals [4].

One of the primary authorized issuers is the government. Many kinds of bonds are issued, and the zero coupon bond and coupon bonds are studied in details in this thesis.

A *zero-coupon bond*, denoted as $B(t,T)$, is a bond bought at present time t, with a prefixed principal repaid at the future time of maturity T. Normally, the price paid for the zero coupon bond $B(t,T)$ at present time t is smaller than its prefixed price. Well known issued zero coupon bonds include U.S. Treasury bills, U.S. savings bonds and long-term zero-coupon bonds.

A *coupon bond*, denoted as $\mathcal{B}(t,T)$, is similar to the zero coupon bond except that a coupon bond is a linear sum of many zero coupon bonds with different maturities. A coupon bond will also pay the principal at maturity time T, and some quantities of coupon bond $B(t_*,T_i)$ are also paid at different future times T_i. Consider a coupon bond issued at time t_* pays fixed dividends a_i being paid at different future times T_i, $i = 1,2,....,N_c$, and pays a principal L when it matures at future time T. The value of the coupon bond is as follows

$$\mathcal{B}(t,T) = \sum_{i=1}^{N_c} a_i B(t_*,T_i) + LB(t_*,T_i) = \sum_{i=1}^{N_c} c_i B(t_*,T_i), \tag{1.11}$$

where $c_i = a_i$ $(i = 1,2,...,N_c - 1)$ and $c_{N_c} = a_{N_c} + L$.

§ 1.4 Interest rate derivatives

An interest rate derivative is a derivative where the underlying asset has the right to pay or receive a notional amount of money at a given interest rate [3].

The interest rate derivatives market is the largest derivatives market in the world. It was estimated that the notional amount outstanding in June 2009 were US $ 437 trillion for OTC interest rate contracts, and US $ 342 trillion for OTC interest rate swaps. International Swaps and Derivatives Association show that nearly 80 % of the world's top 500 companies use interest rate derivatives to control their cashflows.

§ 1.4.1 Options

Options are a type of financial instrument of derivatives. An option gives its buyer the right, but not the obligation, to buy or to sell some underlying asset at an agreed on price before expiration. There are two main types of options, which are called call option and put option. A call option gives the holder the right but not the obligation to buy the underlying asset at a fixed price, which is called strike price. A put option gives the holder the right to sell the underlying asset at strike price. The options should be traded on or before options' expiration date. Two main traded options are European options and American options, respectively. A European option can only be exercised at the expiration date, while an American option can be exercised at any time before expiration date.

The profit, the contract holder earn at the expiration date, can be expressed by the *payoff function*. For example, the value of an European call option at maturity is given by

$$C = (S-K)_+, \tag{1.12}$$

where $(S-K)_+$ is called payoff function. This payoff function means that, at expiration date, the holder will earn the profit $S-K$ if the underlying price S is larger than strike price K. The holder will not earn any profit if the underlying price S is smaller than strike price K. The payoff function has the identity that

$$(a-b)_+ = (a-b)\Theta(a-b). \tag{1.13}$$

Θ is the Heaviside function, which is given by

$$\Theta(t) = \begin{cases} 1 & t > 0 \\ \frac{1}{2} & t = 0 \\ 0 & t < 0. \end{cases}$$

Similarly, the payoff function of a put option is the reverse of a call option and is given by

$$P = (K-S)_+, \tag{1.14}$$

which means that, at expiration date, the holder will earn the profit $K-S$ if the underlying price S is smaller than strike price K. The holder will lose the underlying asset if the underlying price S is larger than strike price K.

§ 1.4.2 Martingale

In finance, *arbitrage* is the practice of taking advantage of a price difference between two (or more) markets. When an arbitrage happen, the profit can be earn from the difference between the market prices.

In principle, an arbitrage means risk-free. For example, if an arbitrary transaction between two states arbitrary is made, the cash flow from one state is different from another state and the profit can be obtained with no risk. Such transactions are the possibilities of a risk-free profit at zero cost.

To avoid arbitrage, the *Rational pricing* with no arbitrage should be used in pricing fixed income securities and derivatives. Rational pricing is the assumption in financial economics that asset prices (and hence asset pricing models) will reflect the arbitrage-free price of the asset as any deviation from this price will be "arbitraged away" [3].

Risk-neutral measure, also called *martingale measure* is the fundamental theorem of arbitrage-free pricing. In a financial market, one risk-neutral measure is corresponding to one unique arbitrage-free price for each asset. If there are more such measures, no arbitrage is possible in an interval of prices. If no martingale measure exists, there will be some arbitrage opportunities which can be used for getting risk-free profit.

A martingale is a special kind of stochastic process; a *martingale* is a stochastic process in which the conditional expected value of an observation at some time t is equal to the observation at that earlier time t_0. An arbitrary discrete stochastic process X_i, is a martingale, satisfies the following

$$E[X_{n+1}|x_1, x_2, , ..., x_n] \quad = \quad x_n. \tag{1.15}$$

If the expectation value of random variables X_1, X_2,... X_n is already known to be x_1, x_2,...,x_n, the expectation value of the random variable X_{n+1} is simply x_n.

A martingale is a model of a fair game. For example, x_n denotes the amount of money which the gambler has after nth game, and X_{n+1} represents the various possible outcome of the $n+1$th game. Under the martingale condition, the expectation value of the outcomes of the $n+1$th game is equal to the money which the gambler has at the end of the nth game, namely x_n. The expectation value of the outcomes of the $n+1$th game only depend on x_n and doesn't have any relation with the historical outcomes. $E[X_{n+1}] = E[X_n]$ can be proved

by using Equation 1.15, and is given by

$$\begin{aligned} E[X_{n+1}] &= \int dx_1 dx_2, ..., dx_n dx_{n+1} E[X_{n+1}|x_1, x_2, , ..., x_n] p(x_1, x_2, ..., x_{n+1}) \\ &= \int dx_1 dx_2, ..., dx_n dx_{n+1} x_n p(x_1, x_2, ..., x_{n+1}) \\ &= E[X_n] \\ \Rightarrow E[X_{n+1}] &= E[X_n] = E[X_{n-1}] = ... = E[X_1]. \end{aligned} \tag{1.16}$$

§ 1.4.3 Numeraire

Numeraire is a basic standard by which values are measured. In a financial market, a particular numeraire is chosen to yield a martingale evolution for the forward bonds in the market. Money market numeraire, forward bond numeraire, forward numeraire and common Libor numeraire is introduced in this section.

Choose $M(t, t_*)$ as a numeraire for the money market, and $M(t, t_*)$ is given by [5]

$$M(t, t_*) = e^{\int_t^{t_*} r(t')dt'}; \quad t : \text{fixed}, \tag{1.17}$$

where $r(t)$ is the spot interest rate. The martingale condition is then given by

$$\begin{aligned} \frac{B(t,T)}{M(t,t)} &= E_M\left[\frac{B(t_*,T)}{M(t,t_*)}\right] \\ \Rightarrow B(t,T) &= E_M[e^{-\int_t^{t_*} r(t')dt'} B(t_*,T)], \end{aligned} \tag{1.18}$$

where $E_M[...]$ denotes taking the expectation value with respect to the money market measure.

$B(t, T_I)$ is chosen for the forward bond numeraire, and the martingale condition for zero coupon bonds $B(t, T)$ is given by [5]

$$\begin{aligned} \frac{B(t,T)}{B(t,T_I)} &= E_I\left[\frac{B(T_I,T)}{B(T_I,T_I)}\right] \\ \Rightarrow B(t,T) &= B(t,T_I) E_I[B(T_I,T)], \end{aligned} \tag{1.19}$$

where $E_I[...]$ denotes taking the expectation value with respect to the forward neutral measure.

The forward numeraire is a collection of zero coupon bonds which is defined on Libor time.

An collection of zero coupon bonds defined on Libor time from T_0 to T_{n+1} is given by

$$B(t,T_0), B(t,T_1), ..., B(t,T_n), B(t,T_{n+1}); \quad T_n = T_0 + \ell n. \tag{1.20}$$

Suppose a zero coupon bond matures at future time T_{n+1}, the forward value of the bond at present time t_0 is given by

$$F(t_0,T_n,T_{n+1}) = e^{-\int_{T_n}^{T_{n+1}} dx f(t_0,x)} = \frac{B(t_0,T_{n+1})}{B(t_0,T_n)}. \tag{1.21}$$

The martingale condition for the forward bond is given by

$$F(t_0,T_n,T_{n+1}) = E_F[F(t_*,T_n,T_{n+1})] \tag{1.22}$$

$$\Rightarrow e^{-\int_{T_n}^{T_{n+1}} dx f(t_0,x)} = E_F[e^{-\int_{T_n}^{T_{n+1}} dx f(t_*,x)}]. \tag{1.23}$$

For modeling the Libor term structure, a common Libor numeraire is chosen for the the martingale evolution of all the Libor rates [6].

The Libor rate, which is defined on Libor time, can be expressed by using the Libor forward interest rate $f(t,x)$. Suppose $L(t,T_n)$ represents the Libor rate from T_n to $T_{n+\ell}$ and the tenor $\ell = T_{n+\ell} - T_n$, the Libor $L(t,T_n)$ is given by

$$L(t,T_n) = \frac{1}{\ell}(e^{\int_{T_n}^{T_{n+\ell}} dx f(t,x)} - 1). \tag{1.24}$$

Because $e^{\int_{T_n}^{T_{n+\ell}} dx f(t,x)}$ can be expressed in terms of bond price, which is

$$e^{\int_{T_n}^{T_{n+\ell}} dx f(t,x)} = \frac{B(t,T_n)}{B(t,T_{n+\ell})}. \tag{1.25}$$

Hence, the Libor can be rewritten in terms of bond, which is given by

$$\begin{aligned} L(t,T_n) &= \frac{1}{\ell}\Big(\frac{B(t,T_n)}{B(t,T_{n+\ell})} - 1\Big) \\ &= \frac{1}{\ell}\Big(\frac{B(t,T_n) - B(t,T_{n+\ell})}{B(t,T_{n+\ell})}\Big). \end{aligned} \tag{1.26}$$

From Equation 1.26, the combination $L(t,T_n)B(t,T_{n+1})$ is equivalent to a portfolio of zero coupon bonds. Hence, $L(t,T_n)B(t,T_{n+1})$ is a traded asset and can be made into martingales by using an appropriate forward bond numeraire.

Choose the zero coupon bond $B(t, T_{I+1})$ as the numeraire, the martingale evolution of Libor rates is given by

$$\frac{L(t_0, T_n)B(t_0, T_{n+1})}{B(t_0, T_{I+1})} = E_L\big[\frac{L(t, T_n)B(t, T_{n+1})}{B(t, T_{I+1})}\big], \tag{1.27}$$

where $E_L[...]$ denotes taking the expectation value with respect to the common Libor market measure. The time T_{I+1} can be freely chosen. It is found that different discounting bond $B(t, T_{I+1})$ can be used as the numeraire for Libor $L(t, T_n)$. The expectation value of $L(t, T_n)$ is invariant under different choices for the discounting bond $B(t, T_{I+1})$, this feature of Libor Market Model is because in the LMM drift is come from the nontrivial property of Libor drift. The details of change numeraire is discussed in details in Chapter 4.

§ 1.4.4 Coupon bond options

Suppose a zero coupon bond $B(t_*, T)$ will be issued at a future time t_* ($t_* > t_0$) and expire at time T. For the forward bond numeraire, the price of a zero coupon bond call option at present time t_0, similar to Equation 1.19, is given by

$$C(t_0, t_*, T, K) = B(t_0, t_*)E[\mathcal{P}_*], \tag{1.28}$$

where $\mathcal{P}_*$ is the payoff function and K is the strike price. The payoff function of zero coupon bond is given by

$$\mathcal{P}_* = \Big(B(t_*, T) - K\Big)_+. \tag{1.29}$$

The term $B(t_0, t_*)$ is used to discount the payoff function at time t_* to present time t_0.

Suppose a coupon bond with a principal L is issued at calendar time t_* and matures at future time T. The fixed dividends a_i are paid at different future times T_i for different coupons. The value of the coupon bond, from Equation 1.11, is given by

$$\sum_{i=1}^{N_c} c_i B(t_*, T_i), \tag{1.30}$$

where $c_i = a_i$ $(i = 1, 2, ..., N_c - 1)$ and $c_{N_c} = a_{N_c} + L$.

The payoff function $\mathcal{P}_*$ for coupon bond option is

$$\mathcal{P}_* = \Big(\sum_{i=1}^{N_c} c_i B(t_*, T_i) - K\Big)_+. \tag{1.31}$$

Discounting the payoff function to present time t_0 using the forward bond numeraire, the call price of coupon bond option is given by

$$C(t_0, t_*, T, K) = B(t_0, t_*)\Big(\sum_{i=1}^{N_c} c_i B(t_*, T_i) - K\Big)_+. \tag{1.32}$$

§ 1.4.5 Barrier options

A barrier option is an option which depends on the price of the option reaching a given barrier level. Barrier options are always cheaper than an option without barrier, the reason is discussed in Chapter 3. A barrier option with up barrier means that underlying price starts below the barrier level and it will be knocked out if the price exceeds the up barrier. The barrier option can have one up barrier, one down barrier and double barrier (both up and down barrier). A double barrier option has the same payoff function as a European option except that the barrier option will be knocked out when the underlying price exceeds a given maximum value U or falls below a minimum value L. The dynamic of a double barrier option is shown in Figure 1.5.

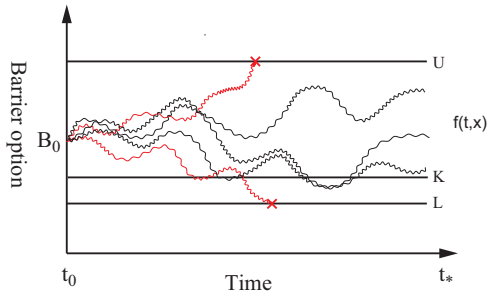

Figure 1.5: The payoff function for a double barrier option, with maturity time t_* and strike price K.

§ 1.4.6 Interest rate caps and floors

An interest rate cap is a popular interest rate options offered by financial institutions in the over-the-counter market [7]. As discussed before, the interest rate is reset periodically equal to Libor. To hedge the interest rate on the floating-rate note rising above some certain level, an interest rate cap is provided for such purpose.

Mathematically, an interest rate cap is a derivative in which the buyer will receive a profit if the interest rate at the end of the tenor (the next reset date) exceeds the prefixed strike price.

Suppose a caplet puts an upper limit of agreed strike price K for the period from T_n to $T_n + \ell$. Then, a mid-curve caplet is defined as an option which is exercised at time t_*, and the operation time T_n is larger than t_*. Let the caplet price, at present time $t_0 < t_*$, is denoted by $Caplet(t_0, t_*, T_n)$. The payoff function of a caplet, which will matures at time t_*, is given by

$$Caplet(t_*, t_*, T_n) \quad = \quad \ell V B(t_*, T_n + \ell)[L(t_*, T_n) - K]_+, \tag{1.33}$$

where V denotes the principal of the interest rate cap, $B(t_*, T_n + \ell)$ is the discounting bond and ℓ is the Libor tenor. Note that this caplet payments will be received at next reset date, which is $T_n + \ell$. Figure 1.6 shows the payoff function for $Caplet(t_*, t_*, T_n)$.

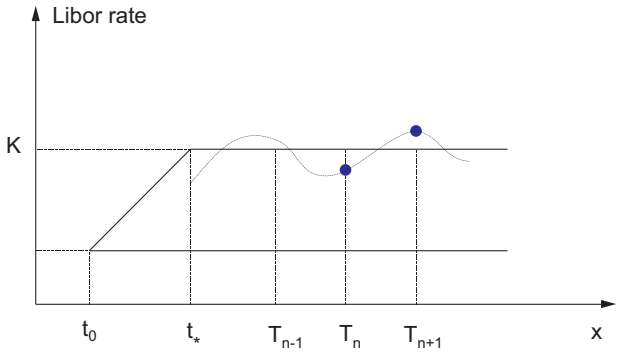

Figure 1.6: Diagram represents the price of $Caplet(t_*, t_*, T_n)$. The holder needs to pay only K interest rate during the Libor time from T_n to $T_n + \ell$.

As discussed in Section § 1.4.3, the forward bond numeraire $B(t, T_{n+1})$ is chosen as the discounting numeraire for the $Caplet(t, t_*, T_n)$. The caplet is a traded instrument, thus it follows a martingale evolution for numeraire $B(t, T_{n+1})$. The present value of a martingale is

equal to its expectation value in the future. The martingale evolution for a caplet is given by

$$\begin{aligned} \frac{Caplet(t_0, t_*, T_n)}{B(t_0, T_{n+1})} &= E\big[\frac{Caplet(t_*, t_*, T_n)}{B(t_*, T_{n+1})}\big] \\ &= \ell V E[L(t_*, T_n) - K]_+. \end{aligned} \tag{1.34}$$

Therefore, the price of a caplet at present time t_0 is given by

$$Caplet(t_0, t_*, T_n) = \ell V B(t_0, T_{n+1}) E[L(t_*, T_n) - K]_+. \tag{1.35}$$

An interest rate floor is a series of European put options or floorlets on LIBOR. If the prefixed rate is below the agreed strike price of the floor on the maturity, the buyer of the floor receives profit. The floorlet looks like the inverse of caplet, which is defined by

$$Floorlet(t_*, t_*, T_n) = \ell V B(t_*, T_n + \ell) E[K - L(t_*, T_n)]_+. \tag{1.36}$$

Similar to the case of caplet, the price of a floorlet at present time t_0 is given by

$$Floorlet(t_0, t_*, T_n) = \ell V B(t_0, T_{n+1}) E[K - L(t_*, T_n)]_+. \tag{1.37}$$

§ 1.4.7 Swaption

Interest rate swaps are the instruments that are contracted between two parities. One party pays at a fixed interest rate and another party pays at a floating interest rate. A floating rate receiver's swap, denoted by $swap_L$, means that the first party will receive the interest rate payments at the floating rate and pay at a fixed interest. Contrary to $swap_L$, a fixed rate receiver's swap, denoted by $swap_R$, means that the first party will receive the payments at a fixed interest rate and pay at the floating rate.

The simplest forward swap is called a forward *swaplet*. Suppose the contract of swaplet, entered at time t, has a notional principal of ℓV and the contract will be kept in a fixed time deposit from future time T_n to $T_n + \ell$. In this swaplet, the Libor rate $L(t, T_n)$ is chosen to be the floating interest rate and R_s denotes the fixed interest rate. The value of a forward floating rate receiver swaplet at present time t_0 is given by

$$swaplet_L(t_0, T_n) = \ell V B(t_0, T_n + \ell)[L(t_0, T_n) - R_s]. \tag{1.38}$$

The swap start at time T_0, with payments made at different Libor time T_n, $n = 1, 2, ...N$, has

the first payment at time T_1 and final payment at time T_N. The present value of the floating rate receiver swap and fixed rate receiver swap is given by

$$swap_L(t_0, R_s) = \ell V \sum_{n=0}^{N-1} B(t_0, T_n + \ell)[L(t_0, T_n) - R_s], \tag{1.39}$$

$$swap_R(t_0, R_s) = \ell V \sum_{n=0}^{N-1} B(t_0, T_n + \ell)[R_s - L(t_0, T_n)]. \tag{1.40}$$

Hence, from above two equations, the following relation can be simply obtained

$$swap_L(t_0, R_s) + swap_R(t_0, R_s) = 0. \tag{1.41}$$

A swaption is an option which the holder has the right but not the obligation to enter into an underlying swap. Swaptions are simply the options on interest rate swaps. Hence, the swaption price of receiving floating rate payments and paying fixed rate is given by

$$\begin{aligned} C_L(t_0, T_0; R_s) &= E[swap_L(T_0, R_s)]_+ \\ &= \ell V E\Big[e^{\int_{t_0}^{T_0} dt r(t)} \sum_{n=0}^{N-1} B(T_0, T_n + \ell)[L(T_0, T_n) - R_s]\Big]_+. \end{aligned} \tag{1.42}$$

Chapter 2

Interest Rates Model in Quantum Finance

A major revolution in quantitative finance starts with the work of Black and Scholes which form the basis of present day's financial theory. This basic concept and model was then developed by Merton and follows with the stochastic models of simulating the term structure of interest rates. The history of interest rate models is briefly introduced in this Chapter. The HJM (Heath-Jarrow-Morton) model and BGM-Jamshidian model based on stochastic calculus are discussed in details. The quantum generalization of forward interest rate model and Libor market model, in which the main advantage is that the whole interest rate dynamics are driven by the quantum field, are studied. The Gaussian Lagrangian for the quantum field and the way of pricing instruments in quantum finance are given. An alternative derivation of the drift in Libor market model is also discussed in this Chapter.

§ 2.1 Brief review of interest rates models

Black and Scholes (1973) [8] proposed the famous Black-Scholes model, which has a strong impact on the fundamental financial theory. This model gives the fundamental economic assumption - the absence of arbitrage opportunities, which is the basis of the option theory of interest rate models. The short rate (short term interest, also means interest rate charged for short term loans) was assumed normally distributed in Black-Scholes-Merton (1973) [9] model, and this model gave a basic method to calculate the option price. However, this model is not able to capture the mean-reverting property of interest rates. This basic assumption proposed in Black-Scholes model was later used by Vasicek to develop the first one-factor

short rate model to capture mean reversion. Vasicek (1977) [10] assumed that the short rate under the real-world measure evolves as a mean reverting-process with constant coefficients. However, a major drawback of this approach is that the short rate in Vasicek model can have negative values; but short rate cannot be negative values in the real market. Cox, Ingersoll and Ross (1985) [11] developed a general equilibrium model by introducing a square root term in the diffusion coefficient in Vasicek model. Their model provides a powerful tool for the study and analysis of interest rate because the instantaneous short rate in their model is always positive. However, all the models mentioned above are time-invariant models. The serious drawback of time-invariant models is that these models endogenously produce the term structure of rates. This led Ho and Lee (1986) [12] to propose an exogenous term-structure model, which is a different approach to short rate models. However, their model is still based on the assumption that the evolution of term structure follows a binomial tree process, and the method cannot give a better understanding of the interest rates. This model therefore cannot be regarded as a proper extension of the Vasicek model. Hull and White (1990) [13] proposed an extended model which is able to fit both term structure and volatilities by introducing one time-varying parameter and gives more flexibility for simulating the spot rate dynamics. However, such a model may be dangerous because it can generate negative interest rates with a positive probability. This shortcoming was solved by Black, Derman and Toy (BDT model) (1990) [14]. In their model, lognormal distribution is firstly combined with the mean reverting process of the short rate. The major achievements of this model are the transparent calibration procedure of the yield curve and positive values generated in the calibration process. However, this model has mutually dependent mean-reversion and volatility terms. Later on, Black and Karasinski (1991) [15] modified this shortcoming of the BDT model in their celebrated lognormal short rate model by introducing independent parameters to avoid mutually dependent mean-reversion.

All the models mentioned above are one-factor short rate models, and many multi-factor models have also been developed to give more flexibility than one-factor models. The best known multi-factor models are Longstaff and Schwartz two-factor model [16] and Chen three-factor model [17]. These one and multi-factor models model the interest rate evolution by means of the instantaneous short rate. The advantage of these models is that one can choose the related dynamics and coefficients in the related diffusion dynamics freely. However, these one and multi-factor models have one serious drawback. All of them are used to model short rate and a clear understanding of correlation structure of forward rates is difficult to achieve. As mentioned before, Ho and Lee (1986) [12] proposed an alternative to short rate models based on a binomial tree process. Their basic idea led Heath, Jarrow and Morton (HJM) (1992) [18] to develop a general framework for modeling interest rate dynamics. Forward

rates were chosen as basic fundamental quantities in HJM model and term structure was also translated to continuous time. The major achievement of HJM model is that forward rates are taken as primary instrument directly because forward rates are directly traded in the debt market. HJM model is also the standard industry interest model nowadays. However, HJM model also has the limitation that it only allows a finite number of factors which determine the structure of the entire forward rate curve. This means that HJM model also cannot capture all the information of the structure of correlation of forward rates between different maturities.

To overcome the limitation of HJM model, Cohen and Jarrow (2000) [19] proposed that the number of factors can be taken to infinity. However, this idea is unrealistic since an infinite number of factors cannot be calculated in practice. In order to avoid the method of using infinite number of factors and to make the model more realistic in application, models with a rich correlation structure by using only a small number of parameters were developed. Some models were proposed by Kenendy (1994) [20], Goldstein (2000) [21], Santa-Clara and Sornette (2001) [22] and Baaquie (2001) [23]. Besides Baaquie's quantum finance approach, all other models are based on a stochastic partial differential equation in infinite variables, and these models have a major limitation that all the processes are based on white noise. White noise is widely used in traditional finance, and short rate models and HJM models mentioned before also use white noise as the main calibration process (also called stochastic process or stochastic calculus). Compared to the stochastic process, the approach of quantum field theory, proposed by Baaquie, is a totally different mechanism. The major advantage of quantum finance approach is that the evolution of forward rates is based on two-dimensional quantum field, and this method can capture more information from the correlated curve of forward rates. Quantum finance takes the similarities of quantum field theory and financial process, and it also offers a different perspective of financial theory. In order to simulate interest rate and interest rate derivatives by generating a two-dimensional quantum field directly, it is therefore necessary to investigate the advantages of quantum finance compared to traditional stochastic calculus.

§ 2.2 Review of interest rates models

§ 2.2.1 Heath-Jarrow-Morton (HJM) model

Heath, Jarrow and Morton (HJM) (1992) [18] developed a general framework for modeling the forward interest rate dynamics, and this model is called HJM model. The one-factor HJM

model is defined by the following

$$\frac{\partial f}{\partial t}(t,x) = \alpha(t,x) + \sigma(t,x)R(t), \tag{2.1}$$

where $\alpha(t,x)$ is the drift term and $\sigma(t,x)$ is the deterministic volatility of the forward interest rates. For each calendar time t, white noise $R(t)$ is an independent Gaussian random variable, which has the following properties

$$E[R(t)] = 0, \tag{2.2}$$
$$E[R(t)R(t')] = \delta(t-t'). \tag{2.3}$$

To get the forward rates at time t, one needs to integrate the differential equation from present time t_0 to t, which is given by

$$f(t,x) = f(t_0,x) + \int_{t_0}^{t} dt'\alpha(t',x) + \int_{t_0}^{t} dt'\sigma(t',x)R(t'), \tag{2.4}$$

where $f(t_0,x)$ is the initial forward rates which are given by the market, and the volatility function $\sigma(t',x)$ is also determined by the market.

From Equation 2.1, the whole differential equation is driven by a single white noise. The one-dimensional white noise cannot describe the correlation function or the volatility structure fully. This drawback leads to the development of K-factor HJM model, in which the time evolution of the forward ratws is driven by K-dimensional white noise, and the K-factor HJM model is given by

$$\frac{\partial f}{\partial t}(t,x) = \alpha(t,x) + \sum_{i=1}^{K} \sigma_i(t,x)R_i(t). \tag{2.5}$$

For each calendar time t, the white noise (stochastic variable) $R_i(t)$ are independent Gaussian random variables, which has the following feature

$$E(R_i(t)R_j(t')) = \delta_{ij}(t-t'). \tag{2.6}$$

As discussed in section § 2.1, the K-factor HJM model still cannot fit the rich correlation of forward rates very well unless the factor K is taken to be infinite. However, taking K to be infinite is not applicable. The quantum finance formulation of the forward rates generalizes the HJM model and fits the market very well.

§ 2.2.2 BGM-Jamshidian model

Besides the drawback discussed in the above section, HJM model also has another shortcoming: the forward rates $f(t,x)$ can be negative with a finite probability. The principles of finance require that the value of interest rates should be strictly positive. As shown in Equation 2.1, the forward rates can be negative if the white noise term is larger than the drift term and this shortcoming cannot be overcome in HJM model. The negative $f(t,x)$ doesn't influence the pricing of bond because bond is the exponential of forward rates. However, the negative value of $f(t,x)$ is not allowed for simulating (positive) interest rates since negative interest rates allow arbitrage.

To overcome this shortcoming, the Libor market model (LMM), also known as the BGM model, was firstly introduced by Brace, Gatarek and Musiela. BGM model was widely used in pricing interest rate derivatives, especially exotic derivatives like caps, floors and swaptions. Compared to the short rate and instantaneous forward rates, a collection of forward rates, which are directly observed in the market, are modeled in BGM model. Another achievement of the Libor market model is that the Black's formula for pricing caplets can be derived from LMM framework directly.

Define $L(t,Tn)$ as the forward interest rate fixed at calendar time t and the cash deposit is from time T_n to $T_n+\ell$. The BGM model is given by [24]

$$\frac{1}{L(t,T_n)}\frac{\partial L(t,T_n)}{\partial t} = \xi_n(t)+\gamma_n(t)R(t), \tag{2.7}$$

where

$$\xi_n(t) = \gamma_n(t)\sum_{m=I+1}^{n}\frac{\ell L(t,T_m)}{1+\ell L(t,T_m)}\gamma_m(t), \tag{2.8}$$

$$\gamma_n(t) = \int_{T_n}^{T_{n+1}} dx\gamma(t,x). \tag{2.9}$$

$\gamma(t,x)$ is the deterministic volatility and $\gamma_n(t)$ is the integration of volatility from T_n to $T_n+\ell$ on the future time. The new feature of Libor market model is that the drift term $\xi_n(t)$ is stochastic and depends on the volatility structure.

Similarly, the K-factor BGM model is given by

$$\frac{1}{L(t,T_n)}\frac{\partial L(t,T_n)}{\partial t} = \sum_{m=I+1}^{n}\frac{\ell L(t,T_m)\sum_{i=1}^{K}\gamma_{n,i}(t)\gamma_{m,i}(t)}{1+\ell L(t,T_m)}+\sum_{i=1}^{K}\gamma_{n,i}(t)R_i(t). \tag{2.10}$$

§ 2.3 Quantum field generalization of HJM model

As discussed in Section § 2.2.1, only the drift and volatility term are based on both calendar time t and future time x. A single white noise $R(t)$ is used to drive the entire evolution of forward interest rates and is not enough to describe the rich correlation of forward rates. It is natural to replace the one-dimensional white noise with two-dimensional quantum field $A(t,x)$, which is an random variable defined on both calendar and future time.

Baaquie (2004) [2] gives the quantum generalization of HJM model

$$\frac{\partial f}{\partial t}(t,x) = \alpha(t,x) + \sigma(t,x)A(t,x), \tag{2.11}$$

$$f(t_*,x) = f(t_0,x) + \int_{t_0}^{t_*} dt\alpha(t,x) + \int_{t_0}^{t_*} dt\sigma(t,x)A(t,x), \tag{2.12}$$

where the drift, under the measure of forward numeraire, is given by

$$\alpha_*(t,x) = \sigma(t,x)\int_{t_*}^{x} dx' D(x,x';t)\sigma(t,x'). \tag{2.13}$$

$A(t,x)$ is the quantum generalization of white noise $R(t)$ and it encodes the correlation (or information from data) of the forward rates $f(t,x)$ on future time x. Since $f(t,x)$ is a function of quantum field $A(t,x)$, the forward rate is also a two-dimensional quantum field. From the view of Monte Carlo simulation, all financial instruments, such as coupon bond options, can be obtained by averaging the forward rates over all possible configurations.

The forward interest rate $f(t,x)$ is an independent random variable on both calendar and future time. Since the drift and volatility are deterministic, the random variable $A(t,x)$ is the most important factor in the evolution of $f(t,x)$. The dynamics of the quantum field $A(t,x)$ were extensively studied in [25]; the Lagrangian of $A(t,x)$, which can be used to describe the correlation of forward rates by using parameters μ and λ, is given by

$$\mathcal{L}[A] = -\frac{1}{2}\Big\{A^2(t,x) + \frac{1}{\mu^2}\Big\{\frac{\partial A(t,x)}{\partial x} + \frac{1}{\lambda^4}\Big\{\frac{\partial^2 A(t,x)}{\partial^2 x}\Big\}^2\Big\}\Big\}. \tag{2.14}$$

The partition function, denoted by Z, is the functional integral over total configurations of $A(t,x)$ and is given by

$$Z = \int DAe^{S[A]}. \tag{2.15}$$

$\int DA$ stands for integrating over all configurations of $A(t,x)$. The action $S[A]$ of the Lagrangian is given as follows

$$S[A] = \int_{t_0}^{\infty} dt \int_{t}^{\infty} dx \mathcal{L}[A]. \tag{2.16}$$

A more general Gaussian Lagrangian, which is used for studying the empirical market data, is defined as

$$\mathcal{L}[A] = -\frac{1}{2} A(t,x) D^{-1}(x,x';t) A(t,x). \tag{2.17}$$

As discussed in [5], the generating function is defined by

$$Z[h] = E\Big[\exp\Big\{\int_{t_0}^{\infty} dt \int_{t}^{\infty} dx h(t,x) A(t,x)\Big\}\Big]. \tag{2.18}$$

This generating functional can be evaluated using Gaussian integration, which is shown as follows

$$\begin{aligned} Z[h] &= \frac{1}{Z}\int DA e^{S[A]+\int_{t_0}^{\infty} dt \int_{t}^{\infty} dx h(t,x)A(t,x)} \\ &= \exp\Big(\frac{1}{2}\int_{t_0}^{\infty} dt \int_{t}^{\infty} dx dx' h(t,x) D(x,x';t) h(t,x')\Big). \end{aligned} \tag{2.19}$$

Hence, the propagator $D(x,x';t)$ is given by

$$\begin{aligned} E[A(t,x)A(t,x')] &= \frac{1}{Z}\int DA e^{S[A]} A(t,x)A(t',x') \\ &= \frac{\delta^2}{\delta h(t,x)\delta h(t',x')} Z[h]\big|_{h=0} = \delta(t-t')D(x,x';t). \end{aligned} \tag{2.20}$$

Compared to the correlation function of HJM model, the propagator of quantum generalized model has full information of forward rates. Hence, the expectation value and correlation of $\partial f(t,x)/\partial t(t,x)$ is

$$E\big[\frac{\partial f}{\partial t}(t,x)\big] = E[\alpha(t,x)] = \alpha(t,x), \tag{2.21}$$

$$\begin{aligned} E\big[\frac{\partial f}{\partial t}(t,x)\frac{\partial f}{\partial t'}(t',x')\big] &= \sigma(t,x)\sigma(t',x')E[A(t,x)A(t',x')] \\ &= \delta(t-t')\sigma(t,x)D(x,x';t)\sigma(t,x'). \end{aligned} \tag{2.22}$$

The price of any interest rate instruments $F[A]$ can be evaluated by getting the expectation

value $E[F[A]]$, which is equivalent to average $F[A]$ for all configurations of $f(t,x)$. Performing the Feynman path integral, the expectation value is given by

$$E\big[F[A]\big] \;=\; \frac{1}{Z}\int DAF[A]e^{S[A]};\quad Z=\int DAe^{S[A]}. \tag{2.23}$$

The simulation of European coupon bond options and barrier options using this generalized interest rate model is discussed in Chapter 3, and it is shown that the quantum field formulation of forward rates gives far more accurate option price.

§ 2.4 Quantum field generalization of Libor market model

As discussed in the above section, the white noise $R(t)$ is replaced with quantum field $A(t,x)$. Similar to HJM frame work, the BGM model is also based on the evolution of a single white noise. Intuitively, one is free to replace $R(t)$ with $A(t,x)$ in BGM model. Following Baaquie [26], the Libor market model using quantum finance approach is given by

$$\frac{1}{L(t,T_n)}\frac{\partial L(t,T_n)}{\partial t} \;=\; \xi(t,T_n)+\int_{T_n}^{T_n+\ell}\gamma(t,x)A(t,x), \tag{2.24}$$

where $\xi(t,T_n)$ is fixed under common Libor measure and is given by

$$\xi(t,T_n)=\begin{cases} =\displaystyle\sum_{m=I+1}^{n}\frac{\ell L(t,T_m)}{1+\ell L(t,T_m)}\Lambda_{mn}(t), & T_n>T_I \\ =0, & T_n=T_I \\ =-\displaystyle\sum_{m=n+1}^{I}\frac{\ell L(t,T_m)}{1+\ell L(t,T_m)}\Lambda_{mn}(t). & T_n<T_I \end{cases} \tag{2.25}$$

BGM model is designed to give positive Libor rates, and the above generalized Libor market model can only give positive Libor rates. In order to investigate the properties of quantum field of Libor rates, a method of changing variable is introduced. Define the logarithmic Libor rates $\phi(t,x)$ by

$$\ell L(t,T_n) \;=\; \exp\Big\{\int_{T_n}^{T_{n+1}}dx\phi(t,x)\Big\}\equiv e^{\phi_n(t)}. \tag{2.26}$$

The Libor market model in terms of logarithic Libor rates $\phi(t,x)$ is given by

$$\begin{aligned}\frac{\phi(t,x)}{\partial t} &= -\frac{1}{2}\Lambda_n(t,x)+\rho_n(t,x)+\gamma(t,x)A(t,x), &(2.27)\\ \Lambda_n(t,x) &= \int_{T_n}^{T_{n+1}} dx' M(x,x';t), &(2.28)\end{aligned}$$

and the function $\rho_n(t,x)$ is defined by

$$\xi(t,T_n) = \int_{T_n}^{T_{n+1}} \rho_n(t,x). \tag{2.29}$$

Following the same discussion for forward interest rate model, the Lagrangian for logarithmic Libor field $\phi(t,x)$ is given by

$$\begin{aligned}\mathcal{L}[\phi] &= -\frac{1}{2}A_L(t,x)D^{-1}(x,x';t)A_L(t,x')\\ &= -\frac{1}{2}\Big[\frac{\partial\phi(t,x)/\partial t-\tilde{\rho}(t,x)}{\gamma(t,x)}\Big]D^{-1}(x,x';t)\Big[\frac{\partial\phi(t,x')/\partial t-\tilde{\rho}(t,x')}{\gamma(t,x')}\Big], &(2.30)\end{aligned}$$

where

$$\tilde{\rho}(t,x) = -\frac{1}{2}\Lambda_n(t,x)+\rho_n(t,x). \tag{2.31}$$

The action for this Lagrangian and the partition function Z are given by

$$\begin{aligned}S[\phi] &= \int_{t_0}^{\infty} dt\int_{t}^{\infty} dxdx'\mathcal{L}[\phi],\\ Z &= \int D\phi e^{S[\phi]} = \int DAe^{S[A]},\\ \int DA &= D\phi = \prod_{t=t_0}^{\infty}\prod_{x=t}^{\infty}\int_{-\infty}^{+\infty} d\phi(t,x). &(2.32)\end{aligned}$$

The price of interest rate instruments based on Libor rates is then given by

$$E[\mathcal{O}] = \frac{1}{Z}\int DA\mathcal{O}[A]e^{S[A]} = \frac{1}{Z}\int D\phi\mathcal{O}[\phi]e^{S[\phi]}. \tag{2.33}$$

The quantum generalization of Libor market model is studied in details in Chapter 4, and the advantage of pricing financial instruments using LMM is also demonstrated.

§ 2.5 Derivation of Libor drift

In terms of Libor forward interest rates, Libor $L(t, T_n)$ is given by

$$1 + \ell L(t, T_n) \quad = \quad \exp\Big\{ \int_{T_n}^{T_n+\ell} dx f_L(t, x) \Big\}. \tag{2.34}$$

The Libor forward interest rates $f_L(t, x)$ has same properties as the empirical forward interest rates and the bond forward interest rates. The Libor zero coupon bond is the bond discounted from future time T to present time t and is given by

$$B(t, T) \quad = \quad \exp\big(- \int_t^T dx f_L(t, x) \big). \tag{2.35}$$

Using Equation 2.34, Libor $L(t, T_n)$ can be expressed in terms of Libor zero coupon bond as follows

$$L(t, T_n) \quad = \quad \frac{B(t, T_n) - B(t, T_{n+1})}{\ell B(t, T_{n+1})}. \tag{2.36}$$

Equation 2.36 yields a recursion equation such that the bond $B(t, T_{n+1})$ and forward bond $F(t_0, T_0, T_n + \ell)$ can be expressed solely in terms of Libor rates as follows

$$B(t, T_{n+1}) \quad = \quad B(t, T_0) \prod_{i=0}^{n} \frac{1}{1 + \ell L(t, T_i)}, \tag{2.37}$$

$$F(t_0, T_0, T_n + \ell) \quad = \quad \frac{B(t_0, T_{n+1})}{B(t_0, T_0)} = \prod_{i=0}^{n} \frac{1}{1 + \ell L(t_0, T_i)}. \tag{2.38}$$

Numeraire is a basic concept by which the future cash flow of financial instruments is discounted. As shown in Equation 2.36, the combination $L(t, T_n)B(t, T_{n+1})$ can be expressed as a portfolio of zero coupon bonds. This unique feature of Libor rates leads to the unusual martingale condition of Libor rates given by

$$\chi_n(t) \quad = \quad \frac{L(t, T_n)B(t, T_{n+1})}{B(t, T_{I+1})}; \quad I : \text{fixed}, \tag{2.39}$$

in which all instruments $\chi_n(t)$ are martingales for $n = 0, \pm 1, \pm 2, ..., \pm\infty$. Because of the unique martingale condition, the nonlinear and nontrivial drift can be derived by using common Libor numeraire $B(t, T_{I+1})$. The nonlinear stochastic drift draws a distinction between the linear HJM model and nonlinear BGM-Jamshidian model.

Baaquie (2009) has given a derivation of $\xi(t,T_n)$ in [5]. An alternative derivation of stochastic drift $\xi(t,T_n)$ is discussed here. As shown in [5], the stochastic volatility $v(t,x)$ of Libor forward interest rates can be rewritten in terms of a deterministic Libor volatility function $\gamma(t,x)$ using the following transformation

$$\int_{T_n}^{T_{n+1}} dx v(t,x)A(t,x) = \frac{\ell L(t,T_n)}{1+\ell L(t,T_n)} \int_{T_n}^{T_{n+1}} dx \gamma(t,x)A(t,x). \tag{2.40}$$

Following the results discussed in [26], the drift $\xi(t,T_n)$, from which the new feature of Libor Market Model is obtained , is defined as

$$\xi(t,T_n) = \frac{1+\ell L(t,T_n)}{\ell L(t,T_n)} \times \int_{T_{I+1}}^{T_{n+1}} dx v(t,x) \int_{T_n}^{T_{n+1}} dx' D(x,x';t)v(t,x'). \tag{2.41}$$

According to the Wilson expansion, the equal time singular product of two Gaussian quantum fields is given by [5]

$$A(t,x)A(t,x') = \frac{1}{\epsilon} D(x,x';t). \tag{2.42}$$

Expressing $D(x,x';t)$ in terms of the quantum field $A(t,x)$, the drift $\xi(t,T_n)$ can be rewritten as

$$\xi(t,T_n) = \epsilon \frac{1+\ell L(t,T_n)}{\ell L(t,T_n)} \times \int_{T_{I+1}}^{T_{n+1}} dx A(t,x)v(t,x) \int_{T_n}^{T_{n+1}} dx' A(t,x')v(t,x'). \tag{2.43}$$

Substituting Equation 2.40 into the drift, one obtains

$$\begin{aligned} \xi(t,T_n) &= \epsilon \frac{1+\ell L(t,T_n)}{\ell L(t,T_n)} \times \int_{T_{I+1}}^{T_{n+1}} dx A(t,x)v(t,x) \times \frac{\ell L(t,T_n)}{1+\ell L(t,T_n)} \int_{T_n}^{T_{n+1}} dx' A(t,x')\gamma(t,x') \\ &= \epsilon \int_{T_{I+1}}^{T_{n+1}} dx A(t,x)v(t,x) \int_{T_n}^{T_{n+1}} dx' A(t,x')\gamma(t,x'). \end{aligned} \tag{2.44}$$

We obtain one integral $A(t,x')\gamma(t,x')$ over one Libor tenor time and another integral over $v(t,x)$ that remains to be transformed to $\gamma(t,x)$. Notice that the integral on x is from T_{I+1} to T_{n+1}, which can be expanded in terms of only one Libor tenor time. For the case of $T_n > T_I$,

Equation 2.44 yields the following

$$\begin{aligned}\xi(t,T_n) &= \epsilon\Big\{\int_{T_{I+1}}^{T_{I+2}} + \int_{T_{I+2}}^{T_{I+3}} + \cdots + \int_{T_n}^{T_{n+1}} dx A(t,x)v(t,x)\Big\} \\ &\times \int_{T_n}^{T_{n+1}} dx' A(t,x')\gamma(t,x'). \end{aligned} \tag{2.45}$$

Taking the integration from T_{I+1} to T_{I+2} for instance, this integration can be solved by using Equation 2.40 again and is given by

$$\begin{aligned}\int_{T_{I+1}}^{T_{I+2}} dx A(t,x)v(t,x) \int_{T_n}^{T_{n+1}} dx' A(t,x')\gamma(t,x') &= \frac{\ell L(t,T_{I+1})}{1+\ell L(t,T_{I+1})} \int_{T_{I+1}}^{T_{I+2}} dx A(t,x)\gamma(t,x) \\ &\times \int_{T_n}^{T_{n+1}} dx' A(t,x')\gamma(t,x'). \end{aligned} \tag{2.46}$$

Using the singular product of two Gaussian quantum field again, one obtains

$$\begin{aligned}\int_{T_{I+1}}^{T_{I+2}} dx A(t,x)v(t,x) \int_{T_n}^{T_{n+1}} dx' A(t,x')\gamma(t,x') &= \frac{1}{\epsilon}\frac{\ell L(t,T_{I+1})}{1+\ell L(t,T_{I+1})} \int_{T_{I+1}}^{T_{I+2}} dx \int_{T_n}^{T_{n+1}} dx' \\ &\times \gamma(t,x)D(x,x';t)\gamma(t,x'). \end{aligned} \tag{2.47}$$

Hence, the integration of the rest of the time intervals can be solved following the same procedure discussed above. Integrating the whole time interval from T_{I+1} to T_{n+1} and collecting all the results, the drift $\xi(t,T_n)$ is given by

$$\xi(t,T_n) = \sum_{m=I+1}^{n} \frac{\ell L(t,T_m)}{1+\ell L(t,T_m)} \Lambda_{mn}(t), \quad n > I, \tag{2.48}$$

where the Libor correlator $\Lambda_{mn}(t)$ is given by

$$\begin{aligned}\Lambda_{mn}(t) &= \int_{T_m}^{T_{m+1}} dx \int_{T_n}^{T_{n+1}} dx' \gamma(t,x)D(x,x';t)\gamma(t,x') \\ &= \int_{T_m}^{T_{m+1}} dx \int_{T_n}^{T_{n+1}} dx' M_\gamma(x,x';t). \end{aligned} \tag{2.49}$$

For the case of $T_n = T_I$, the drift $\xi(t,T_n)$ is equal to zero.

For the case of $T_n < T_I$, the integration from T_{I+1} to T_{n+1} is simply the inverse of the case

of $T_n > T_I$ and is shown as follows

$$-\int_{T_{I+1}}^{T_{n+1}} = \int_{T_{n+1}}^{T_{I+1}} = \int_{T_{n+1}}^{T_{n+2}} + \int_{T_{n+2}}^{T_{n+3}} + \cdots + \int_{T_I}^{T_{I+1}}. \tag{2.50}$$

Following the same derivation for the case of $T_n > T_I$, the drift $\xi(t, T_n)$ is given by

$$\xi(t, T_n) = -\sum_{m=n+1}^{I} \frac{\ell L(t, T_m)}{1 + \ell L(t, T_m)} \Lambda_{mn}(t), \quad n < I. \tag{2.51}$$

Collecting all the results obtained for $\xi(t, T_n)$, we get the results of $\xi(t, T_n)$ as stated in [5]

$$\xi(t, T_n) = \begin{cases} \displaystyle\sum_{m=I+1}^{n} \frac{\ell L(t, T_m)}{1 + \ell L(t, T_m)} \Lambda_{mn}(t), & T_n > T_I \\ 0, & T_n = T_I \\ \displaystyle -\sum_{m=n+1}^{I} \frac{\ell L(t, T_m)}{1 + \ell L(t, T_m)} \Lambda_{mn}(t). & T_n < T_I \end{cases} \tag{2.52}$$

Chapter 3

Simulation of Coupon Bond European and Barrier Options

Coupon bond European and barrier options are studied in the framework of quantum finance. The prices of European and barrier options are analyzed by generating sample values of the forward interest rates $f(t,x)$ using a two-dimensional Gaussian quantum field $A(t,x)$. The strong correlations of forward interest rates are described by the stiff propagator of the quantum field $A(t,x)$. Using the Cholesky decomposition, $A(t,x)$ is expressed in terms of white noise. The simulation results for European coupon bond and barrier options are compared with approximate formulas, which are obtained as power series in the volatility of the forward interest rates. The simulation shows that the simulated price deviates from the approximate value for large volatilities. The numerical algorithm is flexible and can be used for pricing any kind of option. It is shown that the three-factor HJM model can be derived from the quantum finance formulation.

§ 3.1 Introduction

Coupon bond European and barrier options are widely traded financial instruments. The European option is a fundamental option and is the prototype for other kinds of options. Path dependent coupon bond barrier options are also very important derivatives in the financial market. Both the coupon bond European option and the barrier options are derivatives that depend on the forward interest rates. Simulating the forward interest rate accurately is thus a crucial problem in pricing European and barrier bond options.

The forward interest rates $f(t,x)$ are the interest rates, fixed at time t, for an instantaneous loan at future time $x > t$; $f(t,x)$ has the dimensions of 1/time [27]. Most interest rate models in mathematical finance are based on stochastic calculus, which is discussed in Chapter 2. These models give a description of the evolution of forward interest rates (forward rates) as a stochastic process and have some intrinsic shortcomings. The most famous model for forward interest rates is the HJM (Heath, Jarrow and Morton) model [18], which is currently the industry standard interest rate model. The main limitation of these models is that, since the forward rates are simulated as one-dimensional stochastic process, all the forward rates for different maturities are exactly correlated. The quantum generalization of HJM model was proposed by Baaquie (2004) [2], and shows its advantage for simulating the forward interest rates naturally. The simulation of forward interest rates by using Gaussian quantum field is discussed in details in this Chapter.

Coupon bond and forward interest rates have been extensively studied in [5], and the Hamiltonian formulations of European and barrier bond options have been studied in detail in [27]. Numerical simulation of forward interest rates and pricing European and barrier options are studied in this Chapter using the approach of quantum finance.

§ 3.2 Cholesky simulation of two-dimensional quantum field

Heath, Jarrow and Morton (HJM) (1992) [18] developed a general framework for modeling the forward interest rate dynamics. The evolution of the forward interest rates in the HJM model is defined by the following

$$\frac{\partial f}{\partial t}(t,x) = \alpha(t,x) + \sigma(t,x)R(t). \tag{3.1}$$

The one-factor HJM model drives the evolution of the forward interest rates by using a single white noise $R(t)$. From Equation 3.1, it follows that the fluctuation in the forward interest rates at time t only depends on white noise $R(t)$; this means that, at each instant, the correlation between forward rates for different maturities is equal to 1. The major limitation of the HJM model is that this model cannot capture all the information of the structure of the correlation between forward rates for different maturities.

Baaquie (2004) [2] proposed a quantum finance model for forward interest rates, which is

a generalization of the HJM model. The forward interest rates are defined by

$$\frac{\partial f}{\partial t}(t,x) = \alpha(t,x) + \sigma(t,x)A(t,x), \tag{3.2}$$

where the drift for the forward numeraire is given by [2]

$$\alpha_*(t,x) = \sigma(t,x)\int_{t_*}^{x} dx' D(x,x';t)\sigma(t,x'). \tag{3.3}$$

As given in Equation 3.2, in the quantum finance model, white noise $R(t)$ is replaced by a two-dimensional quantum field $A(t,x)$. The two-dimensional quantum field $A(t,x)$ is the generalization of white noise $R(t)$. The expectation value of the product of $R(t)$ and $A(t,x)$ (correlation function) are given in the following respectively

$$E[R(t)R(t')] = \delta(t-t'), \tag{3.4}$$
$$E[A(t,x)A(t',x')] = \delta(t-t')D(x,x';t), \tag{3.5}$$

where $E[...]$ is expectation value and $D(x,x';t)$ is called the forward interest rate propagator [2]. Equation 3.5 shows that the quantum finance model can incorporate the rich correlation between forward interest rates for different maturities. Assume that $D(x,x';t) = D(\theta,\theta')$, for the remaining future time θ and θ' ($\theta = x - t$ and $\theta' = x' - t$). From equation 3.5, the quantum field $A(t,x)$ satisfies the following [2]

$$E[A(t,x)A(t',x')] = \delta(t-t')D(\theta,\theta'). \tag{3.6}$$

Equation 3.6 is the defining equation for simulating the Gaussian quantum field $A(t,x)$. Because the propagator (correlation function) D is always a positive and symmetric matrix, Cholesky decomposition can be used for decomposing D into the product of a lower triangular matrix and its conjugate transpose. Let $0 \le \theta \le \theta_M$, where $\theta_M = T - t$; the Cholesky decomposition for the propagator yields

$$D(\theta,\theta') = \int_0^{\theta_M} Y(\theta,\zeta)Y^T(\zeta,\theta')d\zeta. \tag{3.7}$$

For $\theta = x - t$, let

$$A(t,x) = \int d\zeta Y(\theta,\zeta)R(t,\zeta), \tag{3.8}$$

where $E[R(t,\zeta)R(t',\zeta')] = \delta(t-t')\delta(\zeta-\zeta')$. $R(t,\zeta)$ is an independent Gaussian random variable for each calendar time t and future remaining time ζ. Equation 3.8 yields

$$\begin{aligned} E[A(t,x)A(t',x')] &= \int_0^{\theta_M} E[R(t,\zeta)R(t',\zeta')]Y(\theta,\zeta)Y^T(\zeta',\theta')d\zeta d\zeta' \\ &= \delta(t-t')\int_0^{\theta_M} Y(\theta,\zeta)Y^T(\zeta,\theta')d\zeta \\ &= \delta(t-t')D(\theta,\theta'). \end{aligned} \tag{3.9}$$

The simulation requires discrete calendar and future time. For infinitesimals ϵ_t and ϵ_x, we have

$$t, x \rightarrow m\epsilon_t, n\epsilon_x, \tag{3.10}$$

$$\theta \rightarrow p = n - m. \tag{3.11}$$

The quantum field $A(t,x)$ and forward interest rates $f(t,x)$ are expressed by

$$A(t,x) \rightarrow A_{m,n}, \tag{3.12}$$

$$f(t,x) \rightarrow f_{m,n}. \tag{3.13}$$

Market data for the forward interest rate $f_{m,n}$ are given daily for calendar time m and in intervals of 90 days for future time n. This means that, in market data, the step sizes of calendar time and future time are 1 day and 90 days respectively. However, for the numerical updating, the step sizes of the calendar time and future time must be same. If unequal steps for calendar time and future time are used for updating, the meaning of the variable $A_{m,n=m+p}$ becomes ambiguous since $m+p$ is not an integer multiple of the time step size when q is larger than m. As shown in Figure 3.1, in the lattice of forward interest rates $f_{m,n}$,the step sizes of calendar time and future time need to be equal. Hence, for the process of updating forward interest rate $f_{m,n}$, the step size of calendar time ϵ_t and the step size of future time ϵ_x are also chosen to be equal

$$\epsilon = \epsilon_t = \epsilon_x. \tag{3.14}$$

In this simulation, the value of the step size ϵ is chosen to be 1 day. As shown in Figure 3.1, suppose the largest value of the calendar time is t_* and that for the future time is T; t_0, t_*

and T are represented on the lattice in the following manner

$$t_0 \;=\; M_0\epsilon, \quad t_* = M_*\epsilon, \quad T = M\epsilon. \tag{3.15}$$

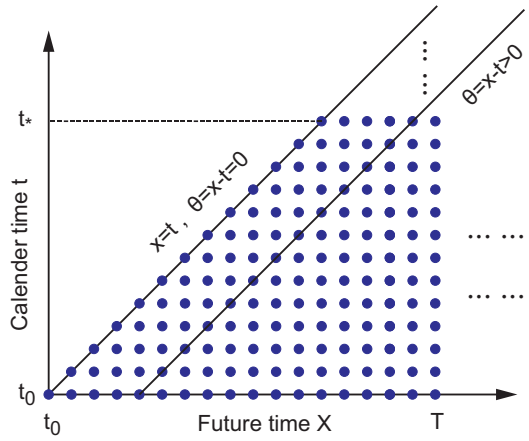

Figure 3.1: The lattice of forward interest rates in discrete time.

Equation 3.2 yields

$$f_{m+1,n} \;=\; f_{m,n} + \epsilon(\alpha_{m,n} + \sigma_{m,n}A_{m,n}). \tag{3.16}$$

The remaining future times $\theta = p\epsilon$ and $\theta' = p'\epsilon$ in discrete time, are $p = n-m$ and $p' = n'-m$, respectively. Equation 3.6 is rewritten as

$$\begin{aligned} E[A_{m,n}A_{m',n'}] &= \delta_{m-m'}D((n-m)\epsilon, (n'-m)\epsilon) \\ &= \delta_{m-m'}D_{p,p'}, \end{aligned} \tag{3.17}$$

where the range for p is $0 \le p \le M - m$.

Define $q = n - m'$ and $q' = n' - m'$;

$$D = YY^T \;\Rightarrow\; D_{p,p'} = \sum_{q=0}^{M-n} Y_{p,q}Y_{q,p'} \tag{3.18}$$

is the Cholesky decomposition.

The quantum field $A_{m,n}$ can be obtained from the following ($R(t,\theta) = \epsilon R_{m,p}$)

$$A_{m,n} = \sum_{p'=0}^{M-n} Y_{p,p'} R_{m,p'}, \quad p = m - n \tag{3.19}$$

with [1]

$$E[R_{m,p} R_{m',p'}] = \delta_{m-m'} \delta_{p-p'}, \tag{3.20}$$

where $R_{m,p}$ is the Gaussian random variable with variance given by $1/\sqrt{\epsilon}$. That is $R = N(0, \frac{1}{\sqrt{\epsilon}})$. In other words

$$\begin{aligned} R &= \frac{1}{\sqrt{\epsilon}} N, \\ N &= N(0,1) \quad ; \quad \text{Normal random variable.} \end{aligned} \tag{3.21}$$

From Equation 3.20 and 3.17

$$\begin{aligned} E[A_{m,n} A_{m',n'}] &= \sum_{q,q'=0}^{M-n} Y_{p,q} Y_{q',p'} E[R_{m,q} R_{m',q'}] \\ &= \delta_{m-m'} D_{p,p'} \\ &= \delta_{m-m'} \sum_{q=0}^{M-n} Y_{p,q} Y_{q,p'}. \end{aligned} \tag{3.22}$$

The bond forward interest rates can be updated using Equation 3.2 as follows (with $p = n - m$)

$$\begin{aligned} f_{m+1,n} &= f_{m,n} + \epsilon \alpha_{m,n} + \epsilon \sigma_{m,n} A_{m,n} \\ &= f_{m,n} + \epsilon \alpha_{m,n} + \epsilon \sigma_{m,n} \sum_{p'=0}^{M-n} Y_{p,p'} R_{m,p'}, \end{aligned} \tag{3.23}$$

[1] $\delta(t-t') = \frac{1}{\epsilon}\delta_{m-m'}$, $\delta(\theta - \theta') = \frac{1}{\epsilon}\delta_{p-p'}$.

where the drift term $\alpha_*(t,x)$ in continuous time in Equation 3.3 can be simplified using

$$\begin{aligned}\alpha_*(t,x) &= \sigma(t,x)\int_{t_*}^{x} dx' D(x,x';t)\sigma(t,x') \\ &= \sigma(x-t)\int_{t_*-t}^{x-t} d\theta' D(x-t,x'-t)\sigma(x'-t); \quad \theta = x-t \\ &= \sigma(\theta)\int_{t_*-t}^{x-t} d\theta' D(\theta,\theta')\sigma(\theta'). \end{aligned} \tag{3.24}$$

Therefore, the drift term $\alpha_{m,n}$ in discrete time is given by

$$\alpha_{m,n} = \epsilon\sigma_p \sum_{p=(M_*-m)}^{M-m} D_{p,p'}\sigma_{p'}.$$

In this study, the empirical stiff propagator is used for the propagator D and given by [2]

$$D(\theta_+;\theta_-) \equiv \frac{\lambda}{2\sinh(2b)}[g_+(\theta_+)+g_-(\theta_-)], \tag{3.25}$$

where

$$g_+(\theta_+) = e^{-\lambda\theta_+\cosh(b)}\sinh\{b+\lambda\theta_+\sinh(b)\}, \tag{3.26}$$

$$g_-(\theta_-) = e^{-\lambda|\theta_-|\cosh(b)}\sinh\{b+\lambda|\theta_-|\sinh(b)\}, \tag{3.27}$$

$$\theta_\pm = \theta \pm \theta'. \tag{3.28}$$

Define the normalized propagator by

$$C(\theta,\theta') = \frac{D(\theta,\theta')}{\sqrt{D(\theta,\theta)D(\theta',\theta')}}. \tag{3.29}$$

The parameters used for the stiff propagator are given in Table 3.1 [5] where $\lambda = \tilde{\lambda}^\eta$.

Table 3.1: The parameters for the stiff propagator used in the simulation.

$\tilde{\lambda}$	$\tilde{\mu}$	b	η
1.79/year	0.40/year	0.85	0.34

Using these parameters, the normalized stiff propagator is generated and this is shown in Figure 3.2(a). In our simulation, we use the stiff propagator without normalization (Figure

3.2(b)) because all the data are generated using formulas instead of market data. If the normalized stiff propagator from market data is used to simulate forward interest rates, the model's volatility σ needs to be transformed to empirical volatility σ_E. The techniques of the transformation of σ_E and empirical analysis are discussed in [5].

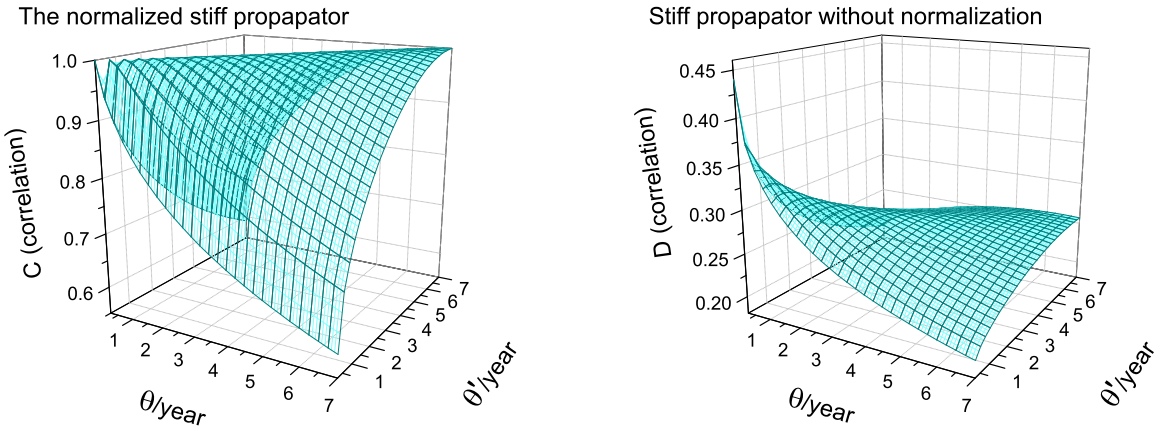

(a) (b)

Figure 3.2: (a) The normalized stiff propagator $C(\theta, \theta')$. (b)The stiff propagator $D(\theta, \theta')$ without normalization.

A well-known formula σ_M for the value of the volatility is given by [28]

$$\sigma_M = 0.061 - 0.014e^{(-1.55(\theta-\theta_{min}))} + 0.074(\theta - \theta_{min})e^{(-1.55*(\theta-\theta_{min}))}. \tag{3.30}$$

This formula is a good fit of the volatility for US forward rates from 1994 to 1999. The curve of $\sigma_M(\theta)$ with θ up to 7 years is shown in Figure 3.3. For the updating of $f(t, x)$, $\sigma(t, x)$ can be obtained using the shift of variables $\sigma(t, x) = \sigma(t, t + \theta)$. The initial value of the forward interest rates $f(t_0, x)$ is generated by using the following formula

$$f(t_0, x) = f_0(1 + e^{-\lambda_f(x-t_0)}), \tag{3.31}$$

where f_0 is chosen to be 0.02 and λ_f is chosen to be 0.3.

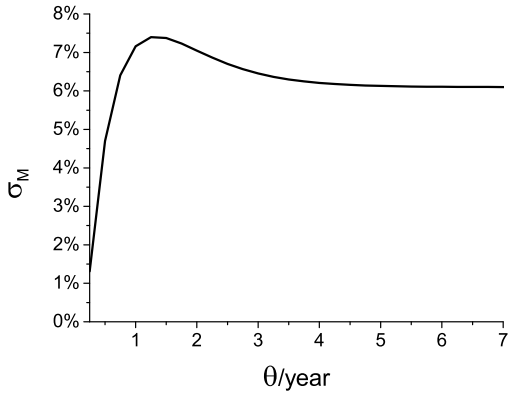

Figure 3.3: The curve of volatility $\sigma_M(\theta)$ which is calculated by using Equation 3.30.

§ 3.3 Zero coupon bond option

The zero coupon bond option is the simplest case of a European bond option. A zero coupon bond's value at time t_0 is $B(t_0, T)$; it has a bond maturity at fixed future time T with $B(T, T) = 1$. The price of this zero coupon bond $B(t, T)$, is obtained by discounting the payoff at future time T to present time t. For $t_* > t_0$, the zero coupon bond $B(t_*, T)$ will be issued at a future time t_* and expire at time T; the forward price of $B(t_*, T)$ at earlier time t, denoted by $F(t, t_*, T)$, is given by

$$F(t, t_*, T) \quad = \quad \exp\Big\{ - \int_{t_*}^{T} dx f(t, x) \Big\}. \tag{3.32}$$

In this simulation, the forward bond price $F(t_0, t_*, T)$ is varied via T; the plot of the forward bond price is shown in Figure 3.4.

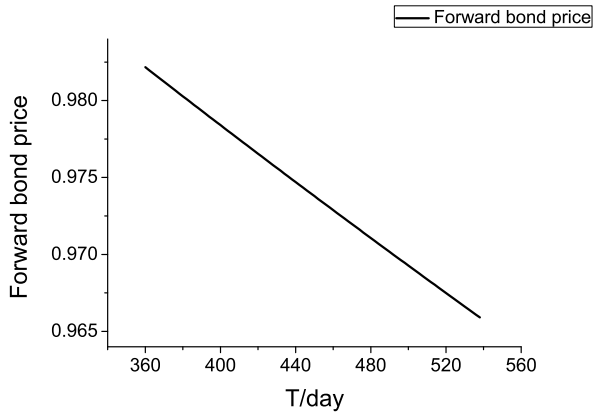

Figure 3.4: Forward bond price of zero coupon bond.

The price of a zero coupon bond call option with strike price K is given by

$$C(t_0, t_*, T, K) = B(t_0, t_*)E[\mathcal{P}_*], \tag{3.33}$$

where $\mathcal{P}_*$ is the payoff function and $C(t_0, t_*, T, K)$ is the price at the earlier time t_0. The payoff function of the zero coupon bond is given by

$$\mathcal{P}_* = \Big(B(t_*, T) - K\Big)_+. \tag{3.34}$$

The exact formula for the call price of the zero coupon bond option can be obtained because a zero coupon bond function is a linear function of forward interest rates. The exact call price for the zero coupon bond is given by [2]

$$C(t_0, t_*, T, K) = B(t_0, t_*)\Big[F(t_0, t_*, T)N(d_+) - KN(d_-)\Big], \tag{3.35}$$

where [2]

$$F \equiv F(t_0, t_*, T) = \exp\Big\{-\int_{t_*}^{T} dx f(t_0, x)\Big\}, \tag{3.36}$$

$$d_\pm = \frac{1}{q}\Big[\ln\frac{F}{K} \pm \frac{q^2}{2}\Big], \tag{3.37}$$

$$q^2 = \int_{t_0}^{t_*} dt \int_{t_*}^{T} dx dx' \sigma(t, x) D(x, x'; t)\sigma(t, x'). \tag{3.38}$$

[2] $N(x) = \frac{1}{\sqrt{2\pi}}\int_{-\infty}^{x} dz e^{-\frac{1}{2}z^2}$.

In this simulation method, the call price is obtained by performing an averaging over the payoff $\mathcal{P}_*^{(n)}$ for each sample configuration namely $f_n(t,x)$, so that the simulated price is

$$\begin{aligned}\tilde{C}(t_0,t_*,T,K,\epsilon) &= B(t_0,t_*)\frac{1}{\mathcal{N}}\sum_{n=1}^{\mathcal{N}}\mathcal{P}_*^{(n)} \\ &= B(t_0,t_*)\frac{1}{\mathcal{N}}\sum_{n=1}^{\mathcal{N}}\Big(B_n(t_*,T)-K\Big)_+ . \end{aligned} \tag{3.39}$$

$\mathcal{N}$ is the total number of configurations and $B_n(t_*,T)$ is the bond price of configuration $f_n(t,x)$. All the configurations are accepted because the zero coupon bond option doesn't have constraints on the configurations.

For the price of the zero coupon bond option, the maturity time t_* of the European call option is set to be 180 days, and the bond maturity time T is from 360 days to 538 days. The parameters for the simulation of the zero coupon bond option are shown in Table 3.2.

Table 3.2: The parameters used in the simulation of the zero coupon bond option.

ϵ	t_*	T	Strike price	Number of configurations
1 day	180 days	360 to 538 days	K = 0.5	$\mathcal{N} = 10^5$

We compare the results of our simulation with the exact price for different values of σ_M. As shown in Figure 3.3, the market volatility is always from 1% to 8% per year. In our simulation, the product of the quantum field $A(t,x)$ and $\sigma(t,x)$ is used in Equation 3.2. This product is very small if market volatility is used. To confirm the validity of our simulation, large fluctuations of the quantum field $A(t,x)$ need to take place in the simulation. A large value of σ is a good test for the correctness of the simulation. Hence, market volatility σ_M is multiplied by a large coefficient of 10 and 50 to obtain a large volatility σ.

$\mathcal{N} = 10^5$ configurations of the two-dimensional quantum field $A(t,x)$ were generated for obtaining sample values of the forward interest rates $f_n(t,x)$. The forward interest rates $f_n(t,x)$ are used to calculate the payoff function $\mathcal{P}_*$ for each configuration and the call price is calculated by evaluating the expectation value $E[\mathcal{P}_*]$.

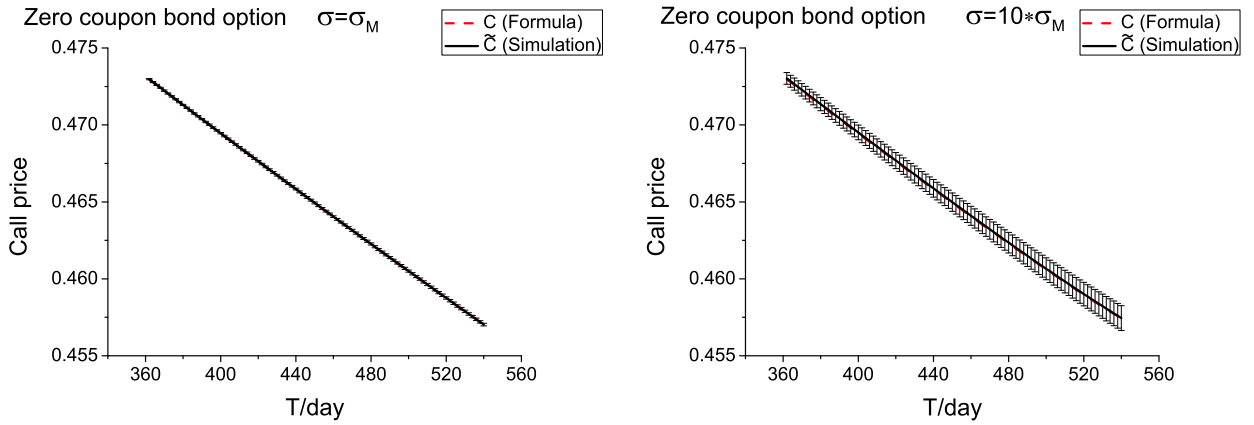

Figure 3.5: Zero coupon bond option with t_*=180 days and strike price=0.5: comparison between simulation and formula. The error bars are Monte Carlo errors of the simulation. (a) $\sigma = \sigma_M$. (b) $\sigma = 10\sigma_M$.

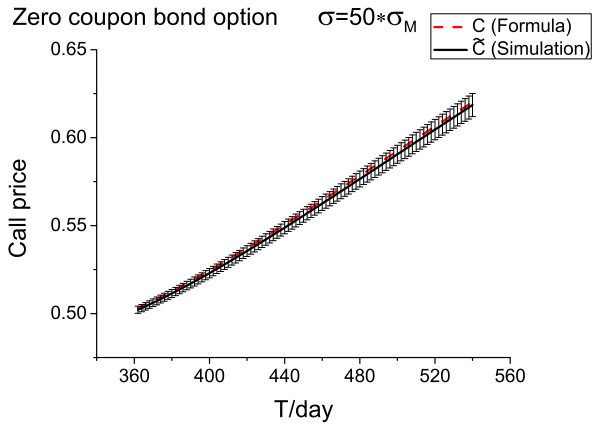

Figure 3.6: Zero coupon bond option with $\sigma = 50\sigma_M$, t_*=180 days and strike price=0.5: comparison between simulation and formula. The error bars are Monte Carlo errors of the simulation.

Figure 3.5(a), 3.5(b) and 3.6 show the comparison between the call price calculated using the formula and Monte Carlo simulation. The error bar of the Monte Carlo simulation is plotted with $\tilde{C}$ in the graphs; the error of the Monte Carlo simulation is given by

$$\text{Monte Carlo error} = \frac{Var(\mathcal{P}_*)}{\sqrt{\mathcal{N}}}, \tag{3.40}$$

where $\mathcal{N}$ is the total number of configurations. $Var(\mathcal{P}_*)$ is the variance of the payoff function $\mathcal{P}_*$ given by

$$Var(\mathcal{P}_*) = \sqrt{E[{\mathcal{P}_*}^2] - E^2[\mathcal{P}_*]}. \tag{3.41}$$

As expected, the call option price of the exact formula is in the range of error bars of the Monte Carlo simulation. Even for the case of $\sigma = 50\sigma_M$, the results of the simulation are nearly same as the results from the formula. The results confirm the correctness of our simulation, and the simulation method can be used for pricing coupon bond European options and barrier options where a formula may be intractable.

§ 3.4 European coupon bond option

A coupon bond is a linear sum of many zero coupon bonds with different maturities. Suppose a coupon bond with a principal L is issued at time t_* and matures at future time T, with fixed dividends a_i being paid at different future times T_i. The value of the coupon bond is as follows

$$\sum_{i=1}^{N_c} a_i B(t_*, T_i) + LB(t_*, T_i) = \sum_{i=1}^{N_c} c_i B(t_*, T_i), \tag{3.42}$$

where $c_i = a_i$ $(i = 1, 2, ..., N_c - 1)$ and $c_{N_c} = a_{N_c} + L$.

The payoff function $\mathcal{P}_*$ for a coupon bond is

$$\mathcal{P}_* = \Big(\sum_{i=1}^{N_c} c_i B(t_*, T_i) - K \Big)_+. \tag{3.43}$$

The simulated price of the European coupon bond option is given by

$$\tilde{C}(t_0, t_*, , T_i, K, \epsilon) = B(t_0, t_*) \frac{1}{\mathcal{N}} \sum_{n=1}^{\mathcal{N}} \Big(\sum_{i=1}^{N_c} c_i B_n(t_*, T_i) - K \Big)_+. \tag{3.44}$$

The price of coupon bond European option is a nonlinear problem, and the exact formula for the option price cannot be obtained directly. The correlator G_{ij} is given by

$$G_{ij} = \int_{t_0}^{t_*} dt \int_{t_*}^{T_i} dx \sigma(t, x) \int_{t_*}^{T_j} dx' D(x, x'; t) \sigma(t, x'). \tag{3.45}$$

The approximate price of a coupon bond European option can be calculated by using a Feynman expansion when the correlator G_{ij} is a small parameter [5] and is divided into the following four parts

$$C(t_0, t_*, K) = P_1 + P_2 + P_3 + P_4 + O(\sigma^4), \tag{3.46}$$

where

$$\begin{aligned}
P_1 &= B(t_0, t_*)\sqrt{\frac{C_2}{2\pi}} I(X), \\
P_2 &= B(t_0, t_*)\sqrt{\frac{C_2}{2\pi}} \frac{C_3}{6C_2^{3/2}} X e^{-\frac{1}{2}X^2}, \\
P_3 &= B(t_0, t_*)\sqrt{\frac{C_2}{2\pi}} \frac{C_4}{24C_2^2} (X^2 - 1) e^{-\frac{1}{2}X^2}, \\
P_4 &= B(t_0, t_*)\sqrt{\frac{C_2}{2\pi}} \frac{C_3^2}{72C_2^3} (X^4 - 6X^2 + 3) e^{-\frac{1}{2}X^2}, \qquad (3.47) \\
X &= \frac{K - F}{\sqrt{C_2}} \qquad (3.48)
\end{aligned}$$

with

$$I(X) = \int_{-\infty}^{+\infty} dQ (Q - X)_+ e^{-\frac{1}{2}Q^2} = e^{-\frac{1}{2}X^2} - \sqrt{2\pi} X (1 - N(X)), \tag{3.49}$$

and $N(x)$ is a cumulative distribution function and F is given in Equation 3.36. The coefficients C_2, C_3 and C_4 are given by

$$C_2 = \sum_{ij=1}^{N} J_i J_j \Big[e^{G_{ij}} - 1 \Big], \tag{3.50}$$

$$C_3 = \sum_{ijk=1}^{N} J_i J_j J_k \Big[e^{G_{ij}+G_{jk}+G_{ki}} - e^{G_{ij}} - e^{G_{jk}} - e^{G_{ki}} + 2 \Big], \tag{3.51}$$

$$\begin{aligned}
C_4 = \sum_{ijkl=1}^{N} J_i J_j J_k J_l \Big[& e^{G_{ij}+G_{ik}+G_{il}+G_{jk}+G_{jl}+G_{kl}} - e^{G_{ij}+G_{jk}+G_{ki}} - e^{G_{ij}+G_{jl}+G_{li}} \\
- & e^{G_{ik}+G_{kl}+G_{li}} - e^{G_{jk}+G_{kl}+G_{lj}} - e^{G_{ij}+G_{kl}} - e^{G_{jk}+G_{il}} - e^{G_{ik}+G_{jl}} \\
+ & 2(e^{G_{ij}} + e^{G_{ik}} + e^{G_{il}} + e^{G_{jk}} + e^{G_{jl}} + e^{G_{kl}}) - 6 \Big]. \qquad (3.52)
\end{aligned}$$

Consider a coupon bond that is issued at time $t_* = 180$ days and pays fixed dividends at

two different times T_i, $i = 1, 2$. In this simulation, $T_1 = 270 + 2i_T$ and $T_2 = 360 + 2i_T$ are assumed as functions of i_T with $0 \leq i_T < 90$. For convenience, the condition of the simulation of the coupon bond European option is restated in Table 3.3. The sum of forward prices of the coupon bond $J = \sum_{i=1}^{2} F_i$ is shown in Figure 3.7.

Table 3.3: The parameters used in the simulation of the coupon bond option.

ϵ	t_*	T_1	T_2	Strike price	Number of configurations
1 day	180 days	270 to 448 days	360 to 538 days	K=0.5	$\mathcal{N} = 10^5$

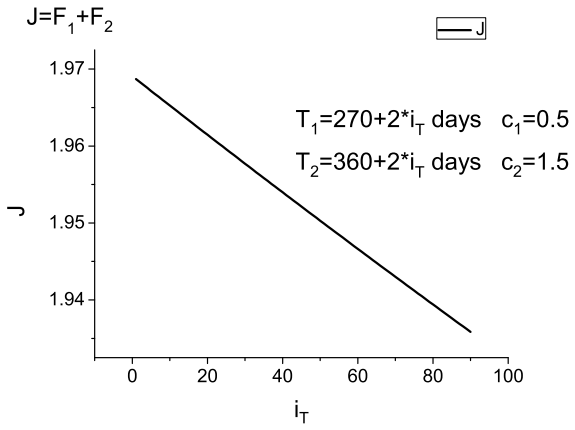

Figure 3.7: The sum of forward prices of the coupon bond $J = \sum_{i=1}^{2} F_i$.

In this simulation, the number of coupon bonds is $N_c = 2$, so the coupon bond has four correlator terms: G_{11}, G_{12}, G_{21} and G_{22}. We choose G_{22} as the axis because the value of G_{22} is the largest. The option price is plotted for different coupon bond maturity times T_i. The value of G_{22} is also given in the graphs because G_{ij} is a function of T_i. As shown in Figure 3.8(a) and 3.8(b), the coupon bond European option prices using the simulation and the Feynman expansion are in the range of error bars of the Monte Carlo simulation when $\sigma = \sigma_M$ and $\sigma = 10\sigma_M$, thus confirming the correctness of the simulation and the validity of the Feynman expansion for small volatility. However, the Feynman expansion is not expected to give the correct approximate price when σ is large. As shown in Figure 3.9(a) , the approximate price of the coupon bond European option even becomes negative when $\sigma = 50\sigma_M$. In contrast, as in Figure 3.9(b), the coupon bond European option price of the simulation works perfectly. The results of the approximate price differ from the results of

the simulation, and this inconsistency can be attributed to the large value of the volatility. As shown in Equation 3.45, the value of the correlator G_{ij} is a function of the volatility and large value of the volatility results in a lack of convergence of the Feynman expansion. These results show that the range of validity of the approximate price needs to be identified.

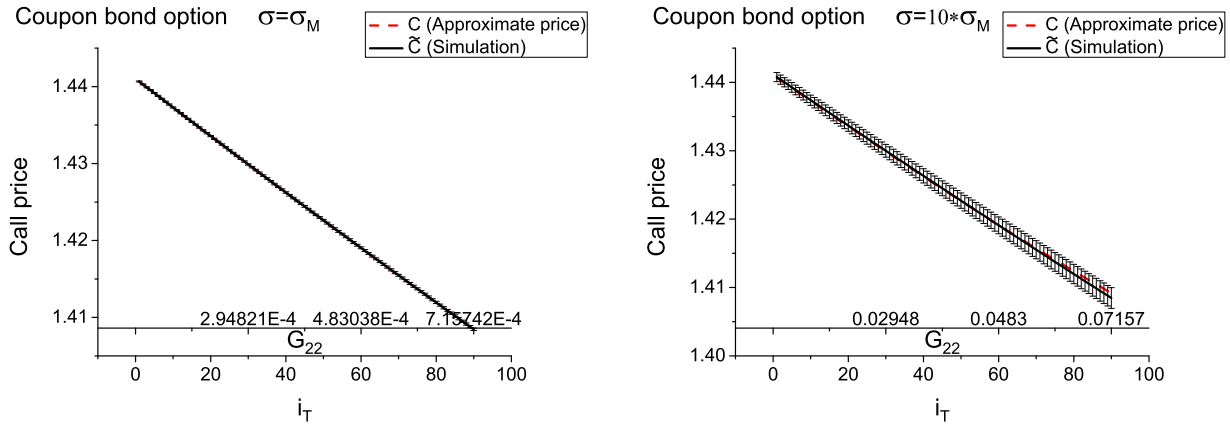

Figure 3.8: Coupon bond European option with number of bonds $N_c = 2$, t_*=180 days and strike price=0.5: comparison between simulation and approximate price. Different future times T_i are $T_1 = 270 + 2i_T$ and $T_2 = 360 + 2i_T$ days with $c_1 = 0.5$ and $c_2 = 1.5$. The error bars are Monte Carlo errors of the simulation. (a) $\sigma = \sigma_M$. (b) $\sigma = 10\sigma_M$.

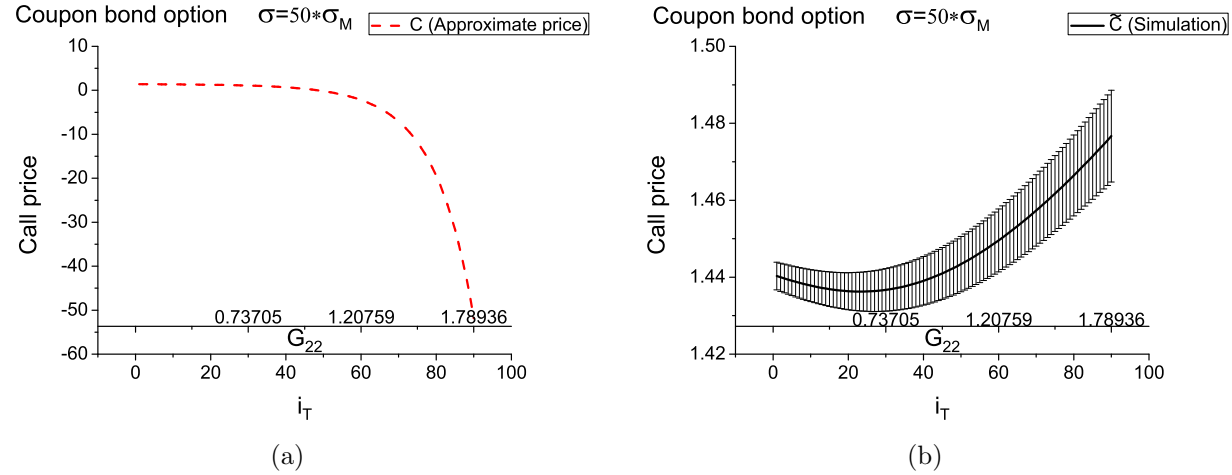

Figure 3.9: Coupon bond European option with number of bonds $N_c = 2$, $\sigma = 50\sigma_M$, t_*=180 days and strike price=0.5. Different future times T_i are $T_1 = 270 + 2i_T$ and $T_2 = 360 + 2i_T$ days with $c_1 = 0.5$ and $c_2 = 1.5$. (a) Results of approximate price. (b) Results of simulation. The error bars are Monte Carlo errors of the simulation.

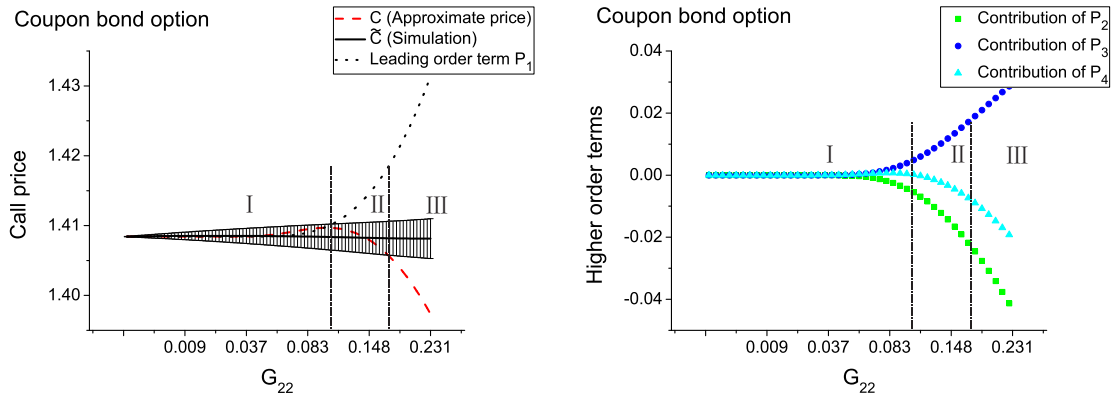

Figure 3.10: Coupon bond European option (number of bonds $N_c = 2$, t_*=180 days and strike price=0.5). Different future times T_1 and T_2 are fixed at 448 and 538 days with $c_1 = 0.5$ and $c_2 = 1.5$. Results of simulation are compared with approximate price when G_{22} is from 0 to 0.2 (the volatility σ is changed from 0 to 1.2 to vary value of G_{22}). (a) The plot of results of simulation, approximate price and leading order term P_1. The error bars are Monte Carlo errors of the simulation. (b) The plot of high order terms P_2, P_3 and P_4.

As shown in Equation 3.46 and 3.47, P_1 is the leading order term, while P_2, P_3 and P_4 are high order terms. From Figure 3.10(a), we see that the leading order term gives a very accurate approximate price in region I, where the correlator value is smaller than 0.11. In region II, where the correlator is from 0.11 to nearly 0.17, the value of the leading order term P_1 increases quickly, but other terms (P_2, P_3 and P_4) rebalance the total value and the approximate price is still in the range of the Monte Carlo error of the simulation (shown in Figure 3.10(b)). In region III, the two higher order terms P_2 and P_4 tend to decrease quickly. The approximate price decreases as the value of the correlator G_{22} further increases, and fails to give the correct results. The results show that Feynman expansion is valid when the value of correlator is smaller than 0.17. From Equation 3.45, we see that the value of the correlator G_{ij} may become extremely large when σ or $T - t_*$ or $t_* - t_0$ is large. From Figure 3.10(a), it can be deduced that the simulation method does not have this limitation and it can be applied in such extreme cases. In the simulation, the stiff propagator without normalization is used. If the market propagator and market volatility are used, the future time T can be up to nearly 10 years when $t_* = 0.5$ years. This means that the Feynman expansion can work for the case of T is smaller than 10 years. Coupon bonds of duration longer than 10 years are widely traded and hence the price of these bonds can only be obtained numerically.

§ 3.5 Barrier option

A double barrier option has the same payoff function $\mathcal{P}_*$ as a European option except that the barrier option will be knocked out when the underlying price exceeds a given maximum value U or falls below a minimum value L. In this section, the price of the out of the money option is analyzed because the price is then large and shows all the relevant features. The case of the at the money zero coupon bond barrier option is also discussed in Section § 3.9. The payoff function of the at the money call option is shown in Figure 3.11(a), and the payoff function of the out of the money call option is shown in Figure 3.11(b).

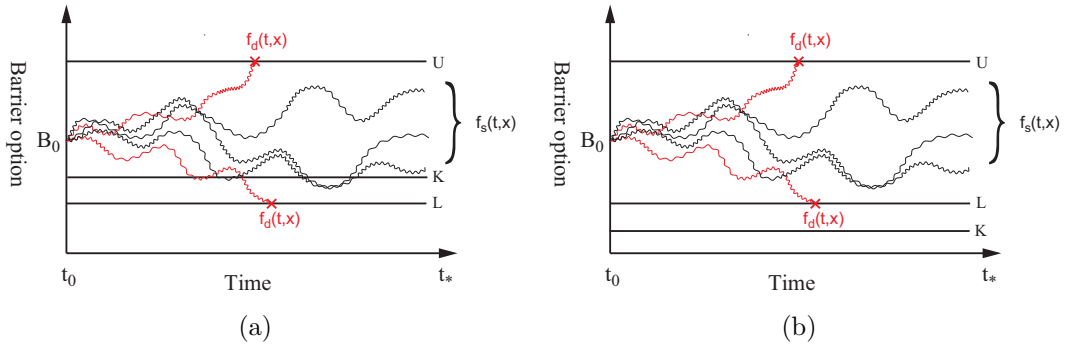

Figure 3.11: The payoff function for a double barrier option, with maturity time t_* and strike price K. The initial bond price B_0 is within the barrier. (a) At the money call option. (b) Out of the money call option.

The price of the barrier option obtained using Monte Carlo simulation,denoted by $\tilde{C}_B(t_0, t_*, T, K, \epsilon)$, is given by, for total number $\mathcal{N}$ configurations

$$\tilde{C}_B(t_0, t_*, T, K, \epsilon) \quad = \quad B(t_0, t_*)\frac{1}{\mathcal{N}}\sum_{s=1}^{\mathcal{N}_s}\Big(B_s(t_*, T) - K\Big)_+, \tag{3.53}$$

where $\mathcal{N}_s$ is the number of successful configurations, namely the configurations that survive until the time t_*. As shown in Figure 3.11(a), $f_s(t, x)$ refers to the configurations that survive at time t_*, while $f_d(t, x)$ refers to the configurations which are terminated in the updating process. $B_s(t_*, T)$ in Equation 3.53 is the bond price calculated using the configurations $f_s(t, x)$, and is given by

$$B_s(t_*, T) \quad = \quad \exp\{-\int_{t_*}^{T} dx f_s(t_*, x)\}. \tag{3.54}$$

The price of the barrier option decreases when the number of successful configurations $\mathcal{N}_s$ decreases. The approximate expansion in Equation 3.53 becomes exact for $\epsilon \to 0$ and $\mathcal{N} \to \infty$.

§ 3.6 Zero coupon bond barrier option: up barrier

The zero coupon bond barrier option price is given by Gaussian quantum field theory and the price can be calculated exactly. The payoff function for the zero coupon bond barrier option is given by

$$\mathcal{P}_* = (e^{-g} - K)_+, \tag{3.55}$$

where

$$g = \int_{t_*}^{T} dx f(t_*, x), \qquad e^{-g} \in [e^{-b}, e^{-a}] \Rightarrow g \in [a, b]. \tag{3.56}$$

As shown in Equation 3.56, the down barrier is $L = e^{-b}$ and the up barrier is $U = e^{-a}$. The exact price of the zero coupon barrier option is given by [27]

$$C_B(t_0, t_*, K) = B(t_0, t_*) e^{-\beta^2/2G} \int_a^b dg e^{(\beta/G)(g-f)} \times \mathcal{Q}[g, f; G; a, b] \mathcal{P}_*(g), \tag{3.57}$$

where $\beta = \frac{1}{2}G$ and $f = \int_{t_*}^{T} dx f(t_0, x)$; the barrier function is given by:

$$\begin{aligned} \mathcal{Q}[g, f; G; a, b] = \quad & \frac{1}{\sqrt{2\pi G}} \sum_{n=-\infty}^{+\infty} \Big\{ \exp(-\frac{1}{2G}[f - g - 2(b-a)n]^2) \\ & - \exp(-\frac{1}{2G}[f + g - 2a - 2(b-a)n]^2) \Big\}. \end{aligned} \tag{3.58}$$

The integration in Equation 3.57 can be calculated directly by using the cumulative normal distribution function. As shown in Equation 3.58, the barrier function has a summation from minus infinity to infinity. To simplify the integration, the case of single up barrier is discussed first in this section.

When the zero coupon bond only has a single up barrier, $b \to +\infty$, and only the $n = 0$ term of the barrier function survives. The barrier function reduces to

$$\mathcal{Q}[g, f; G; a, b] = \frac{1}{\sqrt{2\pi G}} \Big[\exp\big(-\frac{1}{2G}[f - g]^2\big) - \exp\big(-\frac{1}{2G}[f + g - 2a]^2\big) \Big]. \tag{3.59}$$

The integration with the up barrier is given by

$$\int_a^{+\infty} \frac{1}{\sqrt{2\pi G}} e^{\frac{\beta}{G}(g-f)} \Big(e^{-\frac{1}{2G}(f-g)^2} - e^{-\frac{1}{2G}(f+g-2a)^2} \Big) \Big(e^{-g} - K \Big)_+ dg, \tag{3.60}$$

and can be done analytically. The single barrier option price is given as follows

$$C_B(t_0, t_*, K) \;=\; B(t_0, t_*) e^{-\beta^2/2G} (u_1 + u_2 + u_3 + u_4), \tag{3.61}$$

where

$$\begin{aligned}
u_1 &= e^{\frac{1}{2G}(f+\beta-G)^2} e^{-\frac{\beta f}{G} - \frac{f^2}{2G}} \Big\{ N\big(\frac{-\ln K - f - \beta + G}{\sqrt{G}} \big) - N\big(\frac{a - f - \beta + G}{\sqrt{G}} \big) \Big\}, \\
u_2 &= -K e^{\frac{\beta^2}{2G}} \Big\{ N\big(\frac{-\ln K - f - \beta}{\sqrt{G}} \big) - N\big(\frac{a - f - \beta}{\sqrt{G}} \big) \Big\}, \\
u_3 &= -e^{-\frac{1}{2G}\left(-2(fG - 2f\beta - 2aG + 2a\beta) - (G-\beta)^2\right)} \Big\{ N\big(\frac{-\ln K + f - 2a - \beta + G}{\sqrt{G}} \big) - N\big(\frac{f - a - \beta + G}{\sqrt{G}} \big) \Big\}, \\
u_4 &= K e^{-\frac{1}{2G}\left(4\beta f - 4a\beta - \beta^2\right)} \Big\{ N\big(\frac{-\ln K + f - \beta - 2a}{\sqrt{G}} \big) - N\big(\frac{f - \beta - a}{\sqrt{G}} \big) \Big\}.
\end{aligned} \tag{3.62}$$

The payoff function for the function of the zero coupon bond barrier option is the same as for the case of the zero coupon bond option, the only difference being that the zero coupon bond barrier has a constraint on allowed configurations for $f(t, x)$. The up barrier conditions for the simulations for different values of σ are shown in Table 3.4.

Table 3.4: The barrier condition used in the simulation of zero coupon bond single up barrier option.

Simulation	$\sigma = \sigma_M$	$\sigma = 10\sigma_M$	$\sigma = 50\sigma_M$
Up barrier	$U = e^{0.0} = 1$	$U = e^{0.1} = 1.105$	$U = e^{0.8} = 2.226$

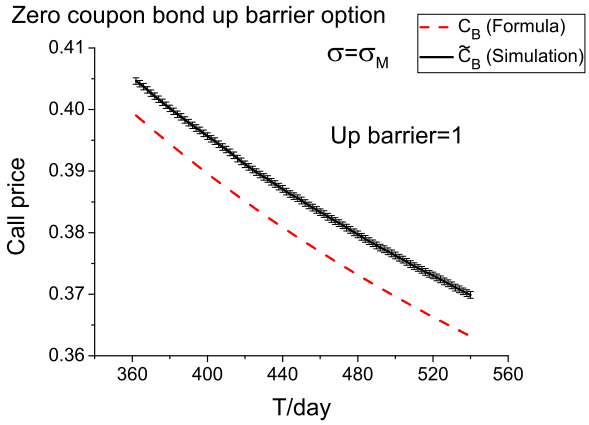

Figure 3.12: Zero coupon bond single up barrier option with $\sigma = \sigma_M$, t_*=180 days and strike price=0.5: comparison between simulation and formula. The error bars are Monte Carlo errors of the simulation.

Figure 3.12 shows the results from the simulation and formula; the option price of the simulation does not agree with the results from the formula. The results of the simulation have a small shift compared to the exact price. We found that this small shift is due to the error from the barrier and can be minimized by using a scaling function. To verify the need for a scaling function, a simulation with the step size of 0.5 day was tested. As shown in Figure 3.13, the call price is closer to the exact price of the formula when the step size is reduced to 0.5 day. If the step size is infinitesimal, the results of the simulation should be equal to the exact result. However, the step size cannot be chosen to be very small since the updating then needs an extremely large matrix of the stiff propagator and generating a large matrix for the quantum field $A(t, x)$ needs a long computing time. Instead, we construct a scaling function to compensate for the error of the barrier option due to the finite time step.

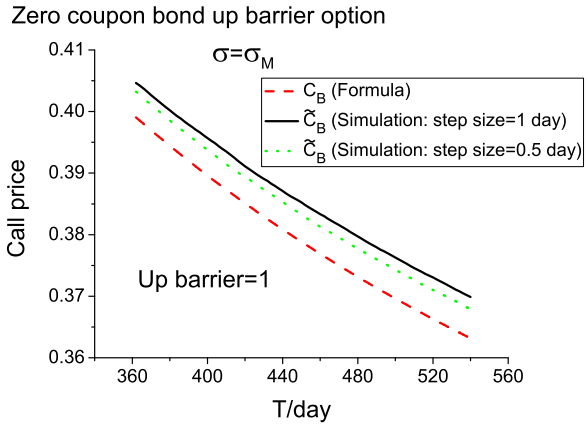

Figure 3.13: The step size of the simulation was reduced to 0.5 day, and the price calculated from the simulation is much closer to the exact price calculated from the formula ($\sigma = \sigma_M$, t_*=180 days and strike price=0.5).

§ 3.7 Scaling function

Figure 3.14 shows the reason for the error in the simulation of barrier options. The updating process starts from t_0 and stops at t_*, and any bond price exceeding the barrier will be eliminated. Consider one process of updating of the bond price from time t to the next instant point at time $t+1$, with the prices at times t and $t+1$ both below U (up barrier). Suppose the bond price near the barrier during the period of t to $t+1$ follows trajectory A. If the updating step is taken to be smaller (e.g. half of 1 day), the bond price could have followed the trajectory B and this would lead to a rejection of the previously accepted outcome at time $t+1$. This means that, due to the finite time step ϵ, the simulation of the barrier option has accounted for more configurations of the updating, thus leading to a larger value of the barrier option price. As shown in Figure 3.12, the curve of the simulated call price is higher than the curve of the exact formula, which matches our explanation because the call option price will increase if more rejected configurations are accounted for. Consistently with our explanation, shown in Figure 3.13, the error decreases when the step size is smaller.

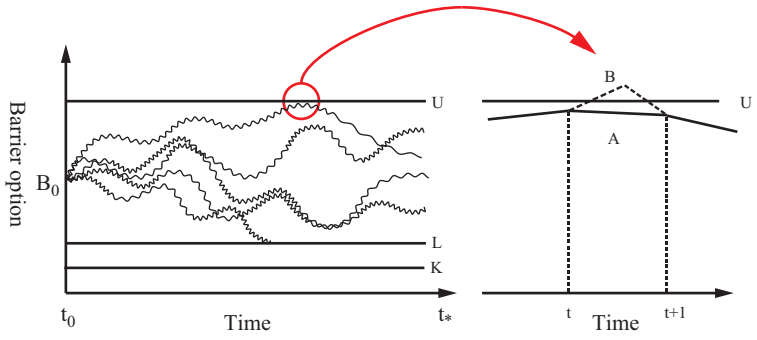

Figure 3.14: The payoff function for a double barrier option (out of money), with strike price K and maturity time t_*. The trajectories A and B are shown for different time step sizes.

The error due to the barrier is a function of the time step size ϵ of the updating, the volatility σ and the maturity time T. A scaling function is used to rescale the simulation results. The error due to the barrier is extracted from the results by using

$$\triangle s_R \quad = \quad \frac{\text{simulation} - \text{formula}}{\text{formula}}. \tag{3.63}$$

The number of total configurations is $\mathcal{N}$ and the number of successful configurations is $\mathcal{N}_s$. The number of default configurations (the configurations that are knocked out during the updating process) is $\mathcal{N}_d = \mathcal{N} - \mathcal{N}_s$. The error $\triangle s_R$ near the up barrier is related to the number of default configurations of the bond price.To simplify the calculation, $\triangle s_R$ is assumed to be proportional to $\mathcal{N}_d$. The real barrier error extracted from the simulation results will be given by

$$\triangle s_R \quad = \quad \triangle s_U \times \frac{\mathcal{N}_d}{\mathcal{N}} = \triangle s_U \times \frac{\mathcal{N} - \mathcal{N}_s}{\mathcal{N}}. \tag{3.64}$$

The simulation results for the zero coupon bond barrier option were compared against the exact formula for the zero coupon bond barrier option in order to fit the parameters of the scaling function. The volatility σ is a curve in time (as shown in Figure 3.3). For simplicity, the mean of the volatility $\bar{\sigma}$ is used as the parameter of the scaling function. After calibration, the error $\triangle s_U$ for the up barrier is fitted and is given by

$$\triangle s_U(T, \bar{\sigma}, \epsilon) \quad = \quad 0.85(\bar{\sigma} + 1)T^{\bar{\sigma}^{0.2}}\epsilon^{0.5}. \tag{3.65}$$

The scaling function for the up barrier is given by

$$\mathcal{S}_U = \frac{1}{1+\triangle s_R} = \frac{1}{1+\frac{\mathcal{N}-\mathcal{N}_s}{\mathcal{N}}\triangle s_U}, \tag{3.66}$$

and the corrected call option price, after using the scaling function, is

$$\tilde{C}_B^I(t_0, t_*, T, K, \epsilon) = \mathcal{S}_U \times \tilde{C}_B(t_0, t_*, T, K, \epsilon). \tag{3.67}$$

After using the scaling function, the results for the zero coupon bond single up barrier option for different magnitudes of σ_M are as shown in Figure 3.15(a), 3.15(b) and 3.16, respectively. The results show that the option price of the simulation is nearly the same as the price from the formula obtained by using the scaling function. The scaling function fits the error quite well for the case of single up barrier.

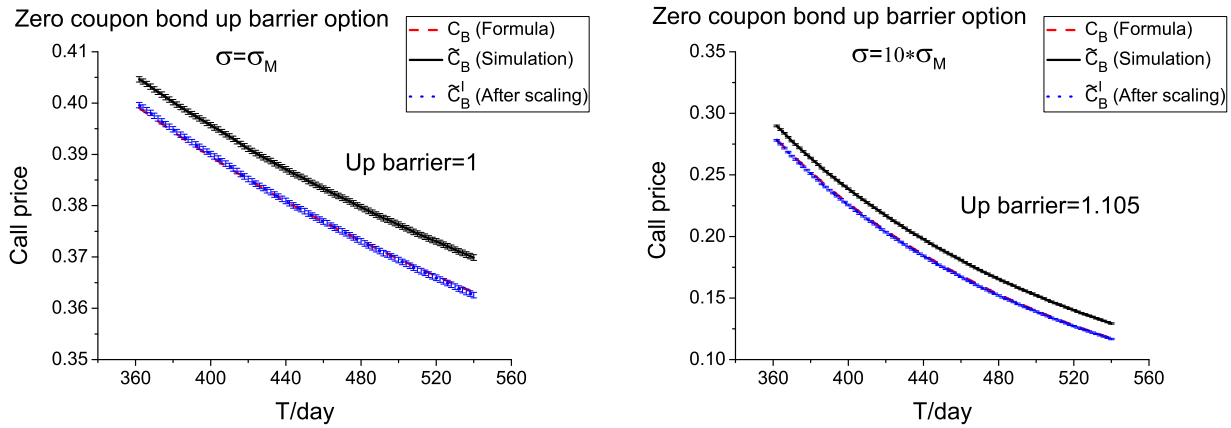

(a) (b)

Figure 3.15: Zero coupon bond single up barrier option with t_*=180 days and strike price=0.5: comparison between simulation and formula, with and without scaling. The error bars are Monte Carlo errors of the simulation. After scaling means that the results of simulation are rescaled using the scaling function. (a) $\sigma = \sigma_M$. (b) $\sigma = 10\sigma_M$.

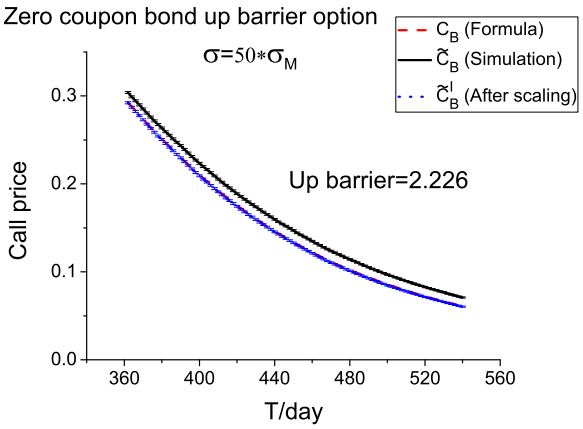

Figure 3.16: Zero coupon bond single up barrier option with $\sigma = 50\sigma_M$, t_*=180 days and strike price=0.5: comparison between simulation and formula, with and without scaling. The error bars are Monte Carlo errors of the simulation.

As given in Equation 3.2, the evolution equation has the drift term $\alpha(t,x)$ which is always positive. The probability of increasing the values of the forward interest rates $f(t,x)$ is larger than the probability of decreasing $f(t,x)$, thus leading to different error mechanism for the up and down barriers. The scaling functions for the up barrier and the down barrier are different because of the positive drift term, and a different scaling function needs to be calibrated for the down barrier.

Following the procedure of the calibration as before, the error $\triangle s_L$ for the down barrier is the following

$$\triangle s_L(T,\bar{\sigma},\epsilon) \quad = \quad (0.03\bar{\sigma}^2 - 0.1\bar{\sigma} + 0.095)T^{\bar{\sigma}^{0.2}}\epsilon^{0.5}. \tag{3.68}$$

The scaling function for the down barrier is given by

$$\mathcal{S}_L \quad = \quad \frac{1}{1+\triangle s_R} = \frac{1}{1+\frac{\mathcal{N}-\mathcal{N}_s}{\mathcal{N}}\triangle s_L}. \tag{3.69}$$

The error of the double barrier is the combination of the errors for the up barrier $\triangle s_U$ and the down barrier $\triangle s_L$. Suppose the numbers of default configurations from the up barrier and down barrier are $\mathcal{N}_U$ and $\mathcal{N}_L$ respectively, and the number of successful configurations is $\mathcal{N}_s$. The scaling function of the double barrier is given by

$$\mathcal{S}_D \quad = \quad \frac{1}{1+\frac{\mathcal{N}-\mathcal{N}_U}{\mathcal{N}_s}\frac{\mathcal{N}_U}{\mathcal{N}}\triangle s_U + \frac{\mathcal{N}-\mathcal{N}_L}{\mathcal{N}_s}\frac{\mathcal{N}_L}{\mathcal{N}}\triangle s_L}. \tag{3.70}$$

The performances of the scaling function for the zero coupon bond single down barrier option and the zero coupon bond double barrier option are discussed in Sections § 3.8 and § 3.9, respectively.

To understand the structure of $\triangle s_U$ and $\triangle s_L$, the graphs of $\triangle s_U$ and $\triangle s_L$ as a function of $\bar{\sigma}$ and ϵ are plotted and shown in Figure 3.17(a) and 3.17(b).

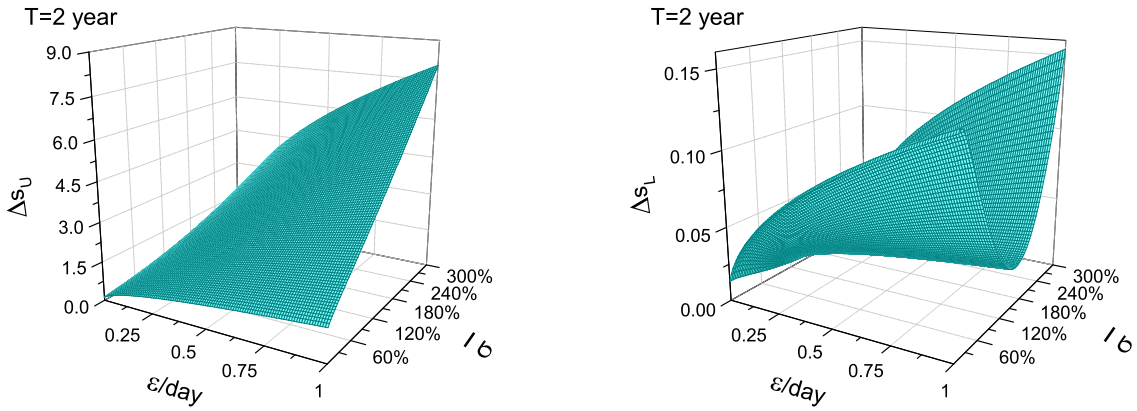

(a) (b)

Figure 3.17: The error of single barrier as a function of $\bar{\sigma}$ and ϵ, and T is fixed at 2 years. (a) $\triangle s_U$ for up barrier. (b) $\triangle s_L$ for down barrier.

§ 3.8 Zero coupon bond barrier option: down barrier

The barrier function for the single down barrier call option is given by $a \to -\infty$ and yields

$$\mathcal{Q}[g, f; G; a, b] = \frac{1}{\sqrt{2\pi G}}\Big[\exp\big(-\frac{1}{2G}[f-g]^2\big) - \exp\big(-\frac{1}{2G}[f+g-2b]^2\big)\Big]. \quad (3.71)$$

The integration for the single down barrier is given by

$$\int_{-\infty}^{b} \frac{1}{\sqrt{2\pi G}} e^{\frac{\beta}{G}(g-f)}\Big(e^{-\frac{1}{2G}(f-g)^2} - e^{-\frac{1}{2G}(f+g-2b)^2}\Big)\Big(e^{-g} - K\Big)_+ dg. \quad (3.72)$$

The exact price of the call option can be obtained by setting $a \to -\infty$, $n = 0$ in terms z_1 and z_2, and $n = 1$ in terms z_3 and z_4 in Equation 3.75.

The parameters of the down barrier simulation for different values of σ are shown in Table 3.5.

Table 3.5: The barrier condition used in the simulation of the zero coupon bond single down barrier option.

Simulation	$\sigma = \sigma_M$	$\sigma = 10\sigma_M$	$\sigma = 50\sigma_M$
Down barrier	$L = e^{-0.05} = 0.951$	$L = e^{-0.3} = 0.741$	$L = e^{-0.4} = 0.670$

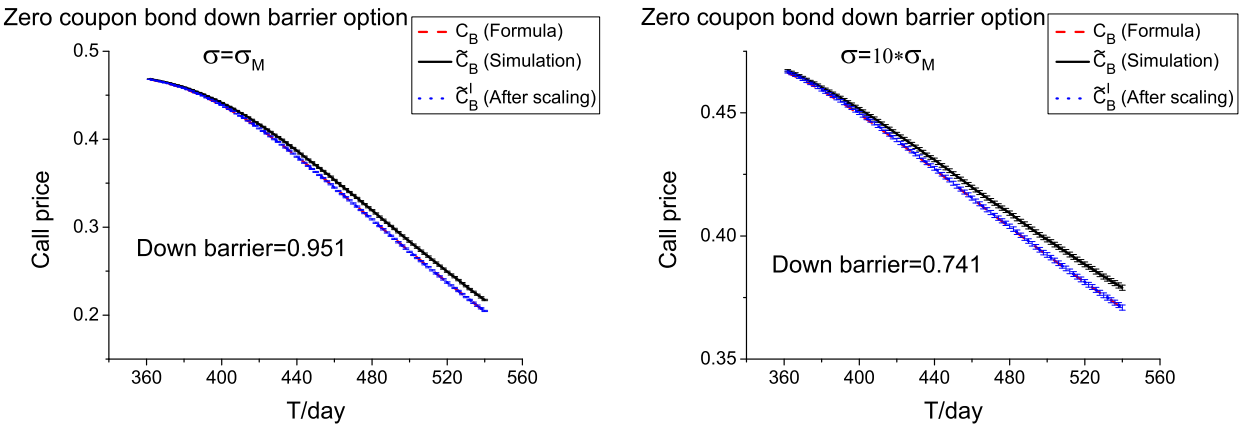

(a) (b)

Figure 3.18: Zero coupon bond single down barrier option with t_*=180 days and strike price=0.5: comparison between simulation and formula, with and without scaling. The error bars are Monte Carlo errors of the simulation. (a) $\sigma = \sigma_M$. (b) $\sigma = 10\sigma_M$.

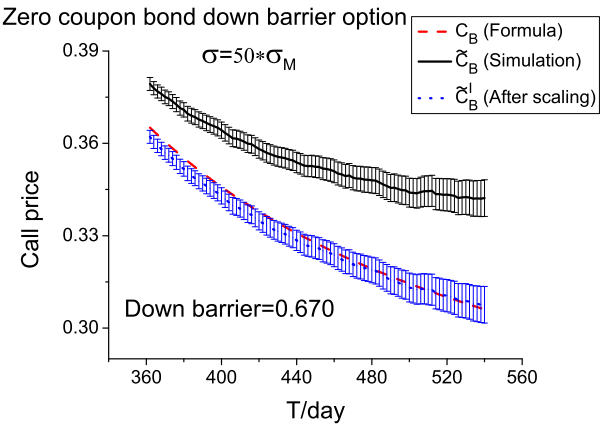

Figure 3.19: Zero coupon bond single down barrier option with $\sigma = 50\sigma_M$, t_*=180 days and strike price=0.5: comparison between simulation and formula, with and without scaling. The error bars are Monte Carlo errors of the simulation.

Figures 3.18(a), 3.18(b) and 3.19 shows the exact option price calculated and the results from the simulation with and without using the scaling function. It can be seen that the scaling function for a single down barrier works quite well for different magnitudes of σ_M.

§ 3.9 Zero coupon bond barrier option: double barrier

The exact results for the zero coupon bond double barrier option are similar to those for the single barrier, except that the double barrier case is more complicated.

The integration with double barrier is given by

$$\int_a^b dg e^{(\beta/G)(g-f)} \times \mathcal{Q}[g,f;G;a,b]\mathcal{P}_*(g), \tag{3.73}$$

where the barrier function $\mathcal{Q}[g,f;G;a,b]$ is given in Equation 3.58. This integration can also be done analytically, and the price of the double barrier call option is given by

$$C_B(t_0,t_*,K) \quad = \quad B(t_0,t_*)e^{-\beta^2/2G}(z_1+z_2+z_3+z_4), \tag{3.74}$$

where

$$\begin{aligned}
z_1 = & \sum_{n=-\infty}^{+\infty} e^{-\frac{1}{2G}\left(2(2(b-a)n-f)(\beta-G)-(\beta-G)^2+2\beta f\right)}\Big\{N\Big(\frac{\xi+2(b-a)n-f-\beta+G}{\sqrt{G}}\Big), \\
& -N\Big(\frac{a+2(b-a)n-f-\beta+G}{\sqrt{G}}\Big)\Big\} \\
z_2 = & -\sum_{n=-\infty}^{+\infty} Ke^{-\frac{1}{2G}\left(4\beta(b-a)n-\beta^2\right)}\Big\{N\Big(\frac{\xi+2(b-a)n-f-\beta}{\sqrt{G}}\Big)-N\Big(\frac{a+2(b-a)n-f-\beta}{\sqrt{G}}\Big)\Big\}, \\
z_3 = & -\sum_{n=-\infty}^{+\infty} e^{-\frac{1}{2G}\left(-2(G-\beta)(f-2a-2(b-a)n)-(G-\beta)^2+2\beta f\right)}\Big\{N\Big(\frac{\xi+f-2a-2(b-a)n-\beta+G}{\sqrt{G}}\Big) \\
& -N\Big(\frac{f-a-2(b-a)n-\beta+G}{\sqrt{G}}\Big)\Big\}, \\
z_4 = & \sum_{n=-\infty}^{+\infty} Ke^{-\frac{1}{2G}\left(4\beta(f-a-(b-a)n)-\beta^2\right)}\Big\{N\Big(\frac{\xi+f-2a-2(b-a)n-\beta}{\sqrt{G}}\Big) \\
& -N\Big(\frac{f-a-2(b-a)n-\beta}{\sqrt{G}}\Big)\Big\},
\end{aligned} \tag{3.75}$$

and $\xi = \max(b, -\ln K)$.

The parameters for the double barrier simulation for different σ are shown in Table 3.6.

Table 3.6: The barrier condition used in the simulation of the zero coupon bond double barrier option.

Simulation	$\sigma = \sigma_M$	$\sigma = 10\sigma_M$	$\sigma = 50\sigma_M$
Up barrier	$U = e^{0.0} = 1$	$U = e^{0.1} = 1.105$	$U = e^{0.8} = 2.226$
Down barrier	$L = e^{-0.05} = 0.951$	$L = e^{-0.3} = 0.741$	$L = e^{-0.4} = 0.670$

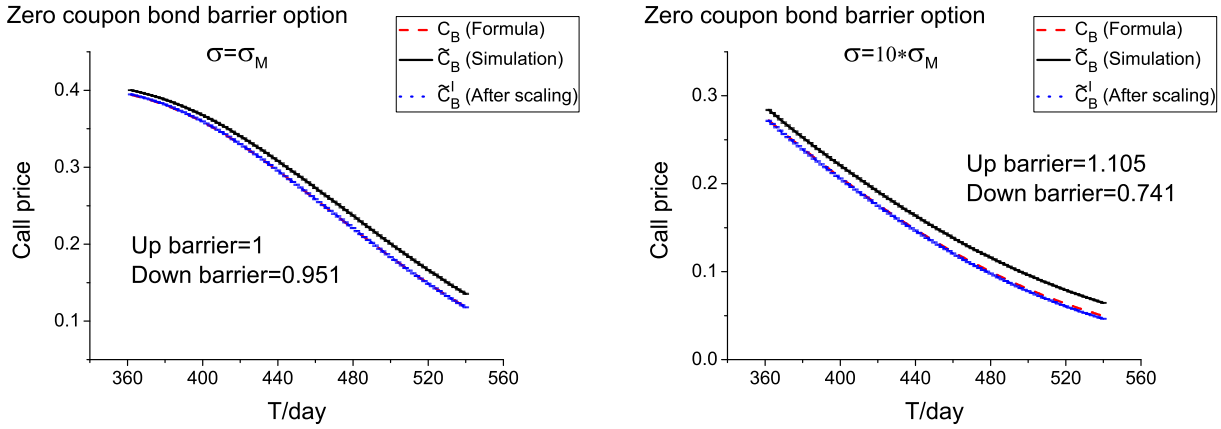

(a) (b)

Figure 3.20: Zero coupon bond double barrier option with t_*=180 days and strike price=0.5: comparison between simulation and formula, with and without scaling. The error bars are Monte Carlo errors of the simulation. (a) $\sigma = \sigma_M$. (b) $\sigma = 10\sigma_M$.

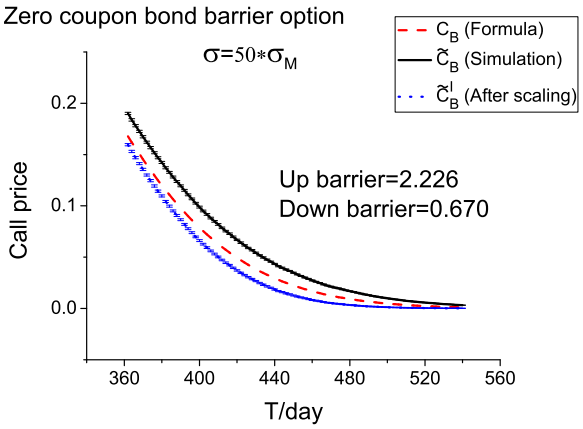

Figure 3.21: Zero coupon bond double barrier option with $\sigma = 50\sigma_M$, t_*=180 days and strike price=0.5: comparison between simulation and formula, with and without scaling. The error bars are Monte Carlo errors of the simulation.

Figures 3.20(a), 3.20(b) and 3.21 show the results from the formula and simulation with and without using the scaling function. It is clear that the scaling function works well for the cases of $\sigma = \sigma_M$ and $\sigma = 10\sigma_M$, but not when $\sigma = 50\sigma_M$. This is because the value of the drift term is quite large and the nonlinear error of the barrier is quite difficult to fit when $\sigma = 50\sigma_M$. For the case of $\sigma = 50\sigma_M$ for a single up barrier, the scaling function works well, and because the ratio of successful configurations to total configurations $\mathcal{N}_s/\mathcal{N}$ is quite high, the error is easy to fit. Figure 3.21 shows that the call price decreases to zero when T increases; this is because the ratio of successful configurations to total configurations $\mathcal{N}_s/\mathcal{N}$ is quite low and the price decreases to nearly zero. When the ratio $\mathcal{N}_s/\mathcal{N}$ is low, the nonlinear error of the barrier is difficult to fit and the scaling function does not work very well. The scaling function given above is quite simple, and a more complicated scaling function needs to be calibrated when the ratio $\mathcal{N}_s/\mathcal{N}$ is very small.

§ 3.10 The stability and convergence of the simulation

A crucial problem in a big simulation is determining the number $\mathcal{N}$ of configurations required for a given accuracy. A low value of $\mathcal{N}$ may result in a large error, while a large value of $\mathcal{N}$ may be inefficient. Thus, how to find a reasonable value of $\mathcal{N}$ is the first question that needs to be considered in the simulation. The stability of the ratio $\mathcal{N}_s/\mathcal{N}$ is very important in simulating barrier options. The ratio of $\mathcal{N}_s/\mathcal{N}$ is plotted for different numbers $\mathcal{N}$ of configurations, as shown in Figure 3.22(a), 3.22(b) and 3.23, for the single up barrier option, single down barrier

option and double barrier option respectively. The ratio of the Monte Carlo error to the option price is also plotted in the graphs. It is seen that the ratio $\mathcal{N}_s/\mathcal{N}$ oscillates when the number of total configurations $\mathcal{N}$ is less than 10^4, and the ratio $\mathcal{N}_s/\mathcal{N}$ becomes stable when $\mathcal{N}$ is larger than 6×10^4. In our simulation, $\mathcal{N}$ is chosen to be 10^5 and this yields the requisite results, accurate enough for our simulation. The ratio of the Monte Carlo error to the option price is smaller than 0.8% when $\mathcal{N} = 10^5$, when the ratio of $\mathcal{N}_s/\mathcal{N}$ is equal to 16.25% (Figure 3.23). In Figure 3.22(a), 3.22(b) and 3.23, the case of $\sigma = 10\sigma_M$ is considered, and this value is large enough for most applications.

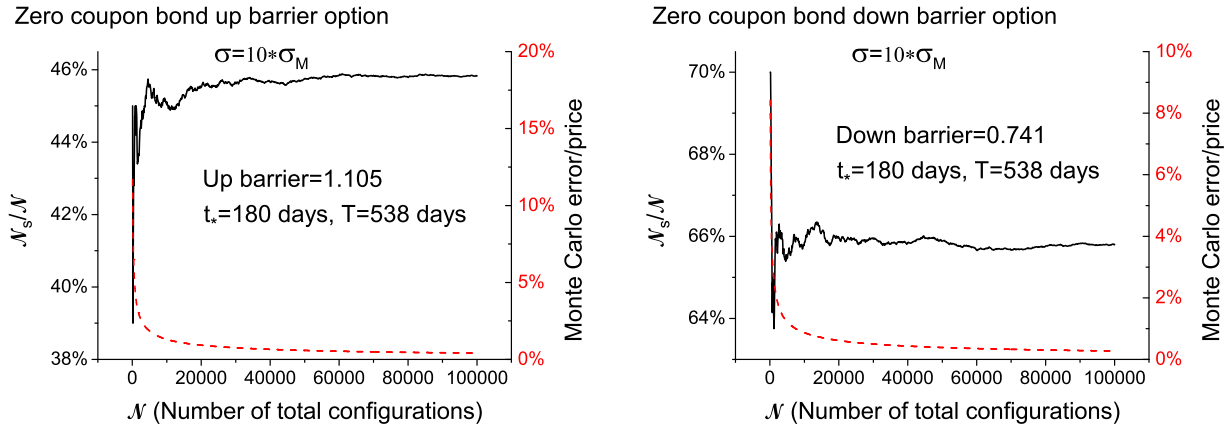

(a) (b)

Figure 3.22: Ratio $\mathcal{N}_s/\mathcal{N}$ is plotted for different values of $\mathcal{N}$ (solid line), and ratio of Monte Carlo error to option price is also plotted (dashed line) with $\sigma = 10\sigma_M$, t_*=180 days, T=538 days and strike price=0.5. (a) Zero coupon bond single down barrier option. (b) Zero coupon bond single down barrier option.

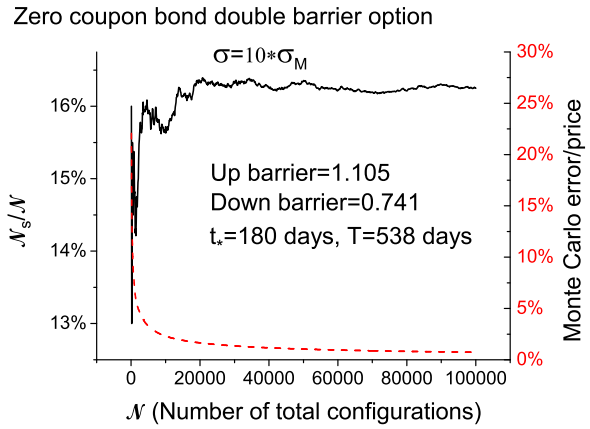

Figure 3.23: Zero coupon bond double barrier option: ratio $\mathcal{N}_s/\mathcal{N}$ is plotted for different values of $\mathcal{N}$ (solid line), and ratio of Monte Carlo error to option price is also plotted (dashed line) with $\sigma = 10\sigma_M$, t_*=180 days, T=538 days and strike price=0.5.

§ 3.11 Coupon bond barrier options

The price of the coupon bond barrier option cannot be obtained exactly because the payoff function with the barrier boundary condition is nonlinear. However, like for the case of the coupon bond option, the approximate price can be calculated when the value of the correlator G_{ij} is small. The technique of linearization of the barrier was used to obtain the approximate price in [27] and is based on the following derivation.

The barrier for the coupon bond is defined by

$$L \leq \sum_{I=1}^{N_c} c_I B(t_*, T_I) \leq U. \tag{3.76}$$

The coupon bond has the following expansion for $g_I = \int_{t_*}^{T_I} dx f(t_*, x)$ and $f_I = \int_{t_*}^{T_I} dx f(t_0, x)$

$$\begin{aligned} \sum_{I=1}^{N_c} c_I B(t_*, T_I) &= \sum_{I=1}^{N_c} c_I e^{-g_I} = \sum_{I=1}^{N_c} c_I e^{-f_I-\beta_I} e^{-(g_I-f_I-\beta_I)} \\ &\equiv \sum_{I=1}^{N_c} d_I e^{-(g_I-f_I-\beta_I)} \\ &\simeq \sum_{I=1}^{N_c} d_I(1+f_I+\beta_I) - \sum_{I=1}^{N_c} d_I g_I + O(\sigma^2), \end{aligned} \tag{3.77}$$

where $d_I \equiv c_I e^{-f_I - \beta_I}$ and $\beta_I = \frac{1}{2} G_{II}$. Note that from Equation 3.2 and 3.3 [27]

$$\begin{aligned} E[(g_I - f_I - \beta_I)^2] &= \int_{t_0}^{t_*} dt \int_{t_*}^{T_I} dx \sigma(t,x) \int_{t_*}^{T_I} dx' D(x,x';t)\sigma(t,x') \\ &= G_{II} \sim O(\sigma^2). \end{aligned} \tag{3.78}$$

Since the value of $(g_I - f_I - \beta_I)$ is of $O(\sigma)$ from Equation 3.78, the barrier can be linearized when σ is small.

The linearized barrier is given by

$$a \leq \sum_{I=1}^{N_c} g_I d_I \leq b, \tag{3.79}$$

where

$$a = \sum_{I=1}^{N_c} d_I (1 + f_I + \beta_I) - U, \tag{3.80}$$

$$b = \sum_{I=1}^{N_c} d_I (1 + f_I + \beta_I) - L. \tag{3.81}$$

The price of the coupon bond barrier option obtained using Monte Carlo simulation, denoted by $\tilde{C_B}(t_0, t_*, T_I, K, \epsilon)$, is given by

$$\tilde{C_B}(t_0, t_*, T_I, K, \epsilon) = B(t_0, t_*) \frac{1}{\mathcal{N}} \sum_{s=1}^{\mathcal{N}_s} \Big(\sum_{I=1}^{N_c} c_I B_s(t_*, T_I) - K \Big)_+, \tag{3.82}$$

where, as before, $\mathcal{N}_s$ refers to the number of successful configurations. The approximate price of the coupon bond barrier option is given by [27]

$$\frac{C_B(t_0, t_*, T, K)}{B(t_0, t_*)} = \frac{1}{\sqrt{2\pi}} C_0^B I(X) \sqrt{D_2 - D_1^2}, \tag{3.83}$$

where $D_1 = C_1/C_0$, $D_2 = C_2/C_0$ with

$$I(X) = \int_{-\infty}^{+\infty} dQ (Q - X)_+ e^{-\frac{1}{2}Q^2} = e^{-\frac{1}{2}X^2} - \sqrt{2\pi} X (1 - N(X)), \tag{3.84}$$

and

$$C_0 = C_0^B, \tag{3.85}$$

$$C_1 = \sum_{I=1}^{N_c} J_I (C_I^B - C_0^B), \tag{3.86}$$

$$C_2 = \sum_{I,K=1}^{N_c} J_I J_K (C_{IK}^B - C_I - C_K + C_0). \tag{3.87}$$

For G_{IJ} defined by Equation 3.45, the coefficients C_0^B, C_I^B and C_{IK}^B are given by the following

$$C_0^B = e^{S_0^B} \int_a^b dh \exp\left\{\frac{1}{\nu^2}\beta d(h - fd)\right\} \times \mathcal{Q}[h, fd; \nu^2; a, b], \tag{3.88}$$

$$S_0^B = -\frac{1}{2\nu^2}(\beta d)^2 \tag{3.89}$$

and

$$C_I^B = e^{S_I^B} \int_a^b dh \exp\left\{\frac{1}{\nu^2}(\beta d - \sum_{J=1}^{N_c} G_{IJ} d_J)(h - fd)\right\} \times \mathcal{Q}[h, fd; \nu^2; a, b], \tag{3.90}$$

$$S_I^B = -\frac{1}{2\nu^2}(\beta d - \sum_{J=1}^{N_c} G_{IJ} d_J)^2 \tag{3.91}$$

and

$$C_{IK}^B = e^{S_{IK}^B} \int_a^b dh \exp\left\{\frac{1}{\nu^2}(\beta d - \sum_{J=1}^{N_c} G_{IJ} d_J - \sum_{J=1}^{N_c} G_{KJ} d_J)(h - fd)\right\} \times \mathcal{Q}[h, fd; \nu^2; a, b], \tag{3.92}$$

$$S_{IK}^B = G_{IK} - \frac{1}{2\nu^2}(\beta d - \sum_{J=1}^{N_c} G_{IJ} d_J - \sum_{J=1}^{N_c} G_{KJ} d_J)^2, \tag{3.93}$$

where

$$\mathcal{Q}[h, fd; \nu^2; a, b] = \sum_{k=-\infty}^{+\infty} e^{-(\nu^2/2)k^2} [e^{-ik(h-fd)} - e^{ik(h+fd-2a)}], \tag{3.94}$$

and βd and ν^2 are defined by

$$\beta d = \sum_{I=1}^{N_c} \beta_I d_I, \tag{3.95}$$

$$\nu^2 = \sum_{I,J=1}^{N_c} d_I G_{IJ} d_J. \tag{3.96}$$

The parameters used for the simulation of the coupon bond barrier option for different magnitudes of σ_M are shown in Table 3.7. The same scaling function is used for the simulation of the coupon bond barrier option as was used for the zero coupon bond barrier option.

Table 3.7: The barrier condition used in the simulation of the coupon bond barrier option.

Simulation	$\sigma = \sigma_M$	$\sigma = 10\sigma_M$	$\sigma = 50\sigma_M$
Up barrier	$U = e^{0.69} = 1.994$	$U = e^{0.9} = 2.460$	$U = e^{1.5} = 4.482$
Down barrier	$L = e^{0.63} = 1.878$	$L = e^{0.4} = 1.492$	$L = e^{0.3} = 1.350$

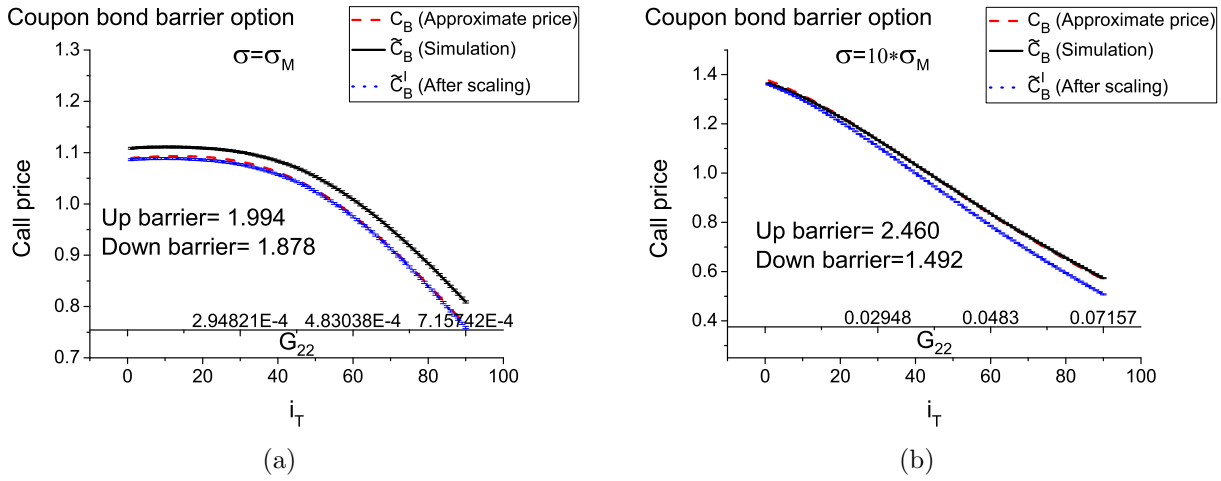

(a) (b)

Figure 3.24: Coupon bond barrier options with number of bonds $N_c = 2$, t_*=180 days and strike price=0.5: comparison between simulation and approximate price, with and without scaling. Different future times T_i are $T_1 = 270 + 2i_T$ and $T_2 = 360 + 2i_T$ days with $c_1 = 0.5$ and $c_2 = 1.5$. The error bars are Monte Carlo errors of the simulation. (a) $\sigma = \sigma_M$. (b) $\sigma = 10\sigma_M$.

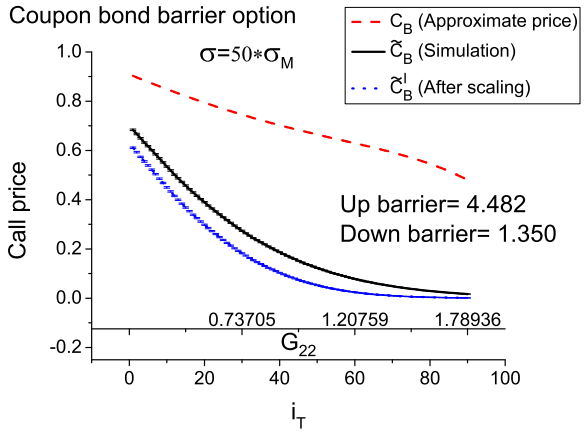

Figure 3.25: Coupon bond barrier options with number of bonds $N_c = 2$, $\sigma = 50\sigma_M$, t_*=180 days and strike price=0.5: comparison between simulation and approximate price, with and without scaling. Different future times T_i are $T_1 = 270 + 2i_T$ and $T_2 = 360 + 2i_T$ days with $c_1 = 0.5$ and $c_2 = 1.5$. The error bars are Monte Carlo errors of the simulation.

As shown in Figure 3.24(a), the results from the formula and simulation after using the scaling function match quite well. In Figure 3.24(b), the error of the approximate formula increases when the bond maturity times T_1 and T_2 increase. However, the largest error is 12%, which is still reasonable for the case of $\sigma = 10\sigma_M$. The results from the approximate formula fail to match the results from the simulation for large $\sigma = 50\sigma_M$, as shown in Figure 3.25. This is due to the fact that the approximate price of formula is valid only when the value of the correlator G_{IJ} is small. In Equation 3.45, the value of the correlator G_{II} is approximately equal to $(t_* - t_0)(T_I - t_*)^2\sigma^2$. In the simulation of the coupon bond barrier option, the value of T_I was changed to find the range of G_{II} for the validity of the linearization of the barrier. Figure 3.26(a) shows the results of the comparison between the simulation and the approximate price for varying T_I. The error is less than 1% if the value of G_{22} is smaller than 0.011, and the error is less than 10% if the value of G_{22} is smaller than 0.057. Compared to the results for coupon bond European option, the range of G_{II} for the accuracy of the approximate barrier option price is smaller. This is because the approximate price of the coupon bond European option only has a limitation on the value of G_{II}. In contrast, for the case of the coupon bond barrier option, the error comes from both the linearization of the barrier and the limitation that the value G_{II} is small. For the case of the coupon bond European options, the higher order terms are computed up to C_4, while only the leading term is calculated for the coupon bond barrier option. The computation of higher order terms is intractable for coupon bond barrier options. If the market propagator and volatility are used, the bond maturity time T can be up to nearly 2.6 years and 6 years for the absolute error of

the approximate price smaller than 1% and 10%, respectively.

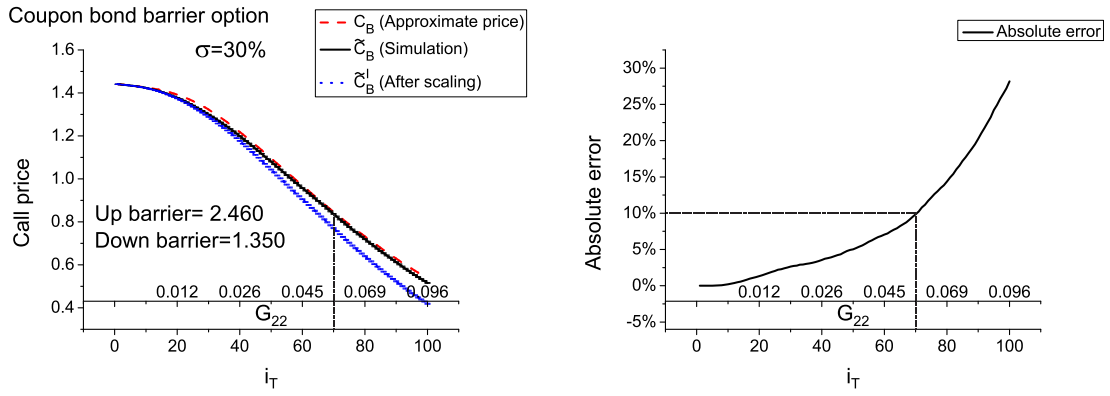

Figure 3.26: (a) Coupon bond barrier options with $\sigma = 30\%$, t_*=180 days and strike price=0.5 : comparison between simulation and approximate price. Different future times T_i are $T_1 = 270 + 8i_T$ and $T_2 = 360 + 8i_T$ days with $c_1 = 0.5$ and $c_2 = 1.5$. (b)The absolute error is calculated by using |(Simulation after scaling−approximate price)/Simulation after scaling|× 100%.

§ 3.12 Eigenfunction expansion of the quantum field $A(t,x)$

The updating step used in the simulation is 1 day, and the bond maturity time T is up to 538 days. The size of the matrix of stiff propagator is 539×539 (including the current time t_0). The number of configurations used for simulation is around 10^5, so the total number of Gaussian random variables is nearly 2.9×10^{10}. Such a large number of Gaussian noise means that nearly 2 hours cpu time is required for each run. The stiff propagator is a positive and symmetric matrix, which can be represented by an eigenfunction expansion. The multi-factor HJM model can be derived from the model of forward interest rates on the basis of quantum finance. From the work of [29], [30], [31] and [32],three factors are enough to express the volatility structure of the forward interest rates. The challenge for the three-factor HJM model is the estimation or calibration of the three volatility functions using empirical analysis, as discussed in [33], [34], [35], [36], [37] and [38]. We show that the three volatility functions can be directly obtained from the eigenvalues and eigenvectors of the stiff propagator.

The eigenvalues and eigenvectors of the stiff propagator are given by

$$\sum_{p'=0}^{M-n} D_{p,p'}\psi_l(p') \;=\; \lambda_l\psi_l(p), \tag{3.97}$$

where λ_l is the eigenvalue of propagator D and ψ_l its eigenvector. Note that

$$\lambda_l \;>\; 0, \quad l = 0, 1, ..., M-n. \tag{3.98}$$

The ψ_l's are orthonormal and satisfy

$$\sum_{l=0}^{M-n} \psi_l^*(p)\psi_l(p') \;=\; \delta_{p-p'}, \tag{3.99}$$

and are shown in Figure 3.27(a) and 3.27(b).

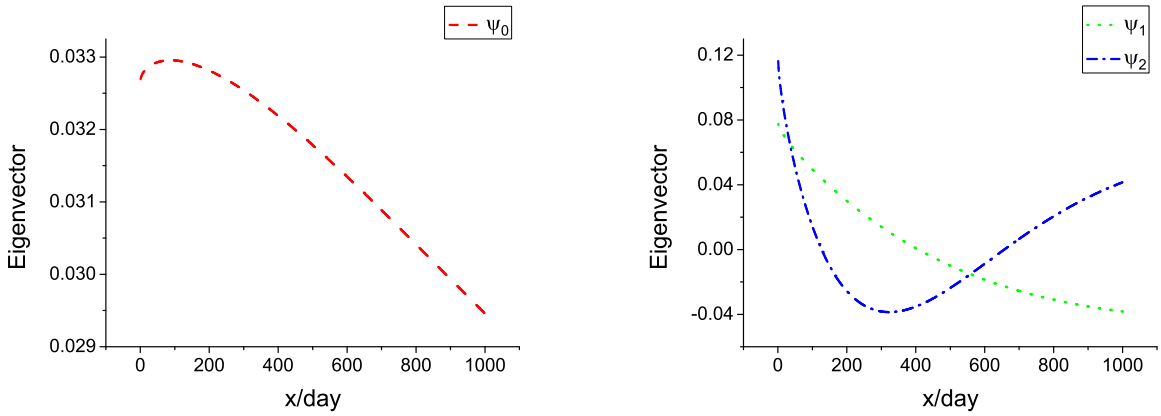

(a) (b)

Figure 3.27: (a) Eigenvector ψ_0 . (b) Eigenvectors ψ_1 and ψ_2 .

Hence, the matrix Y is given by

$$Y_{p,p'} \;=\; \sum_{l=0}^{M-n} \sqrt{\lambda_l}\psi_l^*(p)\psi_l(p'). \tag{3.100}$$

The lattice quantum field $A_{m,n}$ has the following expansion

$$A_{m,n} = \sum_{p'=0}^{M-n} Y_{p,p'} R_{m,p'} \tag{3.101}$$

$$= \sum_{l=0}^{M-n} \sqrt{\lambda_l}\psi_l(p) Q_{m,l}, \tag{3.102}$$

where

$$Q_{m,l} = \sum_{p'=0}^{M-n} \psi_l(p') R_{m,p'}. \tag{3.103}$$

Note that $Q_{m,l}$ is a Gaussian white noise for each m and l.

The first eigenvalue is nearly 96% of the sum of eigenvalues $\sum_{l=0}^{M-n}\lambda_l$; 3% and 0.4% are accounted for by the second and third eigenvalues, respectively. This fact suggests that three eigenvalues are enough for constructing the structure of the propagator, which confirms the studies of [29], [30], [31] and [32].

Equation 3.16 can be written as

$$\begin{aligned} f_{m+1,n} &= f_{m,n} + \epsilon\alpha_{m,n} + \epsilon\sigma_{m,n}A_{m,n} \\ &= f_{m,n} + \epsilon\alpha_{m,n} + \epsilon\sigma_{m,n}\sum_{l=0}^{M-n}\sqrt{\lambda_l}\psi_l(p)Q_{m,l} \\ &= f_{m,n} + \epsilon\alpha_{m,n} + \epsilon\sum_{l=0}^{M-n}\sigma^l_{m,n}Q_{m,l}, \end{aligned}$$

where $p = n - m$ and

$$\sigma^l_{m,n} = \sigma_{m,n}\sqrt{\lambda_l}\psi_l(p) \tag{3.104}$$

is defined as the effective volatility.

l was chosen as 0, 1 and 2 respectively and the one, two and three white noise simulation

is given by

$$f_{m+1,n} = f_{m,n} + \epsilon\alpha_{m,n} + \epsilon\sigma_{m,n}\sqrt{\lambda_0}\psi_0(p)Q_{m,0}, \tag{3.105}$$

$$f_{m+1,n} = f_{m,n} + \epsilon\alpha_{m,n} + \epsilon\sigma_{m,n}\Big(\sqrt{\lambda_0}\psi_0(p)Q_{m,0} + \sqrt{\lambda_1}\psi_1(p)Q_{m,1}\Big), \tag{3.106}$$

$$f_{m+1,n} = f_{m,n} + \epsilon\alpha_{m,n} + \epsilon\sigma_{m,n}\Big(\sqrt{\lambda_0}\psi_0(p)Q_{m,0} + \sqrt{\lambda_1}\psi_1(p)Q_{m,1} + \sqrt{\lambda_2}\psi_2(p)Q_{m,2}\Big). \tag{3.107}$$

As shown in Figure 3.28(a), the white noise $Q_{m,0}$ shifts $f(t_0,x)$, $Q_{m,1}$ tilts the curve $f(t_0,x)$ and $Q_{m,2}$ lifts the far future piece.

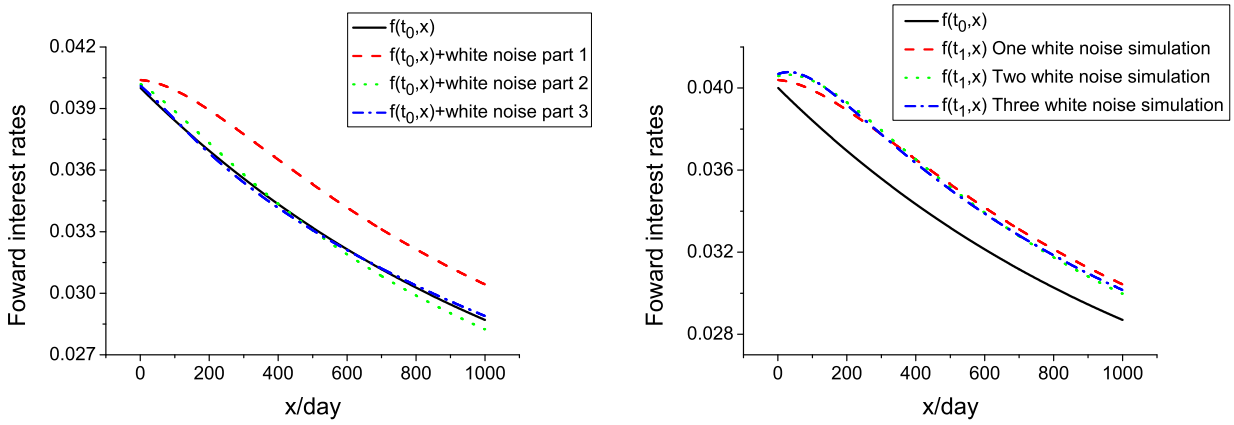

Figure 3.28: (a) The sum of $f(t_0,x)$ and the white noise parts 1 ($\epsilon\sigma_{m,n}\sqrt{\lambda_0}\psi_0(p)Q_{m,0}$), 2 ($\epsilon\sigma_{m,n}\sqrt{\lambda_1}\psi_1(p)Q_{m,1}$) and 3 ($\epsilon\sigma_{m,n}\sqrt{\lambda_2}\psi_2(p)Q_{m,2}$) are plotted respectively. (b) $f(t_1,x)$ of one, two and three white noise simulation, and $t_1 = t_0 + 1$, where the value of the white noise is set to be $Q_{m,l} = 1$.

The results of the white noise simulation are compared with the results of the Cholesky simulation. Only the case of $\sigma = 50\sigma_M$ is presented since the effect of the white noise simulation is large enough to observe in this case. The comparison of the Cholesky and white noise simulations for the zero coupon bond option is shown in Figure 3.29(a). It is seen that the results from the three-factor white noise simulation are almost the same as the results from the Cholesky simulation, with the differences being negligible. The results for the coupon bond European option, zero coupon bond double barrier option and coupon bond barrier option are shown in Figure 3.29(b), 3.30(a) and 3.30(b) respectively. The results obtained using the scaling function are not plotted in Figure 3.30(a) and 3.30(b), because the results from the

simulation and the white noise simulation are nearly the same. After using scaling function, these results are the same. The results suggest that the three white noise simulation is good enough to give accurate results and it also greatly reduces the computing time.

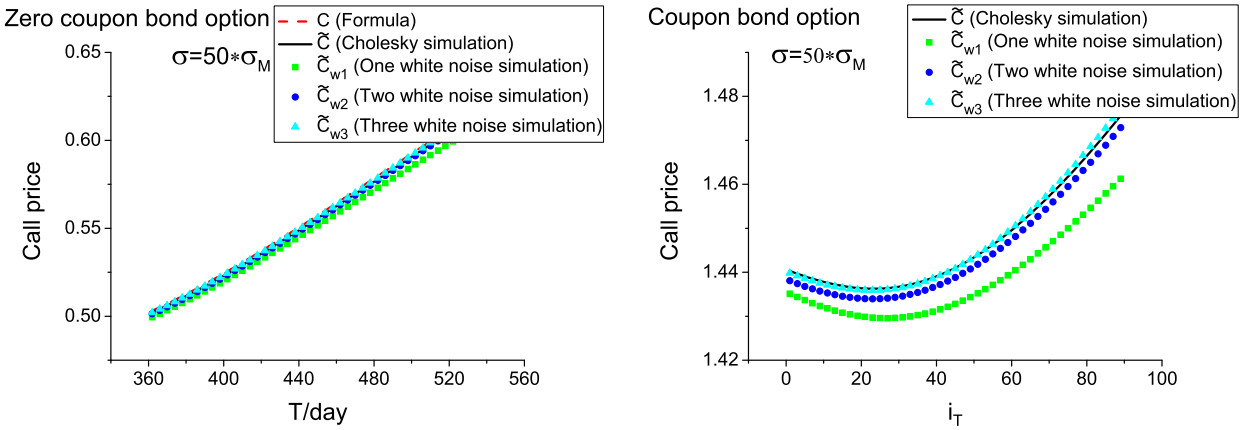

(a) (b)

Figure 3.29: Comparison between Cholesky and white noise simulation ($\sigma = 50\sigma_M$, t_*=180 days and strike price=0.5). (a) Zero coupon bond option. (b) Coupon bond European option.

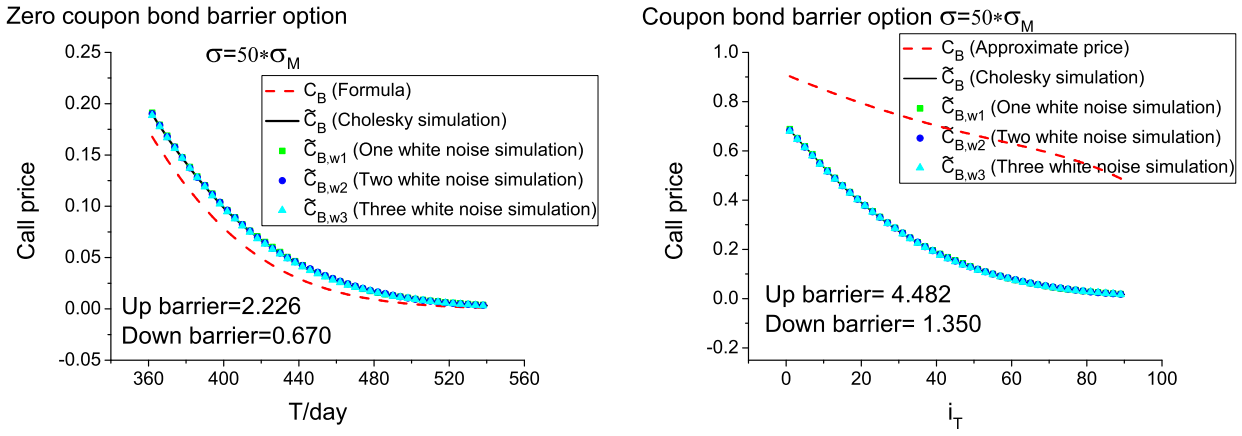

(a) (b)

Figure 3.30: Comparison between Cholesky and white noise simulation ($\sigma = 50\sigma_M$, t_*=180 days and strike price=0.5). (a) Zero coupon bond double barrier option. (b) Coupon bond barrier option.

§ 3.13 Conclusion

The simulation method of quantum field theory for forward interest rates has been shown to yield efficient algorithms for pricing the coupon bond European and barrier options. The quantum field $A(t,x)$ was generated by using the Cholesky decomposition of the stiff propagator. The forward interest rates were constructed by updating the quantum field $A(t,x)$, which contains the rich correlation between forward interest rates for different maturity times.

The zero coupon bond option price was obtained by averaging the payoff function $\mathcal{P}_*$ of each configuration. It was found that the option price of the simulation is nearly equal to the option price obtained from the exact formula. The coupon bond European option price obtained by using simulation was also in agreement with the approximate price when σ was small. The simulation method can also work when the volatility is large, and for this case the approximate price fails. The simulation results show that the method can be used without the limitation of the Feynman perturbation expansion.

The zero coupon bond barrier option price was analyzed and the error of the barrier was also investigated in order to reduce the error between the simulation and the exact formula. Two different scaling functions were calibrated for the up barrier and the down barrier respectively. After using the scaling function, the simulation results for the single barrier and double barrier match the formula very well. The results show that the error of the barrier can be largely removed by using a simple scaling function.

Like the simulation results for the coupon bond European options, the simulation method can be used to analyze the coupon bond barrier option for any value of the correlator G_{IJ}, while the approximate price can only be used when the value of the correlator G_{IJ} is small.

Another key contribution of this study is that the three-factor white noise simulation can be derived from the quantum finance model of forward interest rates. Without any complicated calibration, the effective volatility (volatility structure) of the three-factor HJM model is obtained as the product of the eigenvalue and eigenvector of the propagator. This finding is of crucial importance in terms of the potential and application of quantum finance. The simulation method has been shown to be powerful for a wide variety of options and can be applied to exotic options as well.

§ 3.14 Appendix: Put-call parity for zero and coupon bond barrier option

The results for the at the money call and put prices of the zero coupon bond barrier and coupon bond barrier options are presented in this section. Only the case for $\sigma = 10\sigma_M$ is demonstrated, because it is large enough for the application of the simulation.

Figure 3.11(a) shows the dynamics of the at the money double barrier option. Figures 3.31(a) and 3.31(b) show the call and put prices of at the money zero coupon bond double barrier option. The put option price calculated using simulation with use of scaling function matches the exact result quite well, while the call option price calculated using simulation still has some error. This is due to the fact that the value of the at the money option price is quite small, and the scaling function may not work perfectly for small values of the call option price. However, as discussed before, the scaling function works well for many cases.

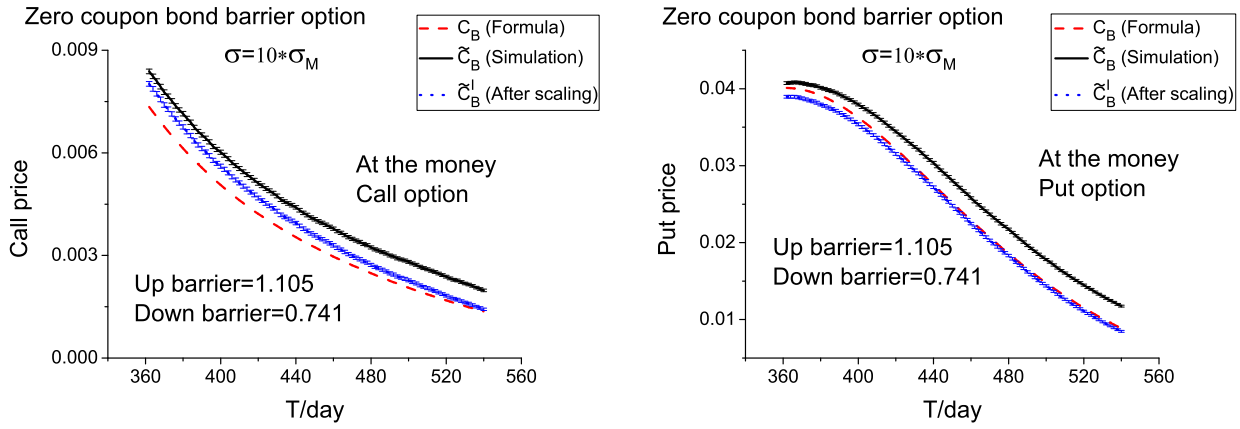

(a) (b)

Figure 3.31: Comparison between simulation and formula ($\sigma = 10\sigma_M$, t_*=180 days and strike price=forward bond price), with and without scaling. The error bars are Monte Carlo errors of the simulation. (a) Zero coupon bond barrier call option (at the money). (b) Zero coupon bond barrier put option (at the money).

Figures 3.32(a) and 3.32(b) show the comparisons between the simulation and formula for call and put prices of the at the money coupon bond barrier option. Echoing the discussion of Section § 3.11, compared to the simulation, the approximate price doesn't work well for the case of $\sigma = 10\sigma_M$. The approximate price is not useful when the value of G_{IJ} is large.

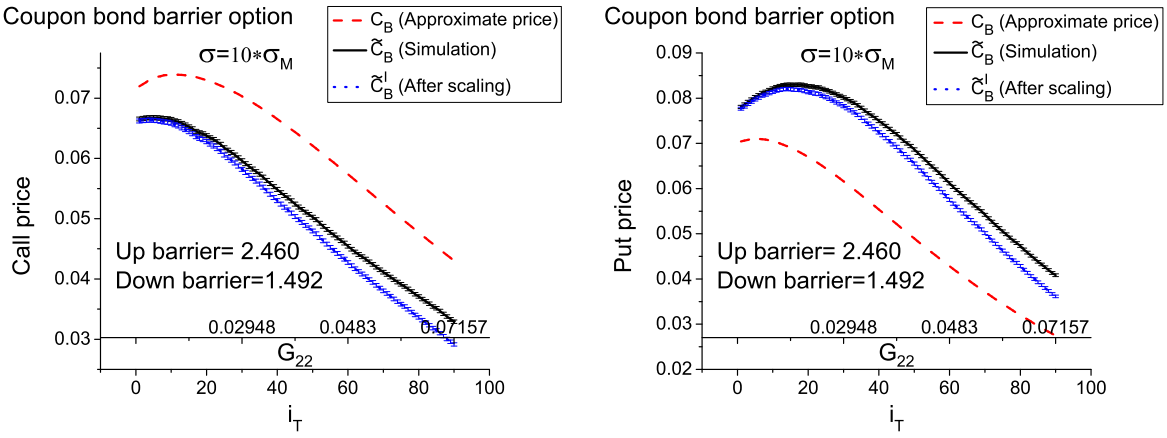

(a) (b)

Figure 3.32: Comparison between simulation and formula ($\sigma = 10\sigma_M$, t_*=180 days and strike price=forward bond price), with and without scaling. Different future times T_i are $T_1 = 270 + 2i_T$ and $T_2 = 360 + 2i_T$ days with $c_1 = 0.5$ and $c_2 = 1.5$. The error bars are Monte Carlo errors of the simulation. (a) Coupon bond barrier call option (at the money). (b) Coupon bond barrier put option (at the money).

Based on the identity in [5]

$$[a-b]_+ - [b-a]_+ \quad = \quad (a-b)\Theta(a-b) - (b-a)\Theta(b-a) = a-b, \tag{3.108}$$

where Θ is the Heaviside function. [3]

The difference of the call and put payoff functions $\mathcal{P}_*$ for the zero coupon bond barrier option is therefore given by

$$[B(t_*,T)-K]_+ - [K-B(t_*,T)]_+ \quad = \quad B(t_*,T)-K. \tag{3.109}$$

The difference of the call and put payoff functions has the constraint that only the successful configurations $f_s(t,x)$ are accepted. Taking the expectation value using the martingale condition, the put-call parity is given by

$$C_B(t_0,t_*,T,K) - P_B(t_0,t_*,T,K) \quad = \quad B(t_0,t_*)E_s[B(t_*,T)-K]_+, \tag{3.110}$$

[3]

$$\Theta(t) = \begin{cases} 1 & t>0 \\ \frac{1}{2} & t=0 \\ 0 & t<0. \end{cases}$$

where $E[...]_s$ is the expectation value over total configurations and the payoff function $\mathcal{P}_*$ is only computed for the successful configurations $f_s(t,x)$, because the configurations which are knocked out during the updating are not accounted for.

The exact formula of the right hand side of Equation 3.110 can be obtained by replacing the payoff function $\mathcal{P}_* = (e^{-g} - K)_+$ with $(e^{-g} - K)$ in Equation 3.73. Hence, the exact results of put-call parity can be calculated by using $\xi = -\ln K$ in Equation 3.75. For the case of the at the money option, $\xi = -\ln K = f$ and $f = \int_{t_0}^{t_*} dx f(t,x)$. The put-call parity of the simulation with scaling can be obtained by using $\tilde{C}_B^I(t_0, t_*, T, K, \epsilon) - \tilde{P}_B^I(t_0, t_*, T, K, \epsilon)$ for the left hand side of Equation 3.110 .

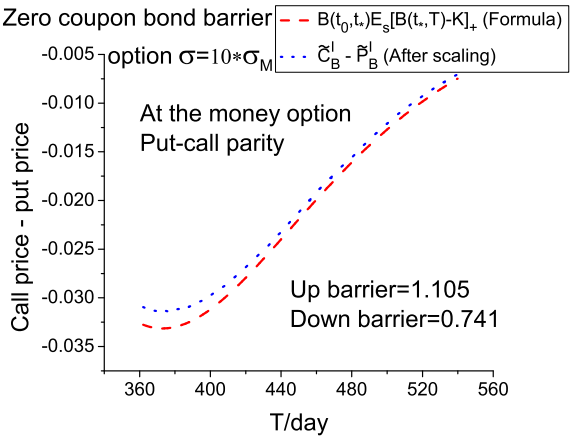

Figure 3.33: Comparison between formula and simulation with scaling for put-call parity of zero coupon bond barrier option ($\sigma = 10\sigma_M$, t_*=180 days and strike price=forward bond price, at the money option).

As shown in Figure 3.33, the difference between the simulation after scaling and the exact formula is very small for put-call parity of zero coupon bond barrier option. The results confirm that our derivation of put-call parity is consistent with the simulation.

Following the procedure of the derivation of put-call parity as before, the put-call parity for the coupon bond barrier option is given by

$$C_B(t_0, t_*, T_I, K) - P_B(t_0, t_*, T_I, K) \quad = \quad B(t_0, t_*) E_s[\sum_{I=1}^{N_c} c_I B(t_*, T_I) - K]_+. \qquad (3.111)$$

The left hand side and the right hand side of Equation 3.111 are compared by using the simulation, since the approximate price doesn't work well for large σ. Figure 3.34 shows the

plots of $\tilde{C}_B^I(t_0, t_*, T_I, K, \epsilon) - \tilde{P}_B^I(t_0, t_*, T_I, K, \epsilon)$ and $B(t_0, t_*)E[\sum_{I=1}^{N_c} c_I B(t_*, T_I) - K]_s$ using the simulation with scaling. The two sides of Equation 3.111 are exactly equal, which confirms the derivation of put-call parity for the coupon bond barrier option.

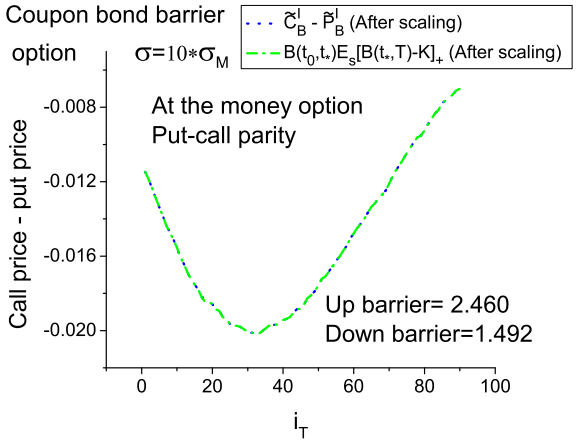

Figure 3.34: Comparison between the left hand side and right hand side of Equation 3.111; the two sides of Equation 3.111 are computed using the simulation with scaling for put-call parity of the coupon bond barrier option ($\sigma = 10\sigma_M$, t_*=180 days and strike price=forward bond price, at the money option).

Chapter 4

Simulation of Nonlinear Interest rates: Libor Market Model

The simulation of Libor Market Model (LMM) is extensively studied in the framework of quantum finance. The imperfectly correlated Libor rates are simulated based on a Gaussian quantum field and a recursion equation of nontrivial stochastic drift. The Libor options are studied using both the simulation method and analytical formula. The caplet price of simulation is compared with Black's caplet formula which can be exactly derived from LMM. The invariance of caplet price for different forward bond numeraire is verified by using the simulation. The simulation results for coupon bond options and swaptions are compared with the approximate price, which are limited for the reason that the approximate price is derived using the small volatility expansion. The simulation method is shown to have great potential in the application of pricing interest rate instruments.

§ 4.1 Introduction

The London interbank offered rate, also called Libor, is often quoted and widely used by banks and financial institutions. Libor is one of the main instruments in the debt market and is the basis for many interest rate instruments such as caplet, coupon bond options and swaptions. The three-month Libor is widely used as the basis of the Libor derivative market. The three-month Libor is simulated directly in this Chapter and all the instruments mentioned above are simulated and discussed.

The HJM model is widely used in the finance industry for describing and simulating the

continuously compounded instantaneous forward interest rates. The instantaneous forward rates are not directly observable in the market, which is one of the main drawbacks of HJM model. Hence, it is difficult to use it to price traded instruments such as caps. Moreover, another intrinsic shortcoming of HJM model is that the forward rates have a finite probability of being negative. Using log-normal interest rates rather than instantaneous interest rates, which was introduced by Bruce-Gatarek-Musiela [24], yields the standard market model known as Libor Market Model (LMM). The main advantage of this model is that the Black's caplet formula can be exactly derived in this framework. The LMM was significantly developed and pricing swap rates was extensively studied by Jamshidian [39].

Similar to the HJM model, BGM-Jamshidian model has a major limitation that the entire Libor rates are driven by a single white noise. In the framework of stochastic process, the instantaneous forward rates as well as the log-normal Libor rates are perfectly correlated. As observed from the market data, the Libor interest rates $L(t, T_n)$, which has dynamics similar to the forward interest rates, shows randomness in both calendar and future time. Hence, in principle and practice, the Libor rates on different future time are imperfectly correlated. Intuitively, the Libor rates can be formulated and simulated using quantum finance approach. Baaquie (2009) [26] gave a generalized formulation of the Libor Market Model and the quantum finance approach is discussed extensively in [5].

The calibration of Libor Market Model has been studied in many books and articles, such as Rebonato (2002) [40], Gatarek (2007) [41] and Brigo (2007)[42]. All of these calibration algorithms are designed and applied using the BGM framework. The empirical study of the quantum formulation of the LMM has been studied in [43]. In this Chapter, the numerical simulations are investigated by using the quantum finance approach, and the financial instruments (such as caplets and swaptions) for the LMM are studied using both Monte Carlo simulation and the volatility expansion.

§ 4.2 Libor market model

Following the work of Bruce-Gatarek-Musiela [24] and Jamshidian [39], the formulation of the single-factor BGM-Jamshidian model is given by

$$\frac{1}{L(t,T_n)}\frac{\partial L(t,T_n)}{\partial t} = \xi_n(t) + \gamma_n(t)R(t), \tag{4.1}$$

$$E[R(t)R(t')] = \delta(t-t'), \tag{4.2}$$

where $R(t)$ is Gaussian white noise and $\xi_n(t)$ is the stochastic drift; the evolution of Libor rate is driven by a single noise $R(t)$. The Libor rates between different future times are perfectly correlated and this assumption is not supported by the market data [43].

To overcome this shortcoming of BGM-Jamshidian model, the volatility structure was studied by Anderson [44]. To capture more information from the correlation of Libor interest rates, another approach is to incorporate a series of white noises coupled with different volatility functions which has been studied by Brigo [42] and Amin [45]. However, the different volatility functions need to be calibrated to agree with the market data and even finite number of white noises are not enough to capture all the information of correlation function. If an infinite number of white noises are introduced, the methods are then not applicable and inefficient in practice.

The quantum generalization of Libor Market Model (LMM) was firstly proposed by Baaquie (2009) [26]; the main improvement of the quantum finance approach is using two-dimensional quantum field $A(t,x)$ as a replacement of one-dimensional stochastic process $R(t)$. The Libor forward rates, denoted by $f_L(t,x)$, are defined for both calendar and future time. The Libor forward rates in quantum finance approach is given as follows

$$\frac{\partial f_L(t,x)}{\partial t} = \mu(t,x) + v(t,x)A(t,x). \tag{4.3}$$

In terms of the Libor rates $L(t,T_n)$, the quantum formulation of LMM is given by

$$\frac{1}{L(t,T_n)}\frac{\partial L(t,T_n)}{\partial t} = \xi(t,T_n) + \int_{T_n}^{T_n+\ell} \gamma(t,x)A(t,x), \tag{4.4}$$

where $\gamma(t,x)$ is a deterministic volatility function and ℓ is Libor tenor and $T_n = n\ell$. Compared to the BGM-Jamshidian framework, the correlation of the Gaussian quantum field $A(t,x)$ is given by

$$E[A(t,x)A(t',x')] = \delta(t-t')D(x,x';t), \tag{4.5}$$

where $D(x,x';t)$ is the correlation function of the Libor forward interest rates between different maturities [43]. $D(x,x';t)$ is also called propagator in terminology of quantum field theory. The quantum generalization of Libor Market Model gives the full description of correlation function and is enough to capture the information from the market data of Libor rates.

§ 4.3 Simulation of Libor Market Model

Suppose the present Libor interest rate is $L(t_0, T_n)$; at calendar time t ,where $t > t_0$, it is given by [5]

$$L(t, T_n) = L(t_0, T_n) e^{\beta(t_0, t, T_n) + W_n}, \tag{4.6}$$

where

$$\beta(t_0, t, T_n) = \int_{t_0}^{t} dt' \xi(t', T_n); \quad q_n^2 = \int_{t_0}^{t} dt' \Lambda_{nn}(t'),$$

and

$$W_n = -\frac{1}{2} q_n^2 + \int_{t_0}^{t} dt' \int_{T_n}^{T_{n+1}} dx \gamma(t', x) A(t', x).$$

Equation 4.6 is used for updating the Libor rates. In the Monte Carlo simulation, the Libor rates are updated on a discrete time lattice. The Libor $L(t, T_n)$ on future time is defined on a lattice with interval of tenor ℓ. The value of $\Lambda_{nn}(t)$ and $A(t, x)$ also requires discrete future time, and hence, discretizing calendar and future time yields

$$\begin{aligned} t &\rightarrow t_i = t_0 + i\epsilon, \\ T_n &\rightarrow T_n = t_0 + n\ell, \end{aligned}$$

where t_0 denotes the initial value of calendar time. The initial value of future time T_i is taken to be the present time t_0.

The updating process for the Libor rates is then given by

$$\begin{aligned} L(t_i + \epsilon, T_n) &= L(t_i, T_n) \exp\left(\epsilon \beta(t_i, t_i + \epsilon, T_n) + \epsilon W_n\right) \\ &= L(t_i, T_n) \exp\left\{\epsilon \xi(t_i, T_n) + \epsilon \int_{T_n}^{T_{n+1}} dx \gamma(t_i, x) A(t_i, x) - \frac{1}{2} \epsilon \Lambda_{nn}(t_i)\right\}. \end{aligned} \tag{4.7}$$

In the above Equation, the approximation $\beta(t_i, t_i + \epsilon, T_n) \simeq \epsilon \xi(t_i, T_n)$ is assumed. In principle the value of $\beta(t_i, t_i + \epsilon, T_n)$ is integrated from t_i to $t_i + \epsilon$. However, for the first updating step $t_0 \rightarrow t_0 + \epsilon$, only the initial value $\xi(t_0, T_n)$ is given. Hence, in the first updating step, the approximation $\beta(t_0, t_0 + \epsilon, T_n) \simeq \epsilon \xi(t_0, T_n)$ is chosen for this simulation. Since the step size ϵ is chosen to be one day, the difference between $\beta(t_i, t_i + \epsilon, T_n)$ and $\epsilon \xi(t_i, T_n)$ is negligible. The

same approximation is also made for W_n. Therefore, the first updating is given by

$$L(t_0+\epsilon,T_n) \;=\; L(t_0,T_n)\exp\Big\{\epsilon\xi(t_0,T_n)+\epsilon\int_{T_n}^{T_{n+1}} dx_j\gamma(t_0,x_j)A(t_0,x_j)-\frac{1}{2}\epsilon\Lambda_{nn}(t_0)\Big\}.$$

Libor for future time T is defined on the Libor lattice of T_n with tenor ℓ. As shown in Equation 4.7, the time step ϵ is needed to be small enough (e.g. ϵ = one day = 1/360 year). However, the step size ℓ is not restricted to be as small as ϵ. It is known that the tenor of Libor is taken to be 3 months = 90 days. This means that the updating step size of calendar time ϵ and future time ℓ are not equal. Figure 4.1 shows the lattice of updating process for Libor Market Model.

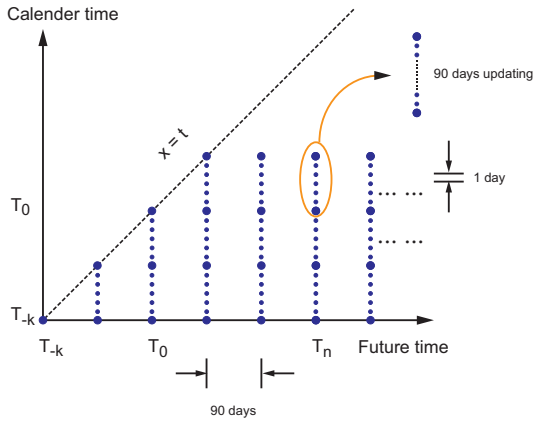

Figure 4.1: The lattice of Libor interest rates in discrete time. The updating step size for calendar time t is 1 day and Libor tenor ℓ = 90 days.

The updating step size of calendar and future time is equal for the case of instantaneous forward interest rates, since calendar time t and future time x are both continuous and the updating step size of t and x need to be equal [46]. However, for the case of Libor interest rates, the Libor Market Model is designed to simulate the traded interest instruments directly. The updating of Libor doesn't require that ℓ should have the same size of ϵ. The simulation of Libor Market Model with unequal step size will be discussed in the following Section.

The updating step size of calendar time is taken to be 1 day and 90 days for future time, namely

$$\begin{aligned}\epsilon &= 1 \text{ day},\\ \ell &= 90 \text{ days}.\end{aligned}$$

The integration over future time $\int dx$ is done by discretizing future time x into a lattice with spacing ϵ.

$$\begin{aligned} x &\rightarrow x_j = x_0 + j\epsilon, \\ \theta = x - t &\rightarrow \theta_i = x_j - t_i. \end{aligned}$$

The Libor correlator $\Lambda_{mn}(t)$, in discrete time, is given by performing the following summation

$$\Lambda_{mn}(t_i) = \epsilon^2 \gamma(\theta_i) \sum_{\theta_i=(T_m-t_i)}^{T_m+\ell-t_i} \sum_{\theta_i'=(T_n-t_i)}^{T_n+\ell-t_i} D(\theta_i, \theta_i')\gamma(\theta_i'). \tag{4.8}$$

After performing the integration for $\Lambda_{mn}(t)$, as shown in Equation 4.7 and 4.8, $\xi(t, T_n)$ and q_n^2 have, in principle, step size of ℓ in future time. However, term $\int_{T_n}^{T_{n+1}} dx\gamma(t, x)A(t, x)$ is the integration from T_n to T_{n+1} in continuous future time. The lattice of $A(t, x)$ is taken to be the same step size for t and x. Three white noise and eigenvectors are enough to describe the empirical stiff propagator $D(x, x'; t)$ [43] [46]. After generating the lattice of $A(t, x)$, the term $\int_{T_n}^{T_{n+1}} dx\gamma(t, x)A(t, x)$ can be obtained by performing the integration on the future time x. Then, three terms on right hand side of Equation 4.7 are all on the same lattice size.

The nonlinear drift $\xi(t, T_n)$ is the most important term in Libor Market Model. Figure 4.2 shows the updating of Libor rates where $T_n > T_I$. As shown in Equation 2.52, one needs the Libor rates $L(t_i, T_{I+1}), L(t_i, T_{I+2})....L(t_i, T_n)$ to obtain the drift $\xi(t_i, T_n)$. Hence, in order to get the Libor rates $L(t_i + \epsilon, T_n)$ of next step, the Libor rates of all time T_i are also needed. This nonlinear feature of Libor Market Model yields some nontrivial and novel properties.

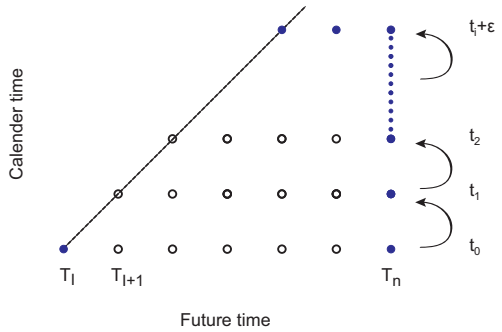

Figure 4.2: The dynamic of updating of Libor rates. The Libor rates $L(t_i, T_{I+1}), L(t_i, T_{I+2})....L(t_i, T_n)$ (demonstrated by open dots) are needed to generate the Libor rates $L(t_i + \epsilon, T_n)$, shown by the full dots.

The parameters for the propagator given in Table 3.1 is used here and the function given in Equation 3.30 is used for generating values of $\gamma(t, x)$.

The initial value for present Libor rates $L(t_0, T_n)$ is generated using the following Equation

$$L(t_0, T_n) \quad = \quad f_0\Big[1.0 + \exp\big\{ - f_x\ell(T_n - t_0)\big\}\Big], \tag{4.9}$$

where f_x is fixed at 1.2 and f_0 is set to be 0.3 for all the interest rate instruments simulated in this Chapter. The large value of Libor ($L(t_0, T_n)$ is around 0.3) is chosen because the payoff function of coupon bond options and swaptions is in terms of bond; if f_0 is small, the bond price does not change much. To clearly observe the dynamics of Libor Market Model, $f_0 = 0.3$ is used for the initial condition. In this simulation, 10 points of three-month Libor rates are generated, which means that $0 \leq n < 10$.

§ 4.4 Caplet

The Black's caplet price was derived exactly in the framework of quantum finance in [47]. The Black formula of caplet price is compared with our simulation, since the Black formula yields the exact price for caplet and provides a check the correctness of our simulation. Hence, the Black's caplet formula is of critical importance for our simulation.

The price of a mid-curve caplet on Libor $L(t_*, T_n)$, maturing at time $t_* > t_0$, is given by

$$Caplet(t_*, t_*, T_n) \quad = \quad \ell V B(t_*, T_n + \ell)[L(t_*, T_n) - K]_+, \tag{4.10}$$

where V is the principal of the caplet and is taken to be 1 in this simulation. The price of the caplet at present time, under discounting with the forward bond numeraire $B(t, T_I + \ell)$, is given by

$$\frac{Caplet(t_0, t_*, T_n)}{B(t_0, T_I + \ell)} \quad = \quad E\big[\frac{Caplet(t_*, t_*, T_n)}{B(t_*, T_I + \ell)}\big]. \tag{4.11}$$

If T_I is taken to be equal to T_n, the caplet price is then given by

$$E\big[\frac{Caplet(t_*, t_*, T_n)}{B(t_*, T_n + \ell)}\big] \quad = \quad \ell V E[L(t_*, T_n) - K]_+. \tag{4.12}$$

As shown in Equation 2.52, for numeraire $B(t, T_{n+1})$, the Libor rate from T_n to $T_n + \ell$ has zero drift and the Black's caplet formula can be obtained analytically.

The Black formula for caplet price is given by [47]

$$\begin{aligned} Caplet(t_0, t_*, T_n) &= \ell VB(t_0, T_{n+1}) E[L(t_*, T_n) - K]_+ \\ &= \ell VB(t_0, T_{n+1}) \big[L(t_0, T_n) N(d_+) - K N(d_-) \big], \end{aligned} \tag{4.13}$$

with

$$d_\pm = \frac{1}{q_n} \ln \big[\frac{L(t_0, T_n)}{K} \big] \pm \frac{q_n}{2}, \tag{4.14}$$

where

$$q_n^2 = \int_{t_0}^{t_*} dt \int_{T_n}^{T_{n+1}} dx \int_{T_n}^{T_{n+1}} dx' M_\gamma(x, x'; t). \tag{4.15}$$

In this simulation, the caplet price is obtained by performing an average over payoff $\mathcal{P}_*^{(l)}$ for each sample configuration $L^{(l)}(t, T_n)$, so that

$$\begin{aligned} \tilde{C}aplet(t_0, t_*, T_n) &= \ell VB(t_0, T_{n+1}) \frac{1}{\mathcal{N}} \sum_{l=1}^{\mathcal{N}} E\big[\mathcal{P}_*^{(l)}\big]_+ \\ &= \ell VB(t_0, T_{n+1}) \frac{1}{\mathcal{N}} \sum_{l=1}^{\mathcal{N}} \big[L^{(l)}(t_*, T_n) - K \big]_+, \end{aligned} \tag{4.16}$$

where $\mathcal{N}$ is the total number of configurations used for averaging the expectation values. The domain of the payoff function is shown in Figure 4.3.

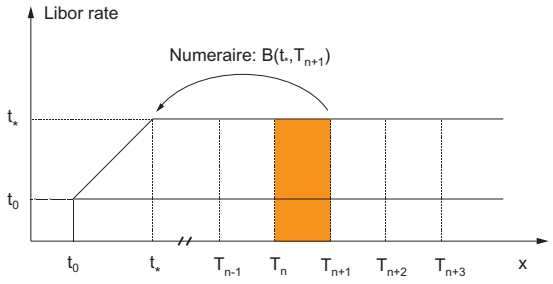

Figure 4.3: The forward bond numeraire $B(t, T_{n+1})$ are used for discounting the caplet price $Caplet(t_*, t_*, T_n)$. The shaded area is the time interval for caplet.

The maturity time t_* of caplet is set to be 180 days and T_n is set to be equal to 360 days. As shown in Equation 4.14, the key term in pricing the caplet is the value of q_n^2 which is of

order γ^2. In order to test the stability of our simulation, the deterministic volatility function $\gamma(t,x)$ is multiplied with different constant number 1 and 100. Other values between 1 and 100 are not tested because the simulation with $\gamma = 100\gamma_M$ also works very well. The parameters for the simulation of caplet are shown in Table 4.1.

Table 4.1: The parameters used in the simulation of a mid-curve caplet.

ϵ	ℓ	t_*	T_I	T_n	Strike price	Number of configurations
1 day	90 days	180 days	360 days	360 days	$0.2 < K < 0.3$	$\mathcal{N} = 10^5$

The simulation results are compared with the exact price of Black's Caplet formula. As expected, shown in Figure 4.4(a) and 4.4(b), the Black's caplet price is in the range of Monte Carlo error even when the value of q_n^2 is up to 1.5.

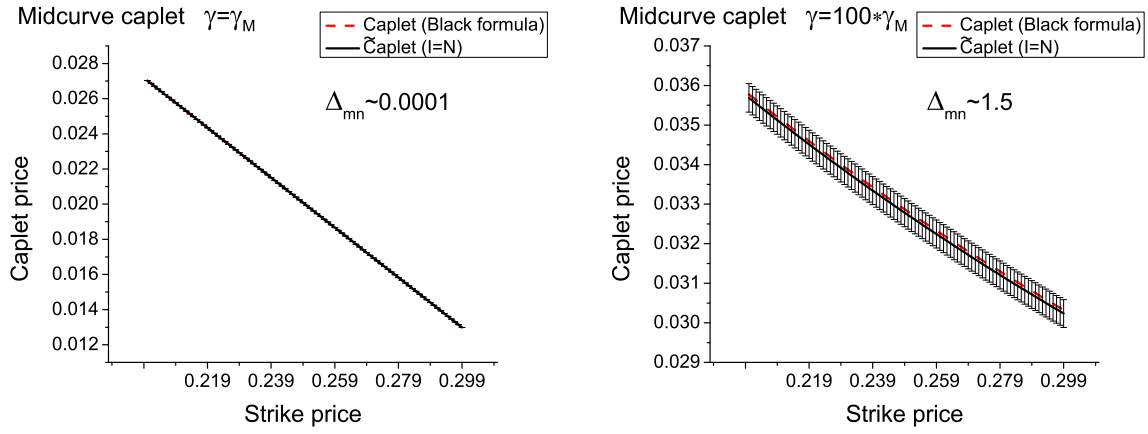

(a) (b)

Figure 4.4: Mid-curve caplet price: comparison between simulation and approximate price. The error bars are Monte Carlo errors of the simulation. (a) $\gamma = \gamma_M$. (b) $\gamma = 100\gamma_M$.

§ 4.5 Pricing Caplet by changing numeraire

Note the above results for the Caplet price have been obtained when the drift $\xi(t,T_n)$ is zero. Since the stochastic drift $\xi(t,T_n)$ is the most important term in the Libor Market Model, the simulation of caplet price with nontrivial drift needs to be investigated. It is well-known that the caplet price $Caplet(t_0,t_*,T_n)$ is invariant under different forward bond numeraire

$B(t, T_{I+1})$, as shown in Equation 4.11. Taking the case of $I = n+1$ for instance, the Equation 4.11 can be rewritten as

$$\begin{aligned}
\frac{Caplet(t_0, t_*, T_n)}{\ell V B(t_0, T_{n+1})} &= \frac{B(t_0, T_{I+1})}{B(t_0, T_{n+1})} E\Big[(L(t_*, T_n) - K)_+ \frac{B(t_*, T_{n+1})}{B(t_*, T_{I+1})}\Big]_+ \\
&= \frac{B(t_0, T_{n+2})}{B(t_0, T_{n+1})} E\Big[(L(t_*, T_n) - K)_+ \frac{B(t_*, T_{n+1})}{B(t_*, T_{n+2})}\Big]_+ \\
&= \frac{1}{1 + \ell L(t_0, T_{n+1})} \times \\
&\quad E\Big[(L(t_*, T_n) - K)_+ \big\{1 + \ell L(t_*, T_{n+1})\big\}\Big]_+ \qquad (4.17)
\end{aligned}$$

in which $L(t_*, T_n)$ from Equation 2.52 has the nontrivial drift $\xi_n = -\frac{\ell L(t, T_{n+1})}{1+\ell L(t, T_{n+1})} \Lambda_{mn}(t)$ for the case of $I = n + 1$. Figure 4.5(a) shows the $Caplet(t_0, t_*, T_n)$ using $B(t, T_{n+2})$ as the forward bond numeraire. Although $Caplet(t_0, t_*, T_n)$ is only defined on the time interval from T_n to T_{n+1}, the Libor rates $L(t_*, T_{n+1})$ is still needed to cancel the negative drift. Hence, the expectation value in Equation 4.17 cannot be solved analytically and can only be evaluated using the simulation method.

To investigate and understand the invariance of caplet price with nontrivial drift, the cases of $I = n-2$, $I = n-1$, $I = n+1$ and $I = n+2$ are simulated and compared with Black's caplet price respectively. Figures 4.5(a), 4.5(b), 4.5(c) and 4.5(d) illustrate the $Caplet(t_0, t_*, T_n)$ using $B(t, T_{n+2})$, $B(t, T_n)$, $B(t, T_{n-1})$ and $B(t, T_{n+3})$ as the discounting numeraire.

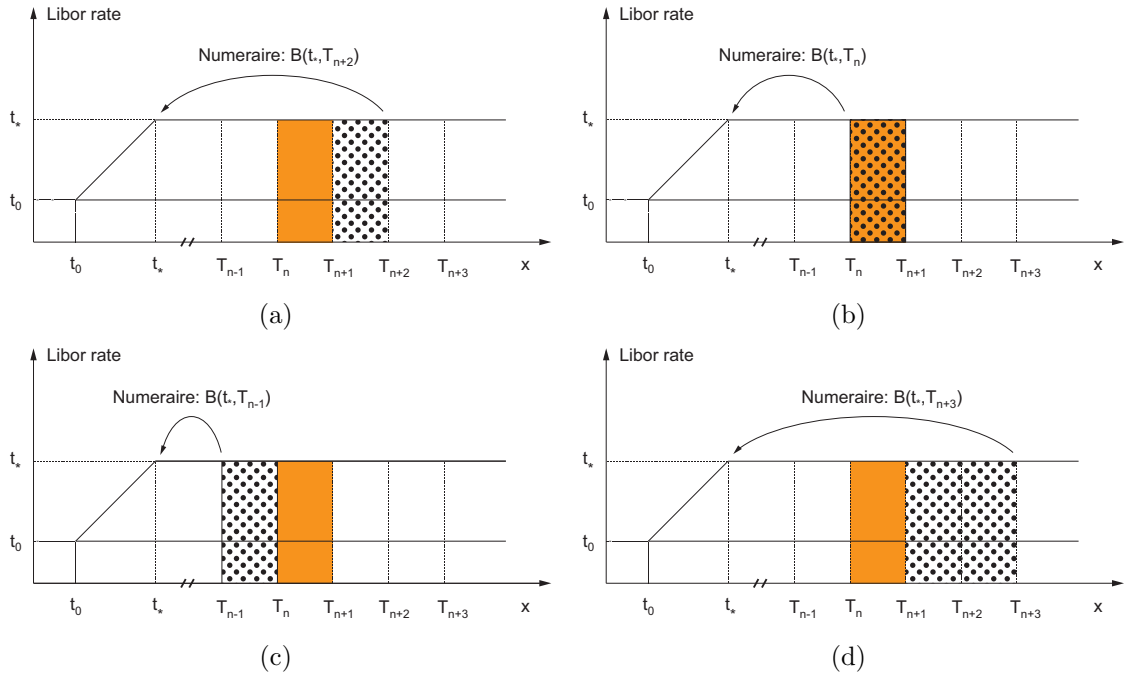

Figure 4.5: Four different forward bond numeraire are used for discounting the caplet price $Caplet(t_*, t_*, T_n)$. The shaded area is the time interval for caplet, and the area of dots denotes the additional Libor rates that are used for different numeraire. (a) $B(t, T_{n+2})$. (b) $B(t, T_n)$. (c) $B(t, T_{n-1})$. (d) $B(t, T_{n+3})$.

Only the results of $60\gamma_M$ and $100\gamma_M$ are stated here since the simulation works for any large value of γ. Figure 4.6 and 4.7(a) shows the caplet price using simulation under different forward bond numeraire for $60\gamma_M$ and $100\gamma_M$ respectively. In all cases, the exact caplet price is in the range of Monte Carlo error of simulation, which is not plotted in Figure 4.6 and 4.7(a). As expected, shown in Figure 4.6, the caplet price is invariant for different forward bond numeraire. However, as shown in Figure 4.7(a), the caplet price of $I = n - 1$ and $I = n - 2$ is lower than zero drift, while the caplet price of $I = n + 1$ and $I = n + 2$ is a little larger. This result is different from the result of $60\gamma_M$ for the reason that the Monte Carlo error can be quite large for the case of $100\gamma_M$. Compared to the case of zero drift $I = n$, shown in Figure 4.7(b), the Monte Carlo error increases as I increases. This is because that the Monte Carlo error is calculated from the expectation value of payoff function, which is

given by

$$\frac{Caplet(t_0,t_*,T_n)}{\ell VB(t_0,T_{I+1})}\begin{cases} = E_I\Big[(L(t_*,T_n)-K)_+\dfrac{1}{(1+\ell L(t_*,T_n))(1+\ell L(t_*,T_{n-1}))}\Big]_+, & I=n-2 \\ = E_I\Big[(L(t_*,T_n)-K)_+\dfrac{1}{(1+\ell L(t_*,T_n))}\Big]_+, & I=n-1 \\ = E_I\Big[(L(t_*,T_n)-K)_+(1+\ell L(t_*,T_{n+1})\Big]_+, & I=n+1 \\ = E_I\Big[(L(t_*,T_n)-K)_+(1+\ell L(t_*,T_{n+1})(1+\ell L(t_*,T_{n+2})\Big]_+, & I=n+2 \end{cases} \tag{4.18}$$

where $E_I[...]$ denotes the expectation value for different numeraire $B(t,T_{I+1})$. As shown in Equation 4.18, the fluctuation of the expectation value increases when I increases, and hence the Monte Carlo error increases with increasing I. The caplet price of $I=n-2$ is closest to the exact price because of its smallest Monte Carlo error while the caplet price of $I=n+2$ has biggest difference with the exact price. All simulation results are within the Monte Carlo error. The Monte Carlo error can be reduced when the sample size $\mathcal{N}$ is increased. As expected, shown in Figure 4.8, the simulation results are nearly the same with the Black's caplet price. This provides clear evidence that the price of Caplet is invariant if a different numeraire is used. The test of changing forward bond numeraire appears to confirm the correctness of our simulation and suggests that other instruments can be priced using the simulation method.

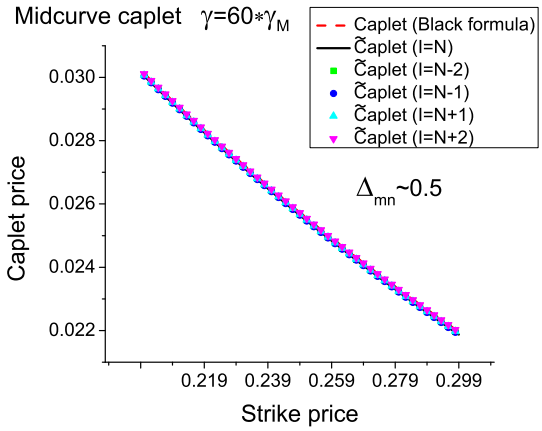

Figure 4.6: The plot of Mid-curve caplet price using different forward bond numeraire with $\gamma = 60\gamma_M$, and the dash line are the caplet price of Black's caplet formula.

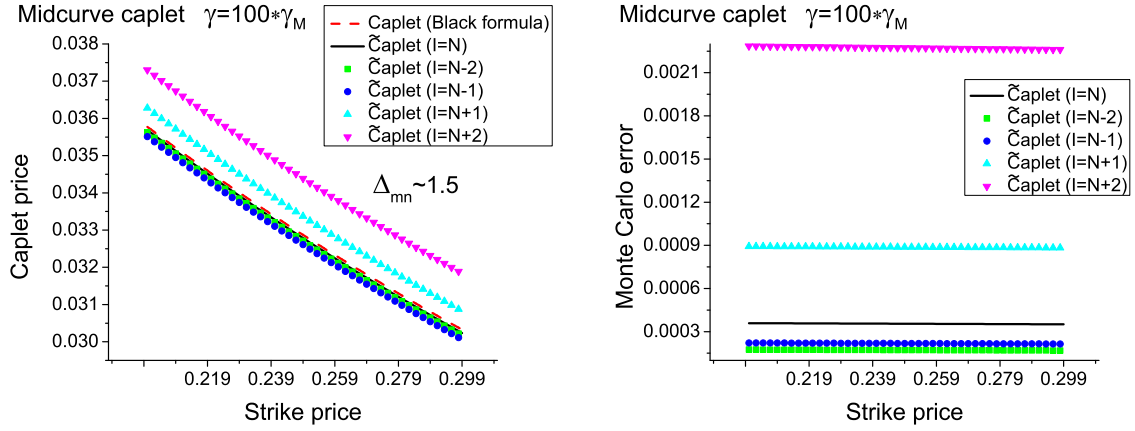

(a) (b)

Figure 4.7: (a) The plot of Mid-curve caplet price using different forward bond numeraire with $\gamma = 100\gamma_M$, and the dash line are the caplet price of Black's caplet formula. (b) Monte Carlo errors of simulation for the cases of using different forward bond numeraire.

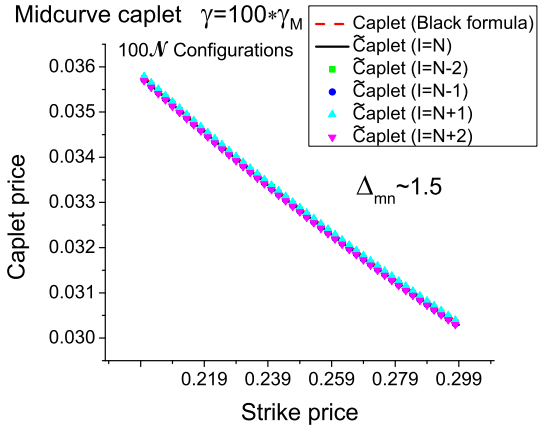

Figure 4.8: The plot of Mid-curve caplet price using different forward bond numeraire with $\gamma = 100\gamma_M$, and the sample configurations is $100\mathcal{N}$ (1×10^7).

§ 4.6 Zero coupon bond option

The volatility expansion for Libor interest rates is extensively studied in [47], with the approximation of integral drift β_n given up to the order of γ^2. Summarizing the results of volatility

expansion yields

$$\begin{aligned} L(t,T_n) &= L(t_0,T_n)e^{\beta_n(t)+W_n(t)} \simeq L(t_0,T_n)e^{\beta_n^{(0)}(t)+W_n(t)} \\ &= \tilde{L}(t_0,T_n) + L(t_0,T_n)(e^{W_n}-1) + O(\gamma^3), \end{aligned} \tag{4.19}$$

where

$$\tilde{L}(t_0,T_n) = L(t_0,T_n)e^{\beta_n^{(0)}}, \tag{4.20}$$

$$\beta_n^{(0)} = \beta_n^{(0)}(t_0,t,T_i) = \sum_{m=0}^{n} \Delta_{mn}\frac{\ell L(t_0,T_m)}{1+\ell L(t_0,T_m)} = O(\gamma^2), \tag{4.21}$$

and

$$\Delta_{mn} = \int_{t_0}^{t} dt' \Lambda_{mn}(t') = O(\gamma^2). \tag{4.22}$$

In Equation 4.19, the drift term is subtracted from Libor rate $L(t,T_n)$. Thus, the expectation value can be calculated analytically because that the expectation value over $(e^{W_n}-1)$ can be obtained by performing Gaussian integration directly. The two expectation values that are used for pricing the options are given by

$$E[e^{W_n}-1] = 0, \tag{4.23}$$

$$E[(e^{W_m}-1)(e^{W_n}-1)] = e^{\Delta_{mn}} - 1 \simeq \Delta_{mn} + O(\gamma^4). \tag{4.24}$$

Suppose a zero coupon bond $B(T_0,T_n)$ is issued at Libor calendar time T_0 and matures at T_n; the payoff function for this zero coupon bond is given by

$$\mathcal{P} = [B(T_0,T_n) - K]_+. \tag{4.25}$$

For the forward numeraire, the call price at present time t_0, denoted by $C(t_0,T_0,K)$, is derived by using forward bond numeraire $B(t_0,T_0)$ and is given by

$$C(t_0,T_0,K) = B(t_0,T_0)E[B(T_0,T_n) - K]_+. \tag{4.26}$$

As discussed in [47], the call price of zero coupon bond is as follows

$$C(t_0,T_0,K) = \frac{1}{\sqrt{2\pi}}B(t_0,T_0)\tilde{F}(t_0,T_0,T_n)I(X)\sqrt{C_2 - C_1^2} + O(\gamma^3), \tag{4.27}$$

where

$$\begin{aligned}
I(X) &= \int_{-\infty}^{+\infty} dQ(Q-X)_+ e^{-\frac{1}{2}Q^2} = e^{-\frac{1}{2}X^2} - \sqrt{2\pi}X(1-N(X)), \\
X &= \frac{\tilde{K}-C_1}{\sqrt{C_2-C_1^2}}; \quad \tilde{K} = \frac{K}{\tilde{F}(t_0,T_0,T_n)} - 1, \\
C_1 &= \frac{1}{2}\sum_{i=0}^{n-1} a_i^2\Delta_{ii} + \frac{1}{2}\sum_{i,j=0}^{n-1} a_i a_j \Delta_{ij}, \\
C_2 &= \sum_{i,j=0}^{n-1} a_i a_j \Delta_{ij}, \\
\tilde{F}(t_0,T_0,T_n) &= \prod_{i=0}^{n-1} \frac{1}{1+\ell\tilde{L}(t_0,T_i)}; \quad a_i = \frac{\ell L(t_0,T_i)}{1+\ell L(t_0,T_i)}.
\end{aligned} \tag{4.28}$$

In order to test our simulation for the mid-curve option that matures at time t_*, the forward bond $F(t_*,T_0,T_n)$ is used to replace the zero coupon bond $B(T_0,T_n)$. The forward price of $B(t,T)$, at earlier time t denoted by $F(t,T_0,T_n+\ell)$, is given by

$$F(t,T_0,T_n+\ell) = \frac{B(t,T_{n+1})}{B(t,T_0)} = \prod_{i=0}^{n} \frac{1}{1+\ell L(t,T_i)}, \tag{4.29}$$

and the mid-curve zero coupon bond option maturing at t_* is hence given by

$$C(t_0,t_*,T_0,K) = B(t_0,T_0)E[F(t_*,T_0,T_n)-K]_+ \tag{4.30}$$

and is more general than the payoff function shown in Equation 4.26. Using Monte Carlo simulation, the call price of zero coupon bond is obtained by performing an average over $\mathcal{N}$ number of configurations and is given by

$$\tilde{C}(t_0,t_*,T_0,K) = B(t_0,T_0)\frac{1}{\mathcal{N}}\sum_{l=1}^{\mathcal{N}} \left[F^{(l)}(t_*,T_0,T_n)-K\right]_+, \tag{4.31}$$

where $F^{(l)}(t_*,T_0,T_n)$ denotes the forward bond price on Libor rates $L(t_*,T_i)$ for the lth configuration and can be calculated in terms of Libor rates using the simulation.

For pricing the Libor zero coupon bond mid-curve option, the maturity time t_* is set to be 180 days while T_n is chosen to be 900 days. The parameters for the simulation of zero coupon bond are shown in Table 4.2.

Table 4.2: The parameters used in the simulation of Libor zero coupon bond option.

ϵ	ℓ	t_*	T_0	T_n	Strike price	Number of configurations
1 day	90 days	180 days	270 days	900 days	$0.4 < K < 0.5$	$\mathcal{N} = 10^5$

The simulation of the option price $\tilde{C}(t_0, T_0, K)$ is plotted and compared with the approximate price, which is based on the volatility expansion with an accuracy of $O(\gamma^2)$. As expected, shown in Figure 4.9(a), the simulation results are exactly the same with approximate price when $\gamma = \gamma_M$ in which γ is order of 0.01. However, the approximate price has a little difference with the option price of simulation when $\gamma = 30\gamma_M$ in which Δ_{mn} is around 0.1 (shown in Figure 4.9(b)). The absolute error for this case is around 2% and this small difference can still be accepted in practice. The approximate price tends to have large error when $\gamma = 60\gamma_M$ and $\gamma = 100\gamma_M$ (shown in Figure 4.9(c) and 4.9(d)), and the volatility expansion fails to give the accurate approximation.

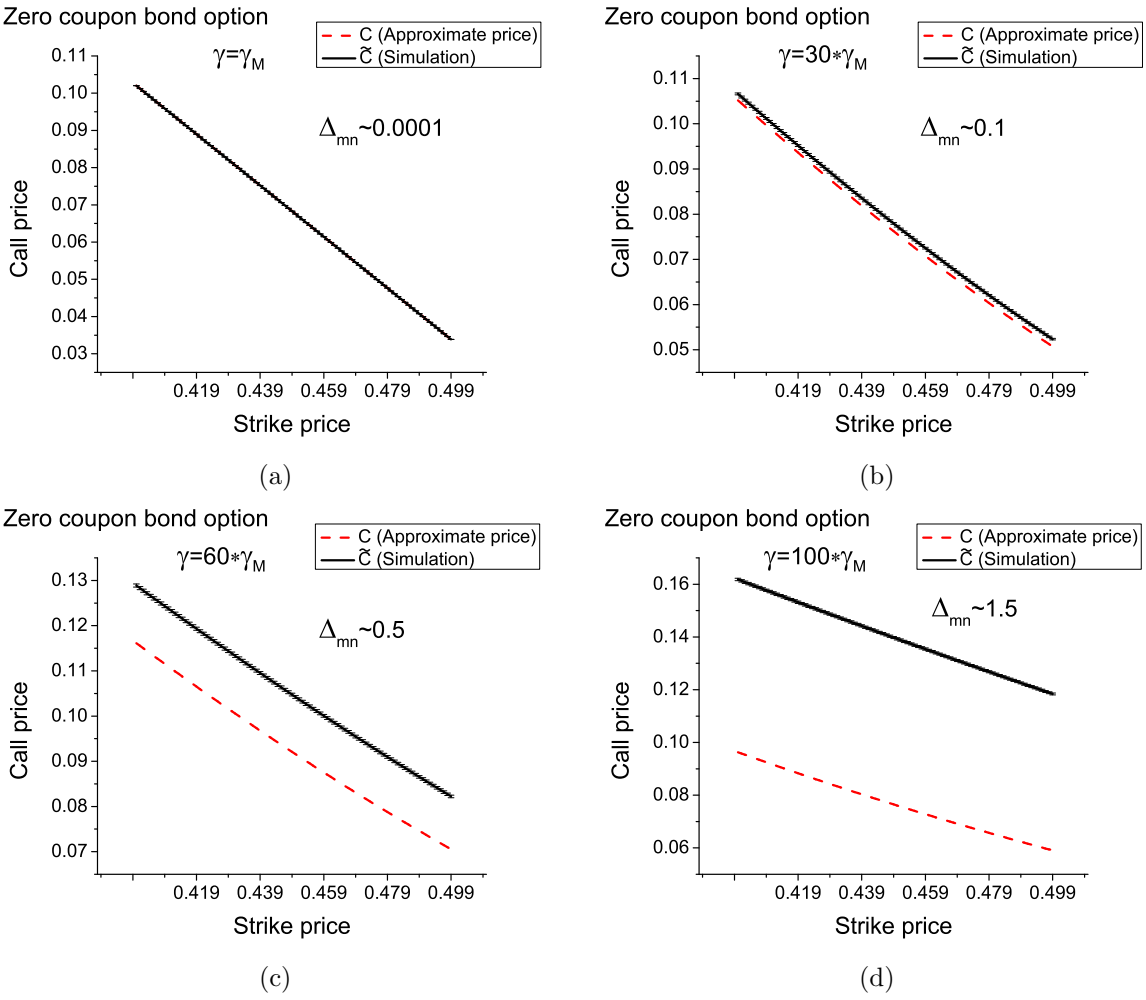

Figure 4.9: Libor zero coupon bond option with maturity $t_* = 180$ days: comparison between simulation and approximate price. The error bars are Monte Carlo errors of the simulation. (a) $\gamma = \gamma_M$. (b) $\gamma = 30\gamma_M$. (c) $\gamma = 60\gamma_M$. (d) $\gamma = 100\gamma_M$.

The approximation price is based on the value of Δ_{mn}, hence the reasonable range of Δ_{mn} is critical for the validity of approximate price. To investigate the relationship between the accuracy of approximate price and value of Δ_{mn}, the simulation results are obtained by varying the value of constant γ. This means that the value of γ is fixed to be a constant for all future time and the call price is calculated for different value of γ. In order to reduce the influence of strike price on the comparison, the strike price is fixed to be $B(t_0, T_n)$ which is the case of at the money option. Figure 4.10 shows the comparison between simulation results and approximate price for different value of γ. Since the expansion is in term of Δ_{mn} and the value of Δ_{nn} is the largest value among Δ_{mn}, the value of Δ_{nn} is given as the x axis instead of

γ. It is shown that the approximate price works well when $\Delta_{mn} < 0.1$ and differs much with simulation results when Δ_{mn} becomes larger than 0.4. This finding is of crucial importance because that one can calculate the Δ_{mn} from market data and apply the approximate formula in the accepted range.

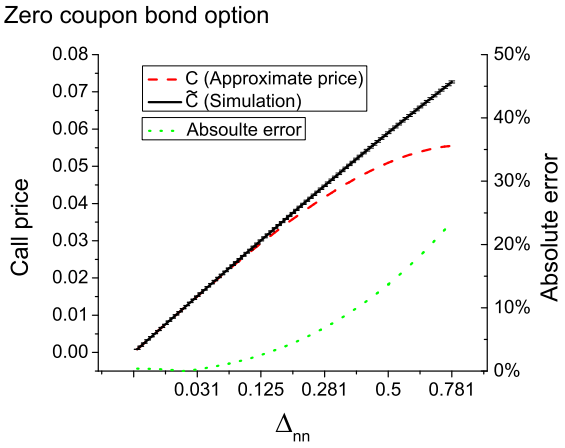

Figure 4.10: Libor zero coupon bond option price is calculated. Results of simulation are compared with approximate price when Δ_{nn} is from 0 to 0.8 (the volatility γ is changed from 0 to 5 to vary the value of Δ_{nn}).

§ 4.7 Coupon bond option

The price of a coupon bond that matures at time T_0 and pays coupons C_I at time T_I, is given by

$$\mathcal{B}(T_0) = \sum_{I=1}^{N_c} c_I B(T_0, T_I). \tag{4.32}$$

The call option price of this coupon bond option at present time $t_0 < T_0$, under the measure $B(t, T_0)$, is given by

$$\begin{aligned} C(t_0, T_0, K) &= B(t_0, T_0) E[\mathcal{P}]_+ \\ &= B(t_0, T_0) E\Big[\sum_{I=1}^{N_c} c_I B(T_0, T_I) - K\Big]_+. \end{aligned} \tag{4.33}$$

The approximate price of coupon bond option is discussed in [47]. However, an different expansion of $L(T_0, T_n)$ is used and is given by

$$L(T_0, T_n) = L(t_0, T_n) + L(t_0, T_n)(\beta_n^{(0)} + e^{W_n} - 1) + O(\gamma^3). \tag{4.34}$$

This expansion has, in principle, small difference with Equation 4.19. To make the approximate price of coupon bond same as the approximation used in zero coupon bond, we use Equation 4.19 for the expansion of coupon bond option. Using the same approach of expansion used for zero coupon bond, we get the following approximate price

$$C(t_0, T_0, K) = \frac{1}{\sqrt{2\pi}} B(t_0, T_0) I(X) \sqrt{C_2 - C_1^2} + O(\gamma^3). \tag{4.35}$$

where

$$\begin{aligned}
X &= \frac{K - \tilde{F} - C_1}{\sqrt{C_2 - C_1^2}}, \\
\tilde{F} &= \sum_{I=1}^{N_c} \tilde{J}_I; \quad \tilde{J}_I = c_I \tilde{F}(t_0, T_0, T_I), \\
C_1 &= \sum_{I=1}^{N_c} \tilde{J}_I B_I; \quad B_I = \frac{1}{2} \sum_{i=0}^{I-1} a_i^2 \Delta_{ii} + \frac{1}{2} \sum_{i,j=0}^{I-1} a_i a_j \Delta_{ij}, \\
C_2 &= \sum_{I=1}^{N_c} \sum_{L=1}^{N_c} \tilde{J}_I \tilde{J}_L \sum_{i=1}^{I-1} \sum_{j=1}^{L-1} a_i a_j \Delta_{ij}.
\end{aligned} \tag{4.36}$$

Similar with the case of zero coupon bond option, instead of $B(T_0, T_I)$, the forward bond $F(t_*, T_0, T_I)$ is used in the payoff function for the mid-curve and is given by

$$C(t_0, t_*, T_0, K) = B(t_0, T_0) E\Big[\sum_{I=1}^{N_c} c_I F(t_*, T_0, T_I) - K\Big]_+. \tag{4.37}$$

The option price by using simulation, denoted by $\tilde{C}(t_0, t_*, T_0, K)$, is given by

$$\tilde{C}(t_0, t_*, T_0, K) = B(t_0, T_0) \frac{1}{\mathcal{N}} \sum_{l=1}^{\mathcal{N}} \Big[\sum_{I=1}^{N_c} c_I F^{(l)}(t_*, T_0, T_I) - K\Big]_+. \tag{4.38}$$

Consider a coupon bond issued at time $t_* = 180$ days that pays fixed dividends at two different future time $T_1 = 540$ days and $T_2 = 900$ days, with coefficients $c_1 = 0.5$ and $c_2 = 1.5$.

The same set of parameters, which is shown in Table 4.2, is also used for the simulation of coupon bonds except that the range of strike price is from 0.8 to 0.9.

As discussed above, same expansion and approximation used for the zero coupon bond option are used to obtain the approximate price of coupon bond options. The reasonable working range of approximation for coupon bond should be same with for zero coupon bond because the coupon bond is simply the combination of N_c zero coupon bonds. Figure 4.11(a) and 4.11(b) show the comparison between simulation results and approximate price. Similar to the conclusion for zero coupon bond option, the approximate price works quite well for the cases of $\gamma = \gamma_M$ and $\gamma = 30\gamma_M$. As shown in Figure 4.11(c) and 4.11(d), the approximate price fails when $\gamma = 60\gamma_M$ and $\gamma = 100\gamma_M$.

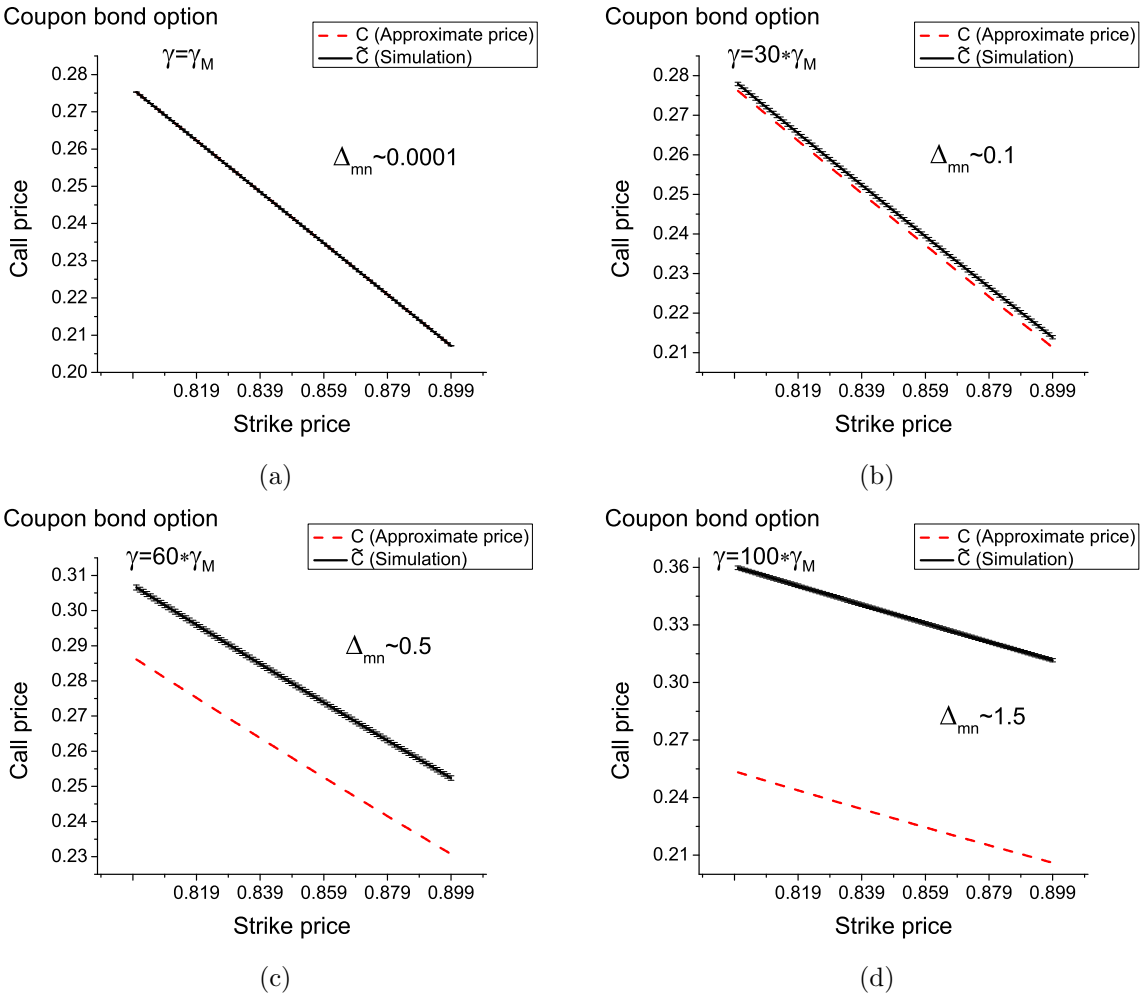

Figure 4.11: Coupon bond European option with number of bonds $N_c = 2$, t_*=180 days: comparison between simulation and approximate price. Different future times T_1 and T_2 are fixed at 540 and 900 days with $c_1 = 0.5$ and $c_2 = 1.5$. The error bars are Monte Carlo errors of the simulation. (a) $\gamma = \gamma_M$. (b) $\gamma = 30\gamma_M$. (c) $\gamma = 60\gamma_M$. (d) $\gamma = 100\gamma_M$.

The simulation results for at the money coupon bond option are calculated. The at the money coupon bond option price at present time t_0 is given by

$$\begin{aligned} C(t_0, t_*, T_0, K) &= B(t_0, T_0) E\big[\mathcal{P}\big]_+ \\ &= B(t_0, T_0) E\Big[\sum_{I=1}^{N} \big(c_I F(t_*, T_0, T_I) - c_I B(t_0, T_I)\big)\Big]_+ . \end{aligned} \tag{4.39}$$

As same with zero coupon bond option, at the money coupon bond option price is calculated for different value of constant γ. As shown in Figure 4.12, the approximate price give accurate

results when Δ_{mn} is smaller than 0.1 and fails when Δ_{mn} is much larger. Likewise, the working range of approximate price for coupon bond options is $0 \leq \Delta_{mn} \leq 0.1$.

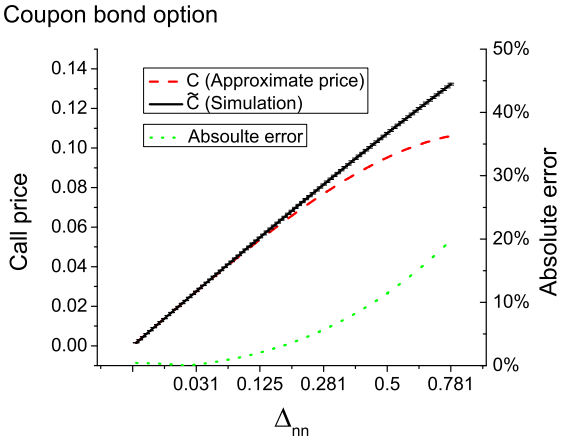

Figure 4.12: Coupon bond European option price is calculated (number of bonds $N_c = 2$, t_*=180 days). Different future times T_1 and T_2 are fixed at 540 and 900 days with $c_1 = 0.5$ and $c_2 = 1.5$. Results of simulation are compared with approximate price when Δ_{nn} is from 0 to 0.8 (the volatility γ is changed from 0 to 5 to vary the value of Δ_{nn}).

§ 4.8 Swaption

Suppose a Libor swaption that matures at calendar time T_0, with swap payments being made at times $T_n = T_0 + \ell n$. The first swap payment is made at time T_1 and final payment is made at T_N. The swaption price for receiving the interest rate payments at the floating rate and paying at a fixed interest, at present Libor time t_0, is given by

$$\begin{aligned} C(t_0, T_0; R_s) &= E\big[swap_L(T_0, R_s)\big]_+ \\ &= \ell V B(t_0, T_0) E\Big[\sum_{n=0}^{N-1} B(T_0, T_n + \ell)\{L(T_0, T_n) - R_s\}\Big]_+ . \end{aligned} \tag{4.40}$$

Based on the volatility expansion of Libor rates, the approximate price of swaption also can be derived. Summarizing the results of approximate price for swaption in [47] yields

$$C(t_0, t_*, T, K) = \frac{1}{\sqrt{2\pi}} \ell V B(t_0, T_0) I(X) \sqrt{C_2 - C_1^2}, \tag{4.41}$$

where

$$
\begin{aligned}
X &= \frac{\tilde{K} - C_1}{\sqrt{C_2 - C_1^2}}, \\
\tilde{K} &= \sum_{n=0}^{N-1} \tilde{F}(t_0, T_0, T_n + \ell)[R_s - \tilde{L}(t_0, T_n)], \\
C_1 &= \sum_{n=0}^{N-1} \tilde{F}(t_0, T_0, T_n + \ell)\Big\{ - L(t_0, T_n) \sum_{i=0}^{n} a_i \Delta_{ni} + \frac{1}{2}[\tilde{L}(t_0, T_n) - R_s] \\
&\quad \times \big(\sum_{i=0}^{n} a_i^2 \Delta_{ii} + \sum_{i,j=0}^{n} a_i a_j \Delta_{ij} \big) \Big\}, \\
C_2 &= \sum_{m,n=0}^{N-1} \tilde{F}(t_0, T_0, T_m + \ell) \tilde{F}(t_0, T_0, T_n + \ell) \Big\{ L(t_0, T_m) L(t_0, T_n) \Delta_{mn} - 2L(t_0, T_m) \\
&\quad \times [\tilde{L}(t_0, T_n) - R_s] \sum_{i=0}^{n} a_i \Delta_{mi} + [\tilde{L}(t_0, T_n) - R_s][\tilde{L}(t_0, T_m) - R_s] \sum_{i=0}^{m} \sum_{j=0}^{n} a_i a_j \Delta_{ij} \Big\}.
\end{aligned}
$$

Following the same procedure used in coupon bond options and replacing the bond $B(T_0, T_n + \ell)$ with the forward bond $F(t_*, T_0, T_n + \ell)$ in the payoff function, the mid-curve swaption price we used is given by

$$
\begin{aligned}
C(t_0, t_*, T_0; R_s) &= E\big[swap_L(T_0, R_s)\big]_+ \\
&= \ell V B(t_0, T_0) E\Big[\sum_{n=0}^{N-1} F(t_*, T_0, T_n + \ell)\{L(t_*, T_n) - R_s\} \Big]_+ . \qquad (4.42)
\end{aligned}
$$

The swaption price of simulation, denoted by $\tilde{C}(t_0, t_*, T_0, K)$, is then given by

$$
\tilde{C}(t_0, t_*, T_0; R_s) = \ell V B(t_0, T_0) \frac{1}{\mathcal{N}} \sum_{l=1}^{\mathcal{N}} \Big[\sum_{n=0}^{N-1} F^{(l)}(t_*, T_0, T_n + \ell)\{L^{(l)}(t_*, T_n) - R_s\} \Big]_+ \qquad (4.43)
$$

The parameters, shown in Table 4.3, are used for pricing European swaptions. T_{N-1} is equal to 900 days and hence n=0,1,... 10.

Table 4.3: The parameters used in the simulation of European swaption.

ϵ	ℓ	t_*	T_0	T_{N-1}	Strike price	Number of configurations
1 day	90 days	180 days	270 days	900 days	$0.25 < K < 0.35$	$\mathcal{N} = 10^5$

Figure 4.13(a), 4.13(b), 4.13(c) and 4.13(d) show the comparison of simulation results with approximate price for European swaption for different magnitude of γ. Similar to the discussion for zero coupon bond and coupon bond options, at the money European swaption is calculated using both simulation and approximate formula. Figure 4.14 shows the comparison for different value of constant γ. Δ_{nn} denotes for the value of $\Delta_{N-1,N-1}$ because that the value of Δ_{nn} is the largest among Δ_{mn} when $n = N - 1$. The value of R_s function used for plotting Figure 4.14 is

$$R_s = L(t_0, T_n). \tag{4.44}$$

It seems that the error of the approximate price of swaption is smaller than zero coupon bond option and the coupon bond option when Δ_{mn} is large. This is because since the swaption is not the combination of zero coupon bond or similar to coupon bond option, the error of approximate prices may cancel and become smaller. However, similar to coupon bond options, the approximate price of swaption works very well when $\Delta_{mn} < 0.1$.

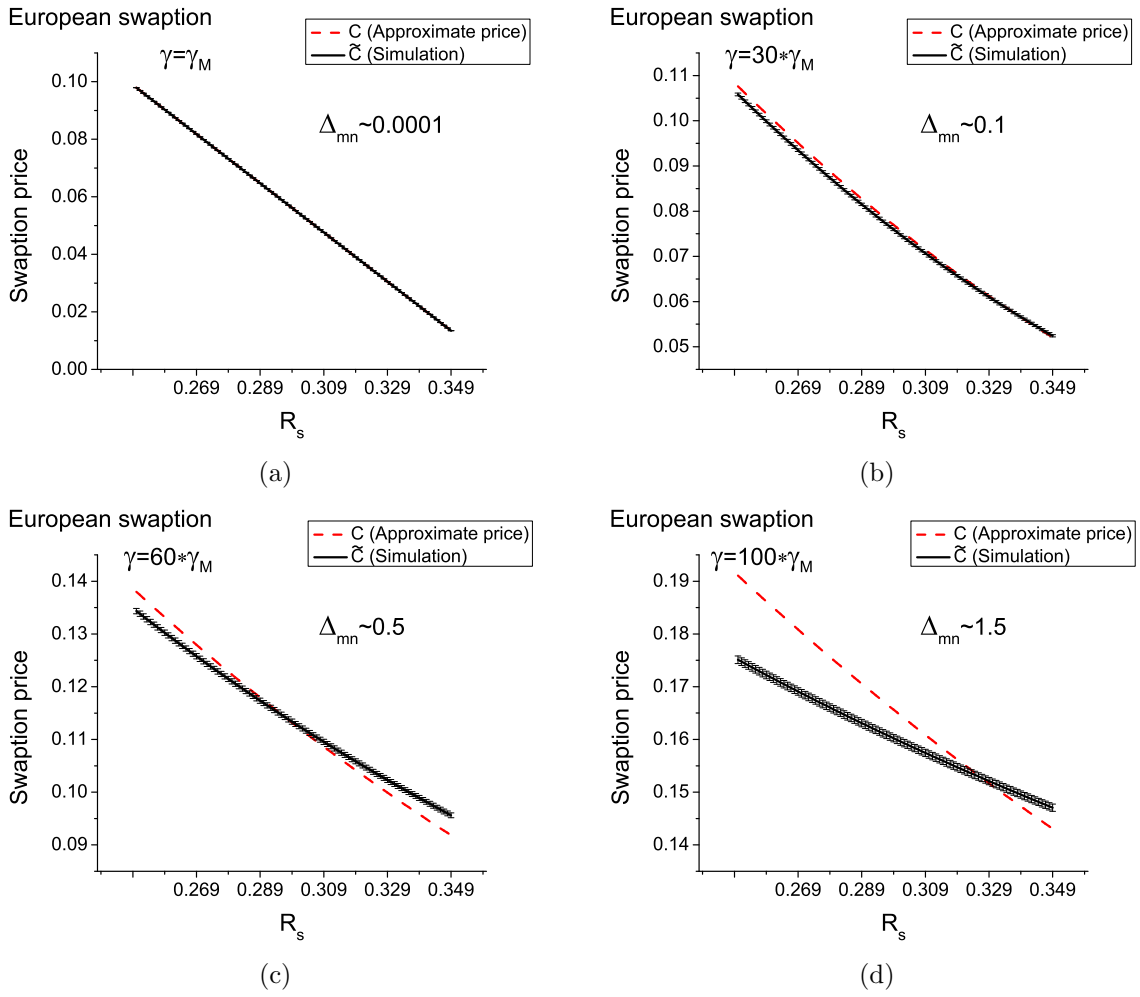

Figure 4.13: European swaption price with maturity t_*=180 days: comparison between simulation and approximate price. The error bars are Monte Carlo errors of the simulation. (a) $\gamma = \gamma_M$. (b) $\gamma = 30\gamma_M$. (c) $\gamma = 60\gamma_M$. (d) $\gamma = 100\gamma_M$.

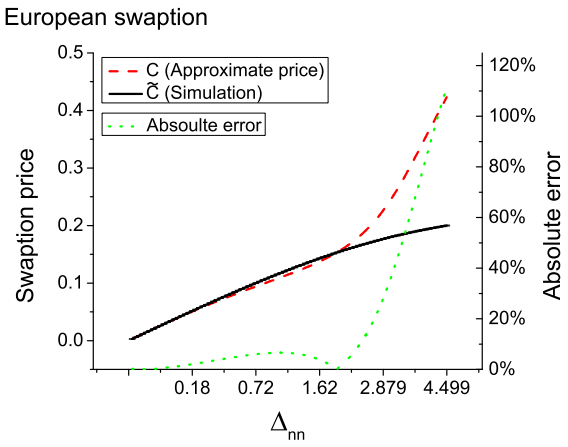

Figure 4.14: European swaption price is calculated. Results of simulation are compared with approximate price when Δ_{nn} is from 0 to 4.5 (the volatility γ is changed from 0 to 12 to vary the value of Δ_{nn}).

§ 4.9 Conclusion

The primary objective of this study was to explore the advantages of numerically simulating Libor Market Model. The simulation method of numerically updating Libor rates, in the frame work of quantum finance, was examined and used to price interest rate instruments. The Libor rates were updated daily in calendar time and ℓ in future time. The quantum field $A(t, x)$ was generated to incorporate the correlation contained in stiff propagator.

The caplet price was analyzed and compared with the well known Black's caplet formula. It was found that the simulated caplet price fits the Black's caplet formula quite well. Caplet price is invariant for different forward bond measure, and this important feature was confirmed by our simulation. This study has provided clear evidence that the nontrivial drift is the key term in Libor Market Model and it yields many novel properties.

The Libor zero coupon bond option, coupon bond option and European swaption were studied in the frame work of quantum finance formulation of the Libor Market Model. The approximate price for these four instruments is based on the volatility expansion which has the limitation on the value of correlator Δ_{mn} . The simulation results show that the approximate price can give accurate results when the correlator $\Delta_{mn} < 0.1$ and fails when Δ_{mn} is much larger. The key advantage of the simulation method is that it can work at any value of correlator Δ_{mn}. This finding is of crucial importance because it shows that the simulation

method is flexible and places no limitations on the parameters. The simulation method has been shown to be a powerful technique for pricing interest rate instruments.

§ 4.10 Appendix A: The approximate price using a more accurate expansion

The comparison between simulation results and approximate price is given in sections § 4.6, § 4.7 and § 4.8 for zero coupon bond option, coupon bond options and European swaptions. The expansion for approximate price is based on Equation 4.24 and is given by

$$E[(e^{W_m} - 1)(e^{W_n} - 1)] \quad = \quad e^{\Delta_{mn}} - 1 \simeq \Delta_{mn} + O(\gamma^4).$$

The approximation of $e^{\Delta_{mn}} - 1$ is made in the above equation. This approximation is valid when value of Δ_{mn} is small and may have large error when Δ_{mn} is a large value. The large volatility γ is tested for both the simulation and approximate formula. Hence, it is reasonable to use $e^{\Delta_{mn}} - 1$ instead of Δ_{mn} for the purpose of comparison. The approximate prices for zero coupon bond option, coupon bond options and swaptions are calculated using $e^{\Delta_{mn}} - 1$, and the results of comparison between simulation and formula are shown in Figure 4.15. It is clearly that the approximate prices are improved for zero coupon bond and coupon bond European option when the value of Δ_{mn} increases. However, the approximate price doesn't give more accurate price for swaption. This result may be because a different expansion is used for obtaining the swaption price. However, these two approximate prices using Δ_{mn} and $e^{\Delta_{mn}} - 1$ are equivalent when the value of Δ_{mn} is in the range of small volatility expansion.

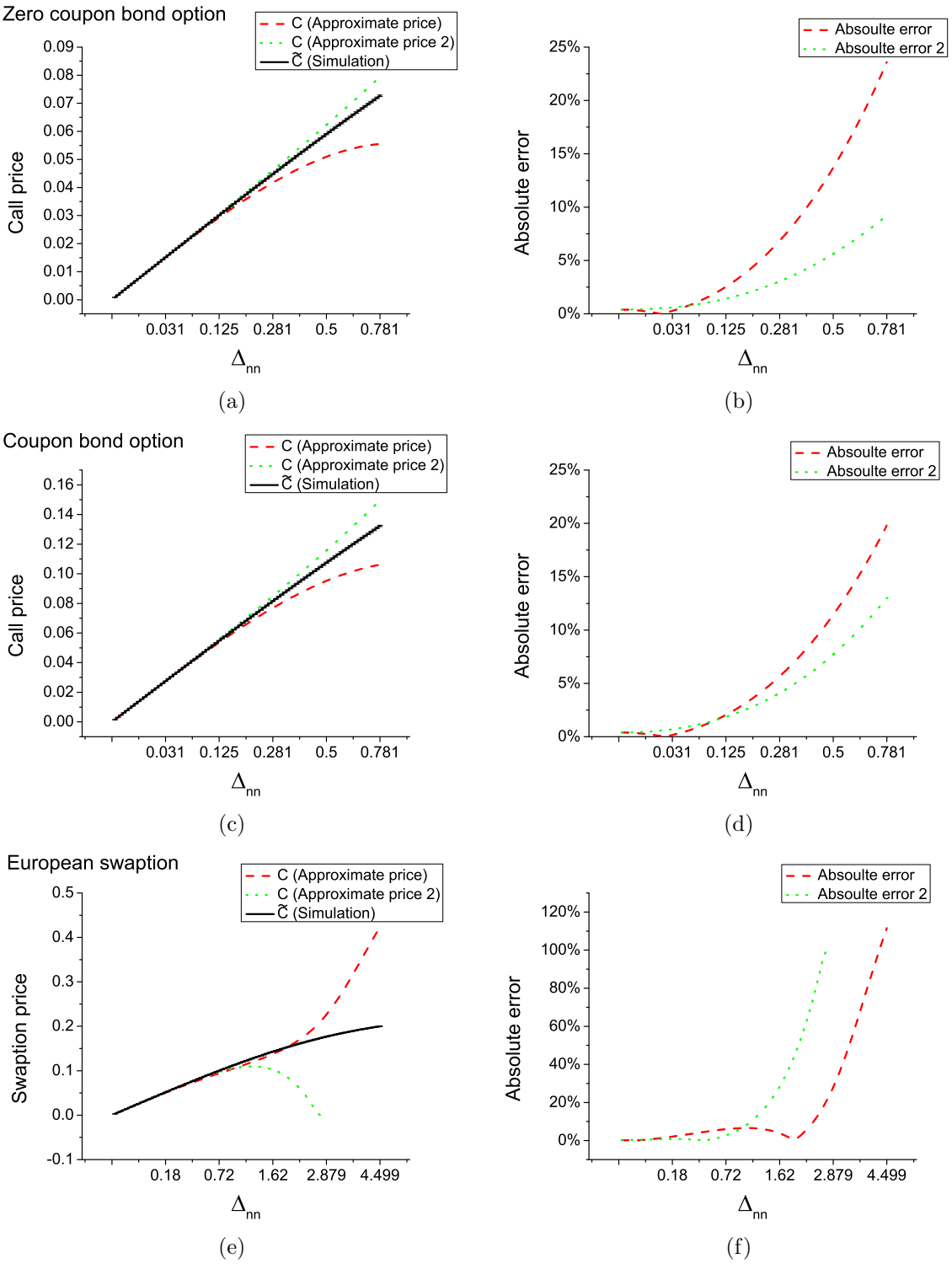

Figure 4.15: Results of simulation are compared with approximate price when the volatility γ is changed to vary the value of Δ_{nn}. Approximate price 2 denotes the results of approximate formula using $e^{\Delta_{mn}} - 1$. (a), (c) and (e) are the plot of option price while (b), (d) and (f) are the plot of absolute error.

§ 4.11 Appendix B: C++ Code

§ 4.11.1 Appendix B.1: Uniform random variables generator

To generate the Gaussian random variables, generating floating-point numbers from 0.0 to 1.0 is the first task. Uniform deviates are random numbers that lie within a specified range with equal probability for each fixed interval. For example, if the floating-point numbers from 0.0 to 1.0 are generated, the probability of generating any interval from x to $x + 0.1$ ($0 < x < x + 0.1 < 1.0$) should equal to 10%. Random number generators are very useful in Monte Carlo method simulations and all the random numbers start from the same seed. The generation of pseudo-random numbers is a critical task in computer programming.

The traditional random generators are the linear congruential generators (LCG) and the multiplicative linear congruential generators (MLCG), which have some weaknesses of such methods. The built-in generators in the C and C++ languages, especially rand() and srand(), also cannot be used for the Monte Carlo simulation because these functions are often badly flawed. To run the Monte Carlo simulation correctly, a efficient generator with long period larger than $2^{64} \approx 2 \times 10^{19}$ should be used. According to the methods introduced in [48], a random number generator with period of 8.5×10^{37} is used for our Monte Carlo simulation. As discussed in [48], this generator is enough for most applications.

The code for uniform random variables generator, denoted as "Ran.h", is given as follows

```
struct Ran {
    unsigned long long v,w;
    Ran(unsigned long long j) : v(4101842887655102017LL), w(1) {
        v ^= j;
        w = int64();
        v = int64();
    }
    inline unsigned long long int64() {
        v ^= v >> 17; v ^= v << 31; v ^= v >> 8;
        w = 4294957665U*(w & 0xffffffff) + (w >> 32);
        return v ^ w;
    }
    inline double doub() { return 5.42101086242752217E-20 * int64(); }
    inline unsigned int int32() { return (unsigned int)int64(); }
};
```

§ 4.11.2 Appendix B.2: Box-Muller transform

The Box-Muller method is used to generate independent standard normally distributed random numbers (Gaussian random variables), and uniformly distributed random numbers are the source of Box-Muller method.

Suppose x_1 and x_2 are independent uniform random variables in the interval $(0, 1]$ (denoted by $x_1, x_2 \in \mathcal{U}(0, 1)$) , the independent Gaussian random variables y_1 and y_2 , denoted by $y_1, y_2 \in N(0, 1)$, are given by [48]

$$\begin{aligned} y_1 &= R\cos(\theta) = \sqrt{-2\ln x_1}\cos(2\pi x_2), \\ y_2 &= R\sin(\theta) = \sqrt{-2\ln x_1}\sin(2\pi x_2). \end{aligned} \tag{4.45}$$

Instead of generating y_1 and y_2 by using x_1 and x_2 directly, an alternative way of expressing uniform random variables in polar form is quite useful. Suppose the independent uniform random variables v_1 and v_2 are the ordinate and abscissa of a random point inside a unit circle. Then $R_2 \equiv v_1^2 + v_2^2$ is also a uniform random variable. If $R = 0$ or $R > 1$, another pair of (v_1, v_2) will be picked up again until $0 < R^2 <= 1$. The value of R can be used for x_1. Furthermore, the ratio of angle θ to 2π is also uniformly distributed in the unit circle. Thus, the cosine and sine in Equation 4.45 can be rewritten as $(\theta = 2\pi x_2)$

$$\begin{aligned} \cos(2\pi x_2) &= \frac{v_1}{\sqrt{R^2}}, \\ \sin(2\pi x_2) &= \frac{v_2}{\sqrt{R^2}}. \end{aligned} \tag{4.46}$$

The Equation 4.45 can be simplified as follows

$$\begin{aligned} y_1 &= R\cos(\theta) = \sqrt{-2\ln R^2}\frac{v_1}{\sqrt{R^2}} = v_1\frac{\sqrt{-2\ln R^2}}{\sqrt{R^2}}, \\ y_2 &= R\sin(\theta) = \sqrt{-2\ln R^2}\frac{v_2}{\sqrt{R^2}} = v_2\frac{\sqrt{-2\ln R^2}}{\sqrt{R^2}}. \end{aligned} \tag{4.47}$$

The code for generating Gaussian random variables, denoted as "Normaldev.h", is given as follows

```
#include"Ran.h"

struct Normaldev_BM : Ran {
    double mu,sig;
    double storedval;
```

```
    Normaldev_BM(double mmu, double ssig, unsigned long long i)
    : Ran(i), mu(mmu), sig(ssig), storedval(0.) {}
    double dev() {
        double v1,v2,rsq,fac;
        if (storedval == 0.) {
            do {
                v1=2.0*doub()-1.0;
                v2=2.0*doub()-1.0;
                rsq=v1*v1+v2*v2;
            } while (rsq >= 1.0 || rsq == 0.0);
            fac=sqrt(-2.0*log(rsq)/rsq);
            storedval = v1*fac;
            return mu + sig*v2*fac;
        } else {
            fac = storedval;
            storedval = 0.;
            return mu + sig*fac;
        }
    }
};
```

§ 4.11.3 Appendix B.3: Cholesky decomposition

If a square matrix A is symmetric and positive definite, this matrix has the following decomposition

$$A = LL^T, \tag{4.48}$$

where L is a lower triangular matrix with strictly positive elements, and L^T is the conjugate transpose of L. This decomposition is called **Cholesky decompisition**. Compared to LU decomposition, the advantage of Cholesky decomposition is that the upper triangular matrix U is the transpose of the lower triangular matrix L. This decomposition can be be interpreted as taking the square root of the matrix A.

Suppose the lower triangular matrix L is a 3×3 matrix, which is given by

$$L = \begin{pmatrix} L_{11} & 0 & 0 \\ L_{21} & L_{22} & 0 \\ L_{31} & L_{32} & L_{33} \end{pmatrix} \tag{4.49}$$

The product of L and its transpose L^T, A, is given by

$$\begin{aligned} A &= LL^T = \begin{pmatrix} L_{11} & 0 & 0 \\ L_{21} & L_{22} & 0 \\ L_{31} & L_{32} & L_{33} \end{pmatrix} \begin{pmatrix} L_{11} & L_{21} & L_{31} \\ 0 & L_{22} & L_{32} \\ 0 & 0 & L_{33} \end{pmatrix} \\ &= \begin{pmatrix} L_{11}^2 & & (symmetric) \\ L_{21}L_{11} & L_{21}^2 + L_{22}^2 & \\ L_{31}L_{11} & L_{31}L_{21} + L_{32}L_{22} & L_{31}^2 + L_{32}^2 + L_{33}^2 \end{pmatrix} \end{aligned} \tag{4.50}$$

The recursion equation of obtaining the elements of L is given as follows

$$\begin{aligned} L_{i,i} &= \sqrt{A_{i,i} - \sum_{k=1}^{i-1} L_{i,k}^2}, \\ L_{i,j} &= \frac{1}{L_{j,j}} \left(A_{i,j} - \sum_{k=1}^{j-1} L_{i,k} L_{j,k} \right), \qquad i = j+1, j+2, ..., N-1. \end{aligned} \tag{4.51}$$

The above Equation 4.51 can be used to decompose the stiff propagator D to be the product of two triangular matrix, and the details of the stiff propagator will be discussed in Chapter 3.

The code for Cholesky decomposition, denoted as "cholesky.h", is given as follows

```
const static int n4=matrixsize;

class Cholesky{
public:
        double m[n4][n4];
        double L[n4][n4];
        void initial()
        {
            for(int i=0;i<n4;i++)
            {
                for(int j=0;j<n4;j++)
                {
                    m[i][j]=0.0;
                    L[i][j]=0.0;
                }
            }
        };
        Cholesky(){};
```

```
        virtual ~Cholesky(){};
        void Decomposition()
        {
            int i,j,k;
            double sum;
            for (i=0;i<n4;i++)
            {
                for (j=i;j<n4;j++)
                {
                    for(sum=m[i][j],k=i-1;k>=0;k--)
                    {
                        sum-=m[i][k]*m[j][k];
                    }
                    if (i==j)
                    {
                        if(sum<=0.0)
                            cout<<"Cholesky failed"<<endl;
                        m[i][i]=sqrt(sum);
                    }
                    else m[j][i]=sum/m[i][i];
                }
            }
            for(int i=0;i<n4;i++)
            {
                for(int j=0;j<i;j++)
                {
                    m[j][i]=0.;
                }
            }

            for(int i=0;i<n4;i++)
            {
                for(int j=0;j<n4;j++)
                {
                    L[i][j]=m[i][j];
                }
            }
        }
};
```

§ 4.11.4 Appendix B.4: Initial parameters

This file "initialparameters.h" is used to define the parameters used in the simulation to be global variable, which can be used in any file of the c++ project.

```
const static int matrixsize=901;
const static int ell=90;
const static int tstar=180;
const static int Tmax=(matrixsize-1)/ell;
const static double e1=1.0/360.0;
const static double e2=1.0/360.0;
const static double sl=e2;
const static double edval=ell/360.0;
const static double fitp=1.2;
const static double f0=0.3;

const static double w1=862.416895633835;
const static double w2=32.4166802133847;
const static double w3=4.38654918617259;

const static int nn=matrixsize;
const static int T0=270;
const static int TI=180;
const static int TL0=T0/ell;
const static int TLI=TI/ell;

const static int nsk=90;
const static double scale=1;
const static int MAX=100000;

double eigenv[nn][nn];
double D[nn][nn];
double gamvol[nn];
double M[nn][nn];

double tlambmnt[tstar];
double tlambMN[tstar][Tmax][Tmax];
double LMN[Tmax][Tmax];

double Libort0[Tmax];
double Libor[Tmax];

double gammaA[tstar][nn];
double intgA[tstar][Tmax];
```

```
double drou[tstar][Tmax];

double SK[nsk];
double avgpay[nsk];
double Call[nsk];
double ep[MAX][nsk];
double error[nsk];
double LBondt0;
```

§ 4.11.5 Appendix B.5: Initial Libor rate and volatility function

Recall Equation 4.9 which is used to give initial values to the present Libor rates $L(t_0, T_n)$

$$L(t_0, T_n) \quad = \quad f_0\Big(1.0 + \exp\big(-f_x\ell(T_n - t_0)\big)\Big).$$

The code for generating $L(t_0, T_n)$ is given as follows

```
struct optionvariable
{
    double GLibor[Tmax];

    void getoptionvariable()
    {
        for(int j=0;j<Tmax;j++)
        {
            GLibor[j]=f0*(1.0+exp(-fitp*j*edval));
        }
    }
};
```

The well known volatility function, shown in Equation 3.30, is used for generating initial values for $\gamma(t, x)$ and is given by

$$\gamma_M \quad = \quad 0.061 - 0.014e^{(-1.55(\theta-\theta_{min}))} + 0.074(\theta - \theta_{min})e^{(-1.55*(\theta-\theta_{min}))}.$$

The code for generating $\gamma(t, x)$ is given as follows

```
struct volgamma
{
    void getgamma()
    {
        for(int i=0;i<matrixsize;i++)
```

```
        {
            gamvol[i]=0.061-0.014*exp(-1.55*(i*sl-0.25))+0.074*(i*sl-0.25)*exp
                (-1.55*(i*sl-0.25));
        }
        for(int i=0;i<matrixsize;i++)
        {
            gamvol[i]=gamvol[i]*scale;
        }
    }
};
```

§ 4.11.6 Appendix B.6: Propagator

The normalized stiff propagator, which is discussed in Chapter 3, is encoded in the c++ file "propagator.h" and is given by

```
#include"initial_parameters.h"
const static int n3=matrixsize;
const static double e3=e1;
const static double lembda=pow(1.79,0.34);
const static double eta=0.34;
const static double bm=0.85;

class stiff{
public:
    double g[n3][n3];
    double zp;
    double zm;
    double gp;
    double gm;
    double gpm;
    double gmp;
    double gz;
    stiff(){};
    virtual ~stiff(){};
    void generateG()
    {
        for(int i=0;i<n3;i++)
        {
            for(int j=0;j<n3;j++)
            {
                zp=pow((i*e3),eta)+pow((j*e3),eta);
```

```
                zm=fabs(pow((i*e3),eta)-pow((j*e3),eta));
                gp=exp(-lembda*zp*cosh(bm))*sinh(bm+lembda*zp*sinh(bm));
                gm=exp(-lembda*zm*cosh(bm))*sinh(bm+lembda*zm*sinh(bm));
                gpm=exp(-lembda*(zp+zm)*cosh(bm))* sinh(bm+lembda*(zp+zm)*sinh
                    (bm));
                gmp=exp(-lembda*(zp-zm)*cosh(bm))* sinh(bm+lembda*(zp-zm)*sinh
                    (bm));
                gz=sinh(bm);
                g[i][j]=(gp+gm)/sqrt((gpm+gz)*(gmp+gz));
            }
        }
    }
};
```

§ 4.11.7 Appendix B.7: Integration for Δ_{mn}

The integration for Δ_{mn} is given by

$$\Delta_{mn} = \int_{t_0}^{t} dt' \int_{T_m}^{T_{m+1}} dx \int_{T_n}^{T_{n+1}} dx' M_\gamma(x, x'; t).$$

and the code for Δ_{mn} is shown as follows

```
struct LambMN{
    double getLambMN(double M[matrixsize][matrixsize],int T1,int T2)
    {
        double SLMN;

        SLMN=0.0;
        for(int t=0;t<tstar;t++)
        {
            tlambmnt[t]=0.0;
        }

        for(int t=0;t<tstar;t++)
        {
          for(int theta=T1-t;theta<T1+ell-t;theta++)
            {
                for(int thetap=T2-t;thetap<T2+ell-t;thetap++)
                {
                    tlambmnt[t]+=M[theta][thetap]*e2*e2;
                }
```

```
            }
        }

        for(int t=0;t<tstar;t++)
        {
            SLMN+=tlambmnt[t]*e1;
        }
        return SLMN;
    }
};
```

§ 4.11.8 Appendix B.8: Program for the Libor zero coupon bond option

As discussed in the above sections, all the c++ head files are included in the main program. The main program is designed to update the Libor rates $L(t+1, T_n)$ from its previous rates $L(t, T_n)$. In this program, the three white noise simulation discussed in Section § 3.12 is used for generating $A(t, x)$. One can use the Cholesky decomposition to improve the accuracy of simulation results. However, as discussed in Section § 3.12, the difference between three white noise simulation and Cholesky decomposition is negligible.

The main program for pricing zero coupon bond option is given as follows

```
#include<iostream>
#include<fstream>
#include<math.h>

//------------ Defined Class ------------------------------
#include"propagator.h"
#include"vol_gamma.h"
#include"option_variables.h"
#include"Lambmn.h"
#include"Normaldev.h"

//---------------- end ------------------------------------


using namespace std;

//---------- use class ------------------------------------
stiff gen;
```

```
volgamma vg;
optionvariable ov;
LambMN lb;
Normaldev_BM myran(0.0,1.0,200);

void initial()
{
//---------- initialise strike price ----------
    for(int i=0;i<nsk;i++)
    {
        SK[i]=0.4+(0.1/nsk)*i;
    }
//---------- read eigenvector ----------

    fstream file2;
    file2.open("eigenvector.txt");

    int m2=0;
    while(!file2.eof())
    {
        for(int j=0;j<nn;j++)
        {
            file2>>eigenv[m2][j];
        }
        ++m2;
    }

    file2.close();

//---------- read gamma and read initial Libor ----------

    ov.getoptionvariable(); // initial Libor
    vg.getgamma();

    for(int j=0;j<Tmax;j++)
    {
        Libort0[j]=ov.GLibor[j];
    }

    LBondt0=1.0;

    for(int i=0;i<TL0;i++)
    {
        LBondt0=LBondt0*(1.0/(1.0+edval*Libort0[i]));
```

```
    }


//------------------------- read propogator and gamma ---------------------
    gen.generateG();
    for(int i=0;i<nn;i++)
    {
        for(int j=0;j<nn;j++)
        {
            D[i][j]=gen.g[i][j];
        }
    }

    for(int i=0;i<nn;i++)
    {
        for(int j=0;j<nn;j++)
        {
            M[i][j]=gamvol[i]*D[i][j]*gamvol[j];
        }
    }
//------------------------- read Lambda (t, M, N) -------------------------

    for(int i=tstar/ell;i<Tmax;i++)
    {
        for(int j=tstar/ell;j<Tmax;j++)
        {
            LMN[i][j]=lb.getLambMN(M,i*ell,j*ell);
            for(int t=0;t<tstar;t++)
            {
                tlambMN[t][i][j]=tlambmnt[t];
            }
        }
    }
}

void recursion()
{
    double ranv1;
    double ranv2;
    double ranv3;
    double temprou;
    temprou=0.0;
    double temprA;
    temprA=0.0;
```

```
    double tempi;
    tempi=0;
    double tempP[nsk];
    double LBond;

    for(int i=0;i<nsk;i++)
    {
        avgpay[i]=0.0;
    }

    for(int mx=0;mx<MAX;mx++)
    {
        cout<<mx<<endl;

//------ set the initial value of Libor for each configurations ----------
        for(int j=0;j<Tmax;j++)
        {
            Libor[j]=Libort0[j];
        }

//------------------------------ updating A (t,x) ---------------------------

        for(int t=0;t<tstar;t++)
        {
            ranv1=myran.dev();
            ranv2=myran.dev();
            ranv3=myran.dev();
            for(int i=0;i<nn;i++)
            {
                gammaA[t][i+t]=gamvol[i]*(sqrt(w1)*eigenv[i][nn-1]*ranv1+sqrt(
                    w2)*eigenv[i][nn-2]*ranv2+sqrt(w3)*eigenv[i][nn-3]*ranv3);
            }
        }

//---------------------- integration of gamma A(t,x) --------------------

        for(int t=0;t<tstar;t++)
        {
            for(int j=0;j<Tmax;j++)
            {
                for(int k=j*ell;k<(j+1)*ell;k++)
                {
                    temprA+=gammaA[t][k]*e2;
                }
```

```
                intgA[t][j]=temprA;
                temprA=0.0;
            }
        }


//------------- updating Libor and get the value of drift ------------

        for(int t=0;t<tstar;t++)
        {
            for(int j=0;j<Tmax;j++)
            {
                if(j<TLI)
                {
                    for(int sm=j+1;sm<=TLI;sm++)
                    {
                        tempi=(Libor[sm]*edval)/(1.0+(Libor[sm]*edval));
                        temprou+=-tempi*tlambMN[t][sm][j];
                    }
                    drou[t][j]=temprou;
                    temprou=0.0;
                }

                else if(j==TLI)
                {
                    drou[t][j]=0.0;
                }
                else
                {
                    for(int sm=TLI+1;sm<=j;sm++)
                    {
                        tempi=(Libor[sm]*edval)/(1.0+(Libor[sm]*edval));
                        temprou+=tempi*tlambMN[t][sm][j];
                    }
                    drou[t][j]=temprou;
                    temprou=0.0;
                }
                Libor[j]=Libor[j]*exp(e1*drou[t][j]+sqrt(e1)*intgA[t][j]-0.5*e1
                    *tlambMN[t][j][j]);

            }
        }
//-------- calculate payoff for each configurations and store the results
    ----------
```

```
        LBond=1.0;
        for(int i=TL0;i<Tmax;i++)
        {
            LBond=LBond*(1.0/(1.0+edval*Libor[i]));
        }
        for(int i=0;i<nsk;i++)
        {
            if((LBond-SK[i])>0)
                tempP[i]=(LBond-SK[i]);
            else
                tempP[i]=0;
        }

        for(int i=0;i<nsk;i++)
        {
            avgpay[i]+=tempP[i];
        }
        for(int i=0;i<nsk;i++)
        {
            ep[mx][i]=tempP[i];
        }
    }
    for(int i=0;i<nsk;i++)
    {
        avgpay[i]=avgpay[i]/MAX;
    }

    for(int i=0;i<nsk;i++)
    {
        Call[i]=LBondt0*avgpay[i];
    }
}

void errorbar()
{
    double mean;
    mean=0.0;
    double var;
    var=0.0;
    for(int i=0;i<nsk;i++)
    {
        for(int mx=0;mx<MAX;mx++)
        {
```

```
            mean+=ep[mx][i];
        }
        mean=mean/MAX;
        for(int mx=0;mx<MAX;mx++)
        {
            var+=pow((ep[mx][i]-mean),2.0);
        }
        var=var/MAX;
        error[i]=LBondt0*(sqrt(var)/sqrt(MAX*1.0));
        mean=0.0;
        var=0.0;
    }
}

void outputcallerror()
{
    ofstream outcallerror("call with error.txt");

    for(int i=0;i<nsk;i++)
    {
            outcallerror<<(i+1)<<'\t'<<Call[i]<<'\t'<<error[i];
            outcallerror<<endl;
    }
    outcallerror.close();
}

void outputCall()
{
    ofstream outCall("Callprice.txt");

    for(int i=0;i<nsk;i++)
    {
            outCall<<(i+1)<<'\t'<<Call[i];
            outCall<<endl;
    }
    outCall.close();
}

void outputLBondt0()
{
    ofstream outLBondt0("LBondt0.txt");

    outLBondt0<<LBondt0;
    outLBondt0<<endl;
```

```
    outLBondt0.close();
}

void outputLibort0()
{
    ofstream outLibort0("Libort0.txt");

    for(int i=0;i<Tmax;i++)
    {
            outLibort0<<(i+1)<<'\t'<<Libort0[i];
            outLibort0<<endl;
    }
    outLibort0.close();
}


void outputLMN()
{
    ofstream outLMN("LMN.txt");

    for(int i=0;i<Tmax;i++)
    {
        for(int j=0;j<Tmax;j++)
        {
            outLMN<<LMN[i][j];
            if(j!=Tmax-1)
                outLMN<<'\t';
        }
            outLMN<<endl;
    }
    outLMN.close();
}

void outputgamma()
{
    ofstream outgamma("gamma.txt");

    for(int i=0;i<nn;i++)
    {
            outgamma<<(i+1)<<'\t'<<gamvol[i];
            outgamma<<endl;
    }
    outgamma.close();
```

```
}

void outputSK()
{
    ofstream outsk("SK.txt");

    for(int i=0;i<nsk;i++)
    {
            outsk<<SK[i];
            outsk<<endl;
    }
    outsk.close();
}


int main()
{
    initial();
    recursion();
    errorbar();
    outputcallerror();
    outputCall();
    outputLBondt0();
    outputLibort0();
    outputLMN();
    outputgamma();
    outputSK();

}
```

Chapter 5

The CEV Process for Pricing Equity Default Swaps

Equity Default Swaps (EDSs) are credit-like instruments that were first introduced in 2003. EDS (Equity Default Swaps) are deep out of the money digital put options that payout a fixed amount (recovery rate) upon the stock price hitting a pre-set low barrier. The premium is paid out as contingent quarterly payments similar to CDS (credit default swaps). Equity default swaps initially soared in volumes as investors used the EDS in capital structure arbitrage strategies involving the simultaneous selling of EDS contracts and buying of CDS contracts as spreads on EDS were several multiples of CDS spreads. However, the contracts diminished in volume as CDS contracts took over. With the recent financial turmoil in the credit derivatives market attention has turned on the credit default swap and its associated structured correlation products such as Nth-to-default basket and synthetic CDOs (Collateralized Debt Obligations) as CDS markets tend to be opaque and difficult to price. In addition, default correlations are not directly observable and recoveries are stochastic making pricing and modeling difficult. As against this, the underlying stock prices in EDS are directly observable and the correlation is also directly observable. The Equity Default Swap may therefore return to the credit fold and may be a complement to the credit default swap market. In this Chapter, we examine the pricing of equity default swaps using the CEV process and calibrate the CEV process to actual observed market prices for EDS and we then draw conclusions on the CEV process, the relationship between stock prices and volatility and the relationship between CDS and EDS prices.

§ 5.1 Introduction

The Equity Default Swap was introduced to the financial markets by JPMorgan and is designed to be a credit-like instrument. The protection buyer makes periodic (usually quarterly) spread payments that are a fixed percentage of the notional contract value to the protection seller for a fixed tenor (usually 5 years) or till a default event takes place. The default event is defined as the price breaching a barrier (usually 30% of the initial price) whereupon all further periodic payments by the protection buyer stop and the protection seller makes a fixed payout (50% of the notional contract value) to the protection buyer. The protection buyer basically buys a deep out of the money American digital put option on the stock with the barrier set at 30% of the initial price. The digital payoff is 50% of the notional value of the contract and the premium is paid in quarterly default contingent payments. Although the EDS is an equity option, the instrument has credit characteristics because the option is deeply out of the money. A fall in stock price by 70% indicates credit impairment and therefore the EDS is a quasi credit derivative.

The Equity Default Swap initially gained popularity with traders and investors as a capital structure arbitrage play. As the EDS spreads in the market were several multiples of the CDS spreads, traders attempted to arbitrage the capital structure by selling EDS and buying CDS or multiples of CDS. For example, selling EDS on XYZ Corp and buying CDS on three times the notional contract value. The position earns a positive carry so long as EDS Spread is greater than three times the CDS spread. If the firm defaults, the stock price would hit the barrier of 30% and become zero. The trader would have to pay out 50% of the notional contract value on the EDS but receive three times Notional $\times$ (1-Recovery Rate). The trader of course takes the risk that an equity default event takes place but the firm remains solvent. The carry in the trade is attractive however and the hedge on the CDS is used to compensate any mark-to-market losses. The EDS soon faded out however, and the contributing factors were limited market participants and illiquidity as only a few banks had the ability to make markets. In comparison the CDS market grew by leaps and bounds aided by a large number of participants entering the market both protection buyers and sellers, high liquidity, demand from banks seeking capital relief and from insurance companies seeking premium. The EDS market was eclipsed by the strong growth of the CDS market. Credit default swaps made their way into more complex structured credit products such as Nth to default baskets and synthetic CDOs.

With the recent sub-prime crisis and financial turmoil, attention has turned toward structured credit and its underlying instrument, the credit default swap. Regulators and investors

have been perplexed to discover the complex pricing procedures of credit default swaps and their associated correlation products, the CDOs. Synthetic CDOs suffered from massive rise in implied correlation in the index tranches causing mark-to-market to suffer steep falls. Markets woke up to the fact that synthetic structured credit revolves around unobservable default, default correlation processes and stochastic recovery rates and this made the structures extremely difficult to model and price. In light of this, the Equity Default Swap makes for a promising alternative in the form of observable stock prices, stock price correlations and fixed recovery rate. While the EDS can never completely replace the CDS, it makes for a promising complement in the credit space providing quasi credit characteristics in a more transparent manner.

In this Chapter, we analyze the pricing of Equity Default Swap using the CEV (Constant Elasticity of Variance) model. We calibrate a CEV process using observed equity default swap prices for 10 European companies over an approximately 1 year period. We find that the parameter of elasticity β must be negative to price EDS. We obtain an optimal β for the pricing of EDS that fits the observed market prices quite well. We find that β values calibrated from the CEV process correspond to the local volatility surface outlined in Albanese and Chen (2005) [49] using credit quality to equity mapping and conclude that the market was correctly pricing the EDS spreads. Finally we calibrate for CDS (stock price falling to zero) and show that CDS spreads as implied by the CEV process calibrated for the EDS spreads were mispriced. We conclude that pricing of EDS by calibrating the elasticity parameter β from CDS spreads is not appropriate but conversely CDS spreads can be obtained from the EDS spreads. The credit risk approach has been adopted in [50] for computing the default of probability and [51] uses the approach of option theory for addressing this problem.

§ 5.2 Simulation and Calibration Process

In this study, we focus on the CEV model for pricing EDS for two main reasons

i Albanese and Chen (2005) [49] show that the local volatility implied by credit quality to equity mapping can be approximated by:

$$\sigma S^{-0.65}.$$

This suggests that a pure diffusion approximation would be a stock price that follows a CEV process.

ii From the boundary classification of the CEV process, the CEV process can have absorption at zero which is analogous to firm default.

Now, the constant elasticity of variance (CEV) process of Cox [52]

$$dS_t = \mu S_t dt + \sigma S_t^{\beta+1} dW; \qquad t \geq 0, S_0 = S(0) > 0, \tag{5.1}$$

where dW is a Wiener process, σ is the volatility, and β is the parameter of elasticity.

We re-write the stochastic differential equation

$$\begin{aligned} dS_t &= \mu S_t dt + \sigma S_0^{\beta} S_t \Big(\frac{S_t}{S_0}\Big)^{\beta} dW \\ &= \mu S_t dt + \sigma_M S_t \Big(\frac{S_t}{S_0}\Big)^{\beta} dW \quad ; \quad \sigma_M = \sigma S_0^{\beta}. \end{aligned} \tag{5.2}$$

The volatility in Equation (5.2), namely σ_M, does not depend on the scale chosen for the stock price $S(t)$ and we identify σ_M as the market volatility of equity. Since σ_M represents the market volatility, it can be calibrated at the initial time $t = 0$, where $S_0 = S(0)$. Note for $\beta = 0$, which is the case for Black-Scholes, we have that $\sigma_M = \sigma$.

In the special case $\beta = 0$, the CEV model is the geometric Brownian motion model of Black and Scholes (1973) [8]. The square root CEV process of Cox and Ross [53] is obtained with $\beta = -0.5$. When $\beta > 0$, the local volatility increases as the stock price increases. When $\beta < 0$, the local volatility increases as the stock price decreases. We observe that implied volatility does not always increase (decrease) as the stock price decreases (increase) in the real market when $\beta < 0$. Implied volatility is not always correlated with the stock price. Two examples of Astra Zeneca Plc and ENI Spa are shown in Figure (5.1) and (5.2).

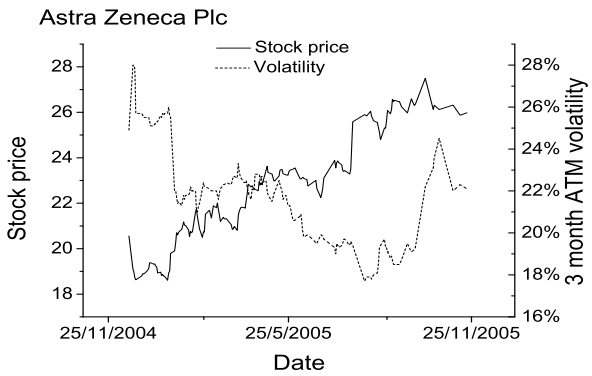

Figure 5.1: Stock price versus implied volatility (Astra Zeneca Plc).

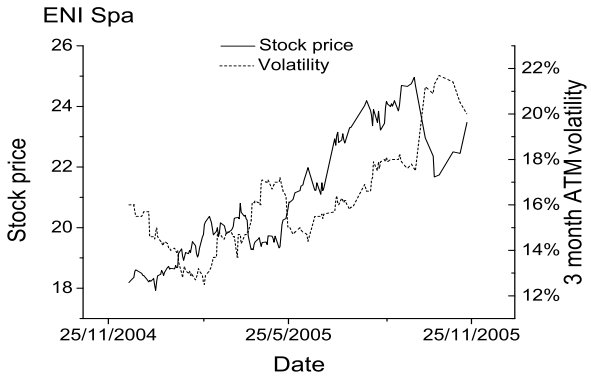

Figure 5.2: Stock price versus implied volatility (ENI Spa).

§ 5.2.1 Calibration of β from Equity Default Swap Spreads

Following the JPMorgan [54] approach, from the Equity Default swap spreads, we obtain the approximate cumulative 5-year probability of default as follows: Consider a firm with cumulative n-year default probability p. In the event of default, the EDS contract will pay out 50% (recovery rate) of notional amount V or $0.5V$. EDS is a binary option with p being the probability that the option is exercised with payoff 0.5P and $1-p$ that it is not exercised with payoff zero. Hence the value of the option

$$p{\times}0.5 \times V.$$

The EDS consists of a stream of payments at a fixed rate of the spread s – over n years until the option is exercised. The total expected payments should be equal to the price of the EDS. The cumulative default probability has a very low sensitivity to interest rates. Also default timing does not significantly impact cumulative default probability for high recovery rates (50% in this case). As an example, a 5 years EDS spread of 100 basis points assuming a recovery rate of 50% implies a cumulative default probability of 9.8% as compared to 10% if we ignore default timing. Therefore, we can ignore interest rate levels and default timing without significant loss of accuracy. We have total premium given by
$s = \text{EDS Spread}{\times}V{\times}n$. Hence, from [54]

$$\text{EDS Spread}{\times}V{\times}n = p{\times}0.5 \times V,$$

$$p \cong \frac{\text{EDS Spread} \times \text{Number of Years}}{100\% - \text{Recovery Rate}}. \tag{5.3}$$

The probability of default p is derived from the market quoted EDS spread, as is the practice in the market. For example, if the EDS for a firm is trading at 250 bps, then,

$$p \cong \frac{2.50\% \times 5}{50\%} = 25\%.$$

For each company we have 160 data points from 24 Dec 2004 to 24 Nov 2005. For each date, we have the Stock Price S_0 , the barrier (which is 30% of S_0 for EDS), the EDS spread, 3 month ATM option implied volatility and μ (drift). We compute drift as $\mu = r - q$ where r is the risk free rate and q is the continuously compounded dividend yield. We obtain 160 values of the cumulative default probability corresponding to the implied probability of equity event as computed in Equation (5.3) for each firm. We regress with least square of errors to obtain a best fit value of probability of default for each company. We then numerically simulate CEV processes using different levels of β till we get a cumulative default probability which gives us the best fit value of probability of default.

We then repeat the procedure and calibrate the CEV process and β values for the traded Credit Default Swap spreads for each of the 10 companies.

We simulate the CEV process at a specific volatility (20%) for different levels of β to compute the default event probabilities and generate a 3 dimensional surface that shows default probability sensitivity to β and barrier level. We also generate a surface to show the sensitivity of default probability to different levels of β and implied volatility for EDS barrier (30%) and CDS barrier (0%) for different levels of μ (drift).

§ 5.2.2 Recursion equation of CEV process

From Equation (5.1), the CEV model, S_t follows the process

$$dS_t = \mu S_t dt + \sigma S_t^{\beta+1} dW(t).$$

The Wiener process $dW(t)$ can be transformed to Gaussian white noise $R(t)$ by doing the following mapping $dW/dt = R$, where the correlator of $R(t)$ is given by

$$\frac{dW(t)}{dt} = R(t), \tag{5.4}$$

$$E[R_t R_{t'}] = \delta(t - t'). \tag{5.5}$$

Equation (5.1) yields

$$\begin{aligned} \frac{dS_t}{dt} &= \mu S_t + \sigma S_t^{\beta+1} R(t) \\ \frac{1}{S_t}\frac{dS_t}{dt} &= \mu + \sigma S_t^{\beta} R(t). \end{aligned} \tag{5.6}$$

For simulating the CEV process, we need to discretize time and convert Equation (5.6) into a finite recursion equation. We discretize time into a lattice with spacing ϵ and this yields $dt = \epsilon$ and $t = n\epsilon$, with $n = 0, 1, 2...\infty$.

Consider the expression $d \ln S/dt$ in discrete time; we obtain the following

$$\begin{aligned} \frac{\Delta \ln S}{\epsilon} &\approx \frac{1}{\epsilon}(\ln S_{t+\epsilon} - \ln S_t) \\ &= \frac{1}{\epsilon}(\ln(S + \epsilon\frac{\Delta S}{\Delta t}) - lnS) \\ &\approx \frac{1}{S}\frac{\Delta S}{\Delta t} - \frac{\epsilon}{2}(\frac{1}{S}\frac{\Delta S}{\Delta t})^2. \end{aligned} \tag{5.7}$$

Equation (5.6) in discrete time, when substituted into Equation (5.7), yields

$$\frac{\Delta \ln S}{\epsilon} = \mu + \sigma S^{\beta} R - \frac{\epsilon}{2}\mu^2 - \epsilon\mu\sigma S^{\beta} R - \frac{\epsilon}{2}\sigma^2 S^{2\beta} R^2 + O(\epsilon). \tag{5.8}$$

Compared to other terms of Equation (5.8), the third and fourth term on the right side are of $O(\epsilon)$ and are neglected. Define variable x defined by $S = S_0 e^x$, and let $x(t) = x_n$ and $x(t + dt) = x_{n+1}$. For $\Delta x = x_{n+1} - x_n$ Equation (5.8) is rewritten as

$$\begin{aligned} \frac{\Delta x}{\epsilon} &= \mu + \sigma S_0^{\beta} e^{\beta x} R - \frac{\epsilon}{2}\sigma^2 S_0^{2\beta} e^{2\beta x} R^2 + O(\epsilon) \\ &= \mu + \sigma_M e^{\beta x} R - \frac{\epsilon}{2}\sigma_M^2 e^{2\beta x} R^2 + O(\epsilon), \end{aligned} \tag{5.9}$$

where the definition of $\sigma = \sigma_M / S_0^{\beta}$ is given in Equation (5.2).

We verify that Equation (5.9) yields the correct continuum limit. For $\epsilon \to 0$, it can be shown from Equation (5.5) that to leading order in any correlation function, white noise $R^2(t)$ becomes deterministic [2]; hence, we obtain for discrete time $t = n\epsilon$

$$E[R_t R_{t'}] = \delta(t - t') \quad \Rightarrow R^2(t) = \frac{1}{\epsilon} + \text{ random terms}, \tag{5.10}$$

and Equation (5.9) yields

$$\frac{dx}{dt} = \mu + \sigma_M e^{\beta x} R - \frac{1}{2}\sigma_M^2 e^{2\beta x}. \tag{5.11}$$

For $\beta = 0$ we recover the Black-Scholes lognormal temporal equation

$$\frac{dx}{dt} = \mu - \frac{1}{2}\sigma^2 + \sigma R. \tag{5.12}$$

From Equation (5.9) we obtain the fundamental recursion for the CEV process in discrete time given by

$$x_{n+1} = x_n + \epsilon\mu + \epsilon\sigma_M e^{\beta x} R - \frac{\epsilon^2}{2}\sigma_M^2 e^{2\beta x} R^2 + O(\epsilon^2). \tag{5.13}$$

From Equation (5.10), we see that white noise R is a Gaussian random variable with variance given by $1/\sqrt{\epsilon}$, namely that $R = N(0, \frac{1}{\sqrt{\epsilon}})$. In other words

$$\begin{aligned} R &= \frac{1}{\sqrt{\epsilon}} N, \\ N &= N(0,1) \quad ; \quad \text{Normal random variable.} \end{aligned} \tag{5.14}$$

For the purpose of simulations, R is changed to normal distribution $N \equiv N(0,1)$. From Equation (5.14), Equation (5.13) is rewritten as

$$x_{n+1} = x_n + \epsilon\mu + \sqrt{\epsilon}\sigma_M e^{\beta x} N - \frac{\epsilon}{2}\sigma_M^2 e^{2\beta x} N^2 + O(\epsilon^2). \tag{5.15}$$

Equation (5.15) is used for simulating the CEV process with ϵ set equal to one day and σ_M is determined from market data.

§ 5.3 Data Analysis and Results

β is calibrated for all 10 firms by computing β for a CEV process for the least squares estimator of the probability of default for a given firm. Examples for Astra Zeneca Plc and ENI Spa are given in Figure (5.3) and Figure (5.4).

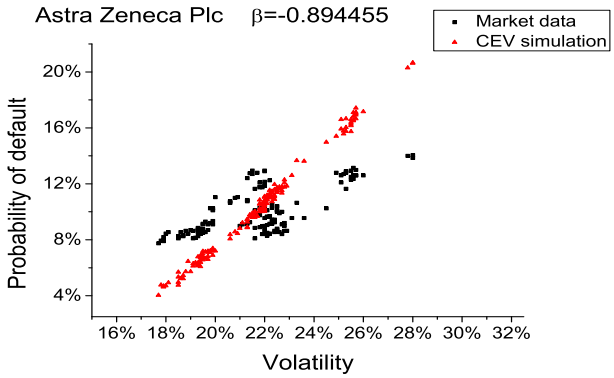

Figure 5.3: Probability of default of market data and CEV simulation for EDS spreads (Astra Zeneca Plc).

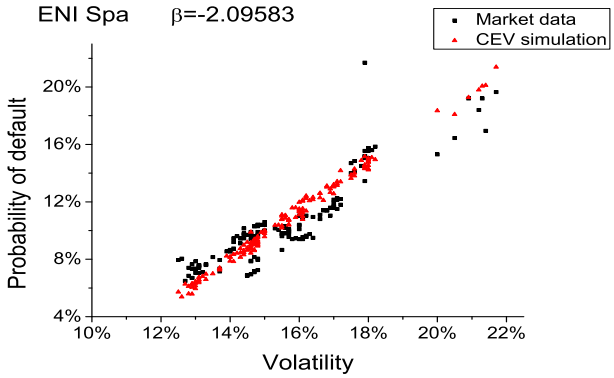

Figure 5.4: Probability of default of market data and CEV simulation for EDS spreads (ENI Spa).

The calibrated β values are shown in table (5.1).

Table 5.1: β values for 10 companies (Barrier: 30% of initial stock price).

Company	β	Company	β
Astra Zeneca Plc	-0.894455	Nokia Oyj	-1.31135
BASF AG	-1.76562	Philips	-1.81191
Carrefour SA	-1.71484	SAP	-1.69077
ENI Spa	-2.09583	Telefonica	-1.73154
L'Oreal	-1.92686	TOTAL S.A	-1.89674

The calibrated β values range from -0.89 to -2.10 with an average value of -1.68. Thus in

terms of the local volatility function outlined by Albanese and Chen [49] the above values of β give a local volatility function in the range from $\sigma S^{0.11}$ to $\sigma S^{-1.10}$ with an average of $\sigma S^{-0.68}$ which corresponds to the credit quality to equity mapping of Albanese Chen [49]. We conclude that the market on average was correctly pricing Equity Default Swap spreads.

We now turn to calibrating β values from the market CDS rates and show the calibration for Astra Zeneca Plc and ENI Spa in Figure (5.5) and Figure (5.6), respectively.

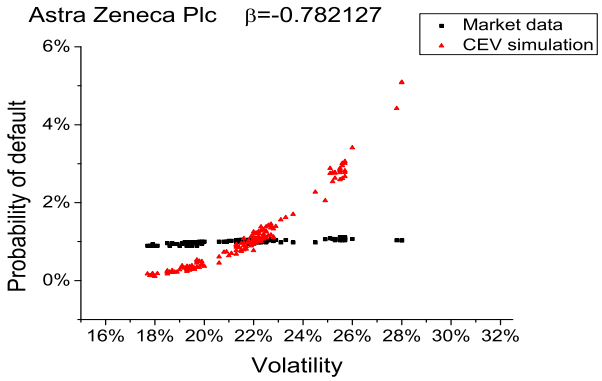

Figure 5.5: Probability of default of market data and CEV simulation for CDS spreads (Astra Zeneca Plc).

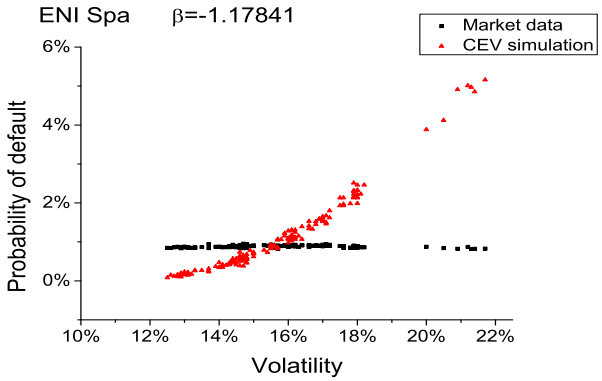

Figure 5.6: Probability of default of market data and CEV simulation for CDS spreads (ENI Spa).

The β values calibrated from the CDS spreads are presented in table (5.2).

The calibrated β values range in value from -0.77 to -1.55 with an average value of -1.09. Thus in terms of the local volatility function outlined by Albanese and Chen (2005) the above values of β give a local volatility function in the range from $\sigma S^{0.23}$ to $\sigma S^{-0.55}$ with an average of $\sigma S^{-0.09}$. This deviates considerably from the EDS mapping of the volatility

Table 5.2: β values for 8 companies (Barrier: zero stock price).

Company	β	Company	β
Astra Zeneca Plc	-0.782127	Nokia Oyj	-0.766586
BASF AG	-1.0712	Philips	-1.04668
Carrefour SA	-1.12685	Telefonica	-1.55293
ENI Spa	-1.17841	TOTAL S.A	-1.17295

surface. We conclude that market CDS spreads do not mesh with the CEV process calibrated from the market EDS spreads. As, on average the EDS spreads implied process corresponds to the credit quality to equity mapping process, we conclude that EDS spreads seem to be correctly priced by the market. However, the CDS spreads seem incorrectly priced, that is they should actually be higher than where the market was pricing them. The CDS spreads also have almost no sensitivity to the implied stock volatility as is evident from the above graphs.

We next examine the CEV process in detail to test what level of β values imply firm default (stock price going to zero). We simulate for a single company with a volatility level of 20% and $\mu = 0.02$, and the plot of probability of default versus values of β is shown in Figure 5.7.

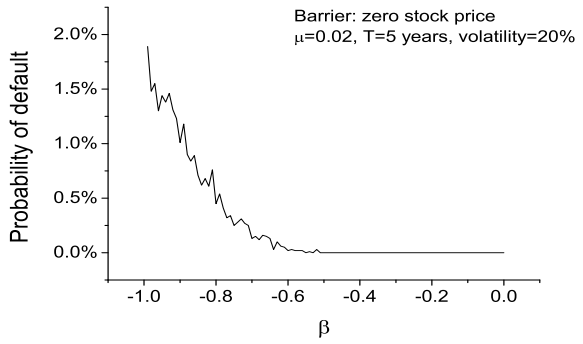

Figure 5.7: Probability of default for different values of β (Barrier: zero stock price).

We investigate further by looking at a 3D plot of default probability versus barrier versus β (Figure (5.8)) and 3D plot of default probability versus barrier versus μ (Figure (5.9)).

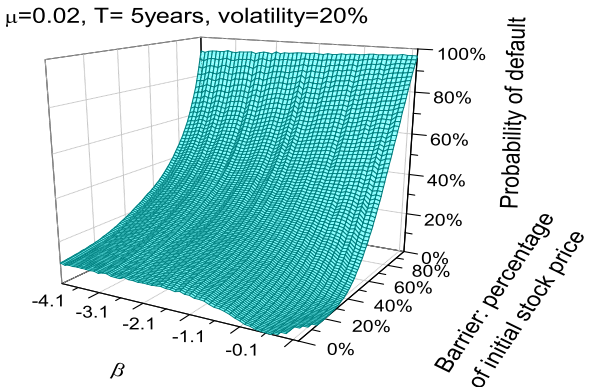

Figure 5.8: 3D plot of probability of default versus barrier versus β.

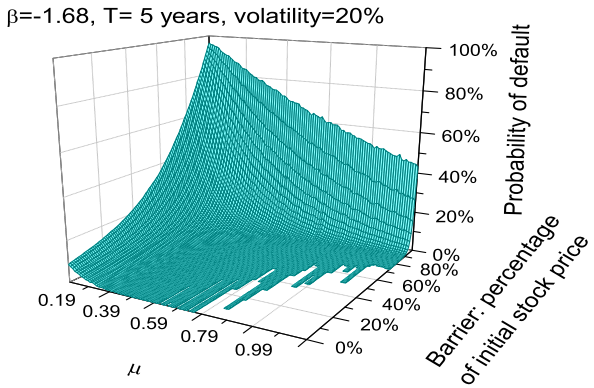

Figure 5.9: 3D plot of probability of default versus barrier versus μ.

It is obvious that the CEV process become highly non-linear near the zero barrier and for β values > -0.5 the probability of default which is positive very near the surface drops to zero when the barrier is zero. The case is different for β values < -0.5 as the default probabilities gradually rise and cap off at about 20%.

We run simulations for a CEV process with variable β and σ for three different values of μ when barrier is set at 30% of initial stock price. The results are presented in Figure (5.10), (5.11) and (5.12).

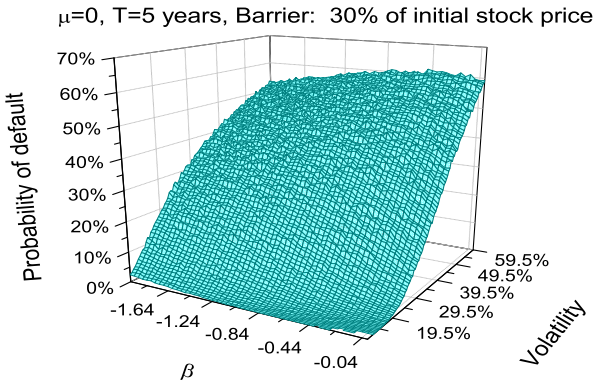

Figure 5.10: 3D plot of probability of default versus β versus volatility ($\mu = 0$, Barrier: 30% of initial stock price).

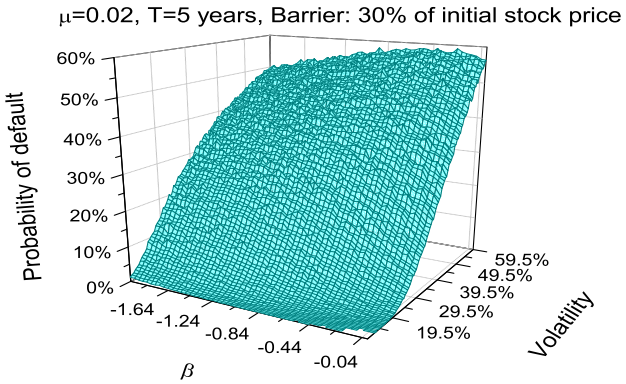

Figure 5.11: 3D plot of probability of default versus β versus volatility ($\mu = 0.02$, Barrier: 30% of initial stock price).

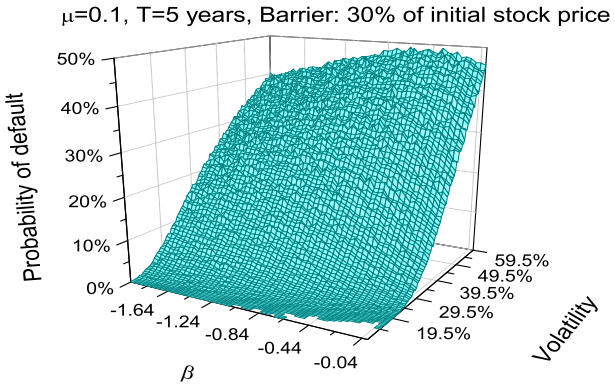

Figure 5.12: 3D plot of probability of default versus β versus volatility ($\mu = 0.1$, Barrier: 30% of initial stock price).

We also run simulations for a CEV process with variable β and σ for three different values of μ when barrier is zero stock price. The results are presented in Figure (5.13), (5.14) and (5.15).

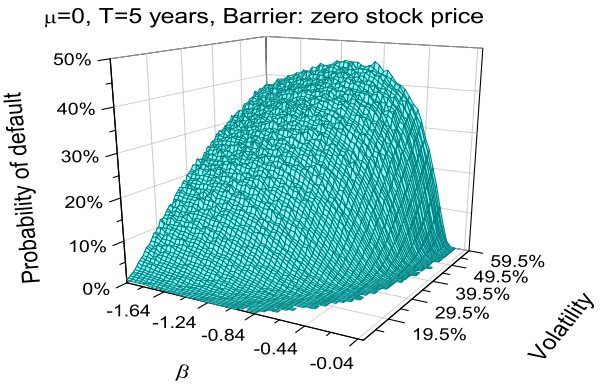

Figure 5.13: 3D plot of probability of default versus β versus volatility ($\mu = 0$, Barrier: zero stock price).

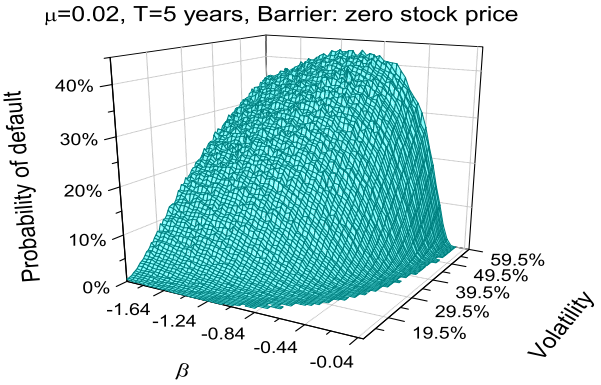

Figure 5.14: 3D plot of probability of default versus β versus volatility ($\mu = 0.02$, Barrier: zero stock price).

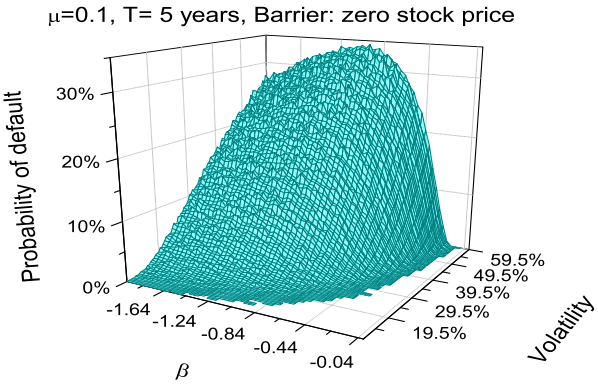

Figure 5.15: 3D plot of probability of default versus β versus volatility ($\mu = 0.1$, Barrier: zero stock price).

It seems for the Figure (5.13), (5.14) and (5.15) that threshold β for default varies with volatility. For probability of default > 0, we find from Monte Carlo simulation, that β must < 0.

§ 5.4 Conclusions

We calibrate a Constant Elasticity of Variance (CEV) process to model the pricing of Equity Default Swaps. We conclude that β values must be negative in order for the process to hit a barrier level of 30% and also for 0%. Negative β values indicate rising volatility with falling stock prices, a phenomenon amply evident in the recent meltdown.

We calibrate a CEV process to market observed EDS spreads over a period of 1 year for 10 large European corporations. We find that on average β for these companies is -1.68 which agrees with the local volatility surface obtained from credit quality to equity mapping (Albanese and Chen [49]). We conclude that the market, on the average, has been pricing the EDSs correctly. Recall that an EDS is a deep out of the money American digital put option. We find that market observed CDS spreads do not correspond to the credit quality to equity mapping. CDS spreads show no sensitivity to implied volatility as shown in Figure (5.5) and (5.6) and hence are deviating from the CEV process. The CEV process implied from the EDS spreads implies higher default probabilities and therefore higher CDS spreads than those observed in the market.

To price Equity Default Swaps, Albanese and Chen [49] suggest calibrating the CEV process with data from the CDS market and then using the calibrated CEV process to price the

Equity Default Swaps. Thus given an implied volatility and a CDS spreads, they compute β for the process. With this calibration, they price the EDS using the EDS pricing formula [49]. We have clearly shown that this process will result in incorrect EDS spreads. Market CDS spreads are shown to be insensitive to implied equity volatilities and the CEV process implied by the CDS spreads have a local volatility surface that deviates from the credit quality to equity mapping. Rather our analysis suggests using the market EDS spreads to calibrate CEV process and then using the process parameters thus obtained to find the CDS spreads.

We now try and offer reasons why the market CDS spreads were so low and consider the EDS as an alternative to the CDS both as a credit risk management tool and as an underlying derivative in structured credit products. As 2005 was a period of feverish structured credit activity, big corporations such as the 10 companies used in our analysis, were frequently included in CDO portfolios. The large buildup in 'long credit' positions by CDO investors possibly depressed CDS spreads to record lows. It is worth mentioning that the record low CDS spreads in the global credit market catalyzed the introduction of the EDS as a higher yielding product. Being equity derivatives, market observed stock prices, market implied volatility, and a non-stochastic recovery rate, contributed to the instruments being more objectively and accurately priced than CDS.

Although CDS can theoretically be priced using structural models such as the Merton model, difficulties in estimating a firm's value can obfuscate the methods, accuracy and utility. Another major difficulty with CDS is pricing synthetic CDOs (tranched portfolios of credit default swaps). CDO prices are sensitive to default correlation. It is virtually impossible to estimate correlation for events for which there is no adequate history. In the case of synthetic CDOs the market relies on the prices of traded tranches on the standard credit indexes (such as ITraxx and CDX) to imply the correlation of the tranches. These were then mapped to the reference CDS portfolios using expected loss.

The EDS has an advantage here in that CDO portfolios of EDS would not only have objectively priced EDS spreads but also correlations would be directly observable. We feel EDS contracts with lower barriers at say 10% would likely be more attractive to the market and would attract both protection buyers and sellers. EDOs (CDOs of such EDS) would also likely generate interest due to the transparency in pricing the spreads and estimating the correlations from observed market stock prices. CDS and CDOs have come under attack from regulators in the recent financial meltdown owing to opaqueness in pricing. An EDS with lower barriers as an exchange traded product may appeal to both regulators and the market.

It would be interesting to see how EDS priced using the CEV model can be hedged effectively by market participants. It would also be useful to test and calibrate the pricing of EDS using structural models such as the Merton model. Any analysis in this direction would be welcome.

§ 5.5 Appendix A: Calibration of simulation of $\beta = 0$ CEV process

The pricing kernel of a stock gives the likelihood of the stock price reach a certain barrier in a certain future time. The formula of pricing kernel for Black-Scholes model is given by [2]

$$P_{BS}(x,\tau;x') = e^{-r\tau}\frac{1}{\sqrt{2\pi\tau\sigma^2}}e^{-\frac{1}{2\tau\sigma^2}(x-x'+\tau(r-\sigma^2/2))^2}. \tag{5.16}$$

The probability of default is given by the likelihood that a stock price having an initial value of $S = e^x$ falls below the barrier price set at $S' = e^{x'}$. The probability of default, appropriately normalized, is given by

$$\begin{aligned} P_D(x,\tau;x') &= \frac{\int_{-\infty}^{x'} dy P_{BS}(x,\tau;y)}{\int_{-\infty}^{+\infty} dx P_{BS}(x,\tau;x')} \\ &= \int_{-\infty}^{x'} dy \frac{1}{\sqrt{2\pi\tau\sigma^2}}e^{-\frac{1}{2\tau\sigma^2}(x-y+\tau(r-\sigma^2/2))^2}. \end{aligned} \tag{5.17}$$

Probability of default calculated by using Black-Scholes pricing kernel is shown in Figure (5.16), while probability of default calculated by using Monte Carlo method under CEV process is shown in Figure (5.17). These two graphs are under the same calibration condition: $10\% \leq \sigma \leq 59.5\%$, $\mu = 0.02$ and $\beta = 0$. The barrier of default is set at 30% of initial stock price.

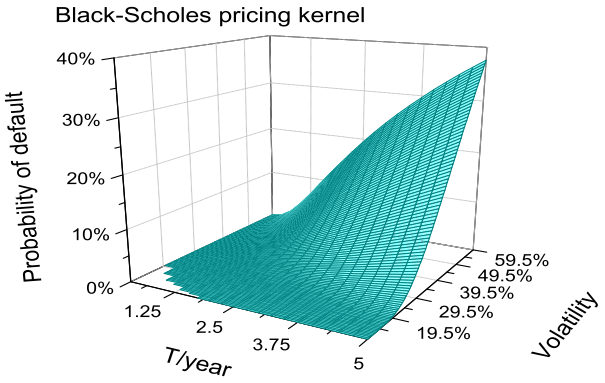

Figure 5.16: Probability of default using Black-Scholes pricing kernel.

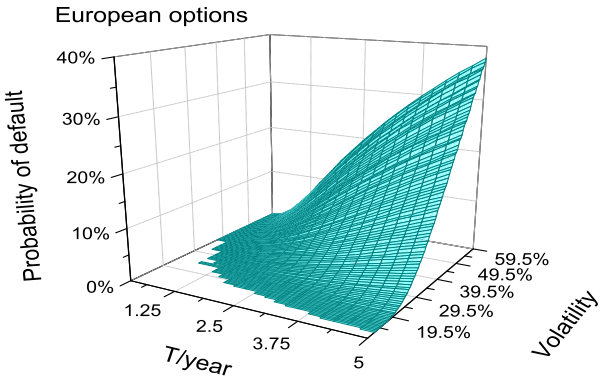

Figure 5.17: Probability of default using CEV simulation for European options.

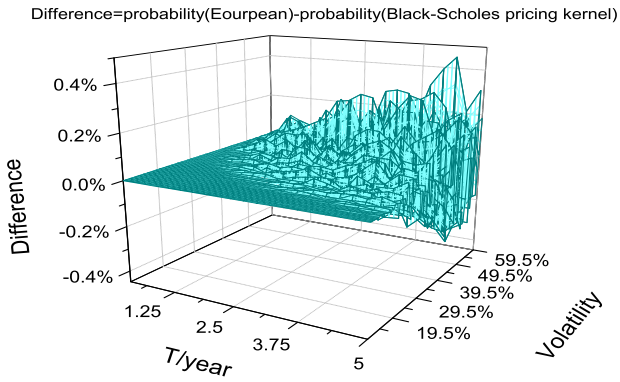

Figure 5.18: Comparison of Black-Scholes pricing kernel and CEV simulation.

The difference of results of simulation and Black-Scholes pricing kernel is shown in Figure (5.18). The error of simulation can be eliminated by increasing the number of configurations of simulation, which shows the properties of Monte Carlo simulation.

The probability of default for American options is shown in Figure (5.19). American options can be exercised at any time before expiration, while European options only can be exercised at certain pre-fixed time before expiration. This property of American options leads to the higher probability of default than European options, which is consistent with our results.

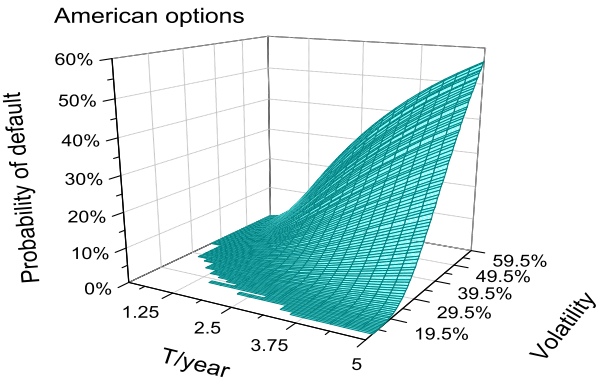

Figure 5.19: Probability of default using CEV simulation for American options.

§ 5.6 Appendix B: Calibration of simulation of $\beta < 0$ CEV process

The term $(S/S_0)^\beta$ for the Black-Scholes does not have influence on the final results since β is equal to zero. The simulation needs to be tested for nonzero values of β. The exact formula of option price is given by Cox [52] for $\beta < 0$ and Emanuel and MacBeth [55] for $\beta > 0$:

$$\begin{aligned} C(S;K,T) &= e^{-qT} S Q(\zeta; n-2, y_0) \\ &- e^{-rT} K (1 - Q(y_0; n, \zeta)), \quad \beta > 0, \\ C(S;K,T) &= e^{-qT} S Q(y_0; n, \zeta) \\ &- e^{-rT} K (1 - Q(\zeta; n-2, y_0)), \quad \beta < 0, \end{aligned} \tag{5.18}$$

where $Q(p, q, r)$ is the cumulative chi-square distribution and

$$\begin{aligned} n &= 2 + \frac{1}{|\beta|}, \\ \zeta &= \frac{2\mu S^{-2\beta}}{\sigma^2\beta(e^{2\mu\beta T} - 1)}, \\ y_0 &= \frac{2\mu K^{-2\beta}}{\sigma^2\beta(1 - e^{-2\mu\beta T})}. \end{aligned} \tag{5.19}$$

For CEV simulation, call price is computed by getting the expectation value of call price of total configurations.

$$C = e^{-rT}E[S - K]. \tag{5.20}$$

The case of $\beta > 0$ is not our interest, the calibration of call price under $\beta < 0$ is made in the following. Call price calculated using CEV simulation is compared with the call price calculated using formula. Two different methods of calibration, call price versus strike price and call price versus time T, are shown in Figures 5.20 5.21 and Figures 5.23 5.24 ,respectively.

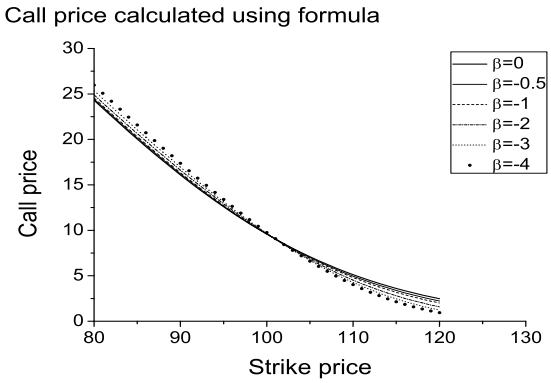

Figure 5.20: Call price calculated using formula (call price versus strike price). $S_0 = 100$, $\mu = 0.1$, $\sigma = 25\%$ and $T = 0.5$ years.

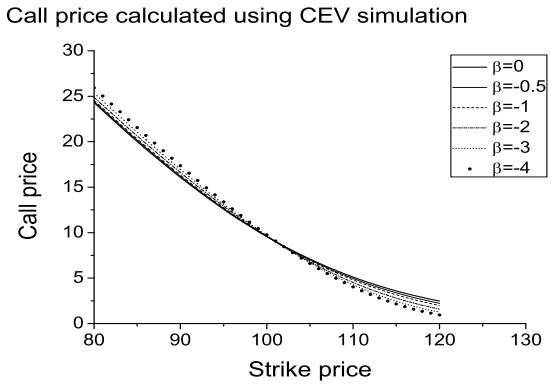

Figure 5.21: Call price calculated using CEV simulation (call price versus strike price). $S_0 = 100$, $\mu = 0.1$, $\sigma = 25\%$ and $T = 0.5$ years.

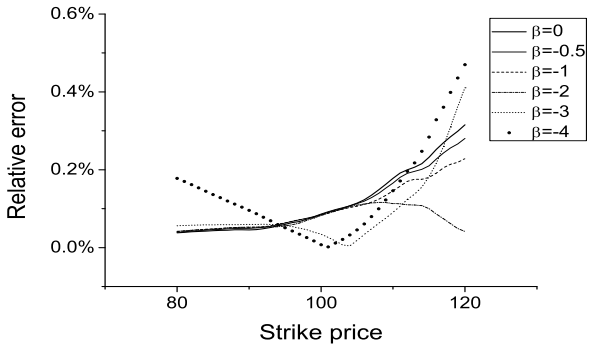

Figure 5.22: Relative error of call price between formula and simulation (call price versus strike price). $S_0 = 100$, $\mu = 0.1$, $\sigma = 25\%$ and $T = 0.5$ years.

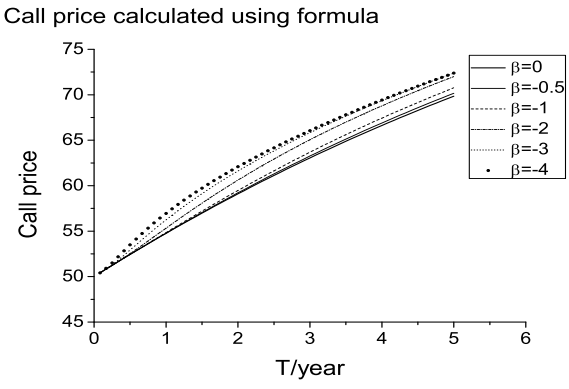

Figure 5.23: Call price calculated using formula (call price versus time T). $S_0 = 100$, $\mu = 0.1$, $\sigma = 25\%$ and strike price $= 50$.

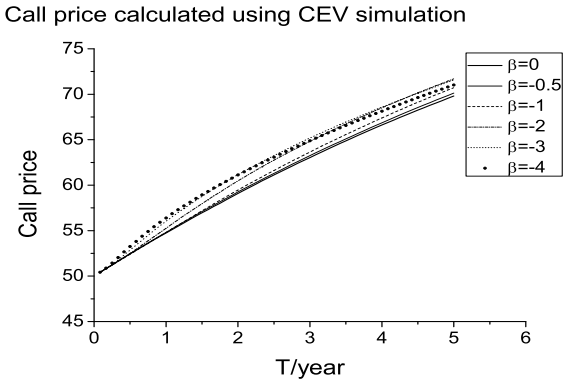

Figure 5.24: Call price calculated using CEV simulation (call price versus time T). $S_0 = 100$, $\mu = 0.1$, $\sigma = 25\%$ and strike price $= 50$.

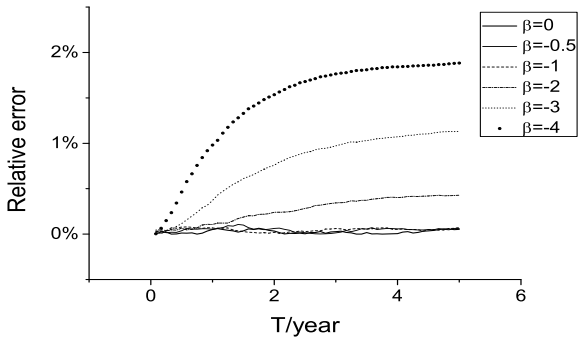

Figure 5.25: Relative error of call price between formula and simulation (call price versus time T). $S_0 = 100$, $\mu = 0.1$, $\sigma = 25\%$ and strike price $= 50$.

Figure (5.22) and (5.25) show the relative error (relative error $= \frac{|\text{Call price(formula)} - \text{Call price(simulation)}|}{|\text{Call price(formula)}|} \times 100\%$) between formula and CEV simulation for call price versus strike price and call price versus time T, respectively. The results of simulation and formula are exactly the same when the number of configurations goes to infinity.

Error is negligible when β is larger than -3. The error becomes large when value of β decreases. This is because the value of each step changes largely when β is too negative. From the EDS and CDS results, the value of β is always from -0.5 to -2.5, the case of too negative β is out of our consideration.

Chapter 6

Dynamic Correlation Model and Empirical Analysis for Equities

The aim of this chapter is to develop a model to describe the unequal time correlation between different stock market data. A nontrivial fourth order derivative Lagrangian was defined to provide an unequal time propagator, which can be simplified to fit the market data. A calibration algorithm is designed to find the empirical parameters for this model and different denoising methods are used to capture the signals concealed in the rate of return. The detailed modeling results of this Gaussian model show that the different stocks of different time can have strong correlation and this empirical unequal time correlator can be described by the propagator. This preliminary study provides a novel solution to calibrate the correlator for different instruments between different times.

§ 6.1 Introduction

Consider N stocks having values $S_I, I = 1, 2, \ldots, N$, the rate of return of single stock $X_I(t)$ is,

$$X_I(t) = \frac{1}{S_I(t)} \frac{dS_I(t)}{dt}. \tag{6.1}$$

In empirical study, the rate of returns are calculated by

$$X_I(t) = \frac{S_I(t) - S_I(t-1)}{S_I(t-1)}. \tag{6.2}$$

The unit of t is set to day and the unit of $X(t)$ is 1/day.

$E[X_I] = d_I$ is the deterministic drift of each stock. The rate of return of each stock $X_I(t)$ can be written as

$$X_I(t) = d_I + \varphi_I(t), \tag{6.3}$$

where $\varphi_I(t)$ are stochastic variables.

The traditional mean-variance analysis proposed by Markowitz is a single-period approach in which there is no time-dependency.

Baaquie and Khan [56] proposed a model that the rate of return of an infinite collection of equities is driven by N random variables. The time evolution of return is governed by the propagator $G_{IJ}(t, t')$, for a finite number of securities,

$$E[\varphi_I(t)\varphi_J(t')] = G_{IJ}(t, t') \quad I, J = 1, 2, \cdots, N. \tag{6.4}$$

Therefore, the correlation between equities is correlated and dynamical, depending on time.

§ 6.2 A Gaussian Model

We now describe $\varphi_I(t)$ by a Gaussian model. First of all, we have to make a change of variable $t \to z = t^\eta, \eta \in (0, 1]$ because the evolution of $\varphi_I(t) = \varphi_I(z)$ needs to be described in market time z instead of physical time t. z reflects the future time anticipated by traders and investors [2]. Define the Lagrangian by

$$\mathcal{L}[\varphi] = -\frac{1}{2}\sum_{IJ}^{N} \varphi_I [D^{-T}U^{-T}\left(\partial_z^4 - \alpha\partial_z^2 + \lambda\right)U^{-1}D^{-1}]_{IJ}\varphi_J, \tag{6.5}$$

where D, U, λ, α are time independent N×N matrix. λ, α are diagonal matrixes, and U is an orthogonal matrix, i.e. $UU^T = 1$.

The action functional is given by

$$S[\varphi] = \int_{-\infty}^{\infty} \mathcal{L}[\varphi] dz. \tag{6.6}$$

We obtain the probability distribution functional

$$P[\varphi] = \frac{1}{Z}\exp(S[\varphi]), \tag{6.7}$$

where

$$\begin{aligned} Z &= \int \mathcal{D}\varphi \exp(S[\varphi]), \\ \int \mathcal{D}\varphi &\equiv \prod_I \prod_{z=-\infty}^{\infty} \int_{-\infty}^{\infty} d\varphi_I(z) \end{aligned} \tag{6.8}$$

is the partition function for the probability distribution.

§ 6.3 The Propagator

The propagator is a quantity of fundamental importance since it governs the evolution of the stochastic variables. According to the above Gaussian model, the propagator of our model $G_{IJ}(t,t')$ is given by

$$\begin{aligned} G_{IJ}(t,t') &= E[\varphi_I(t)\varphi_J(t')] \\ &= \frac{1}{Z}\int \mathcal{D}\varphi \exp(S[\varphi])\varphi_I(z)\varphi_J(z'). \end{aligned} \tag{6.9}$$

According to [2], $G_{IJ}(t,t')$ yields,

$$G^{-1}_{IJ}(t,t') = \left(D^{-T}U^{-T}\left(\partial_z^4 - \alpha\partial_z^2 + \lambda\right)U^{-1}D^{-1}\delta(z-z')\right)_{IJ}. \tag{6.10}$$

Considering $\delta(z,z') = \int_{-\infty}^{+\infty}\frac{d\omega}{2\pi}e^{i\omega(z-z')}$, yields,

$$\begin{aligned} G_{IJ}(t,t') &= \left(DU\frac{1}{\partial_z^4 - \alpha\partial_z^2 + \lambda}U^T D^T\delta(z-z')\right)_{IJ} \\ &= \left(DU\int_{-\infty}^{+\infty}\frac{d\omega}{2\pi}\frac{1}{\partial_z^4 - \alpha\partial_z^2 + \lambda}e^{i\omega(z-z')}U^T D^T\right)_{IJ}. \end{aligned} \tag{6.11}$$

By carrying out the Gaussian integrations and canceling the normalization terms from the partition function Z, we have

$$\begin{aligned} G_{IJ}(t,t') &= \left(DU\left[\int_{-\infty}^{\infty}\frac{d\omega}{2\pi}\frac{e^{i\omega(z-z')}}{\omega^4 + \alpha\omega^2 + \lambda}\right]U^T D^T\right)_{IJ} \\ &= \left(DU\Delta(z,z')U^T D^T\right)_{IJ}, \end{aligned} \tag{6.12}$$

and $\Delta(z,z')$, α, λ is diagonal such that

$$\Delta_{II}(z-z') \equiv \int_{-\infty}^{\infty} \frac{d\omega}{2\pi} \frac{e^{i\omega(z-z')}}{\omega^4+\alpha_I\omega^2+\lambda_I}. \tag{6.13}$$

Let a_I^2 and b_I^2 be the two complex conjugate roots of the quadratic equation

$$x^2+\alpha_I x+\lambda_I = 0, \tag{6.14}$$

so that $a_I^2+b_I^2=\alpha_I$ and $a_I^2 b_I^2=\lambda_I$, and thus $\Delta_{II}(z)$ is

$$\begin{aligned}\Delta_{II}(z,z') &= \frac{1}{a_I^2-b_I^2}\int_{-\infty}^{\infty}\frac{d\omega}{2\pi}\left[\frac{e^{i\omega(z-z')}}{\omega^2+b_I^2}-\frac{e^{i\omega(z-z')}}{\omega^2+a_I^2}\right] \\ &= \frac{1}{2(a_I^2-b_I^2)}\left(\frac{e^{-|b_I||z-z'|}}{b_I}-\frac{e^{-|a_I||z-z'|}}{a_I}\right).\end{aligned} \tag{6.15}$$

Furthermore, we set

$$a_I^2 = r_I e^{i\theta_I}, \quad b_I^2 = r_I e^{-i\theta_I}. \tag{6.16}$$

$\tilde{a}_I$ is defined as $(\tilde{a}_I|t|)^\eta = a_I|z|$, so that the dimension of $\tilde{a}_I$ is t^{-1}, and

$$\begin{aligned}\tilde{a}_I &= a_I^{\frac{1}{\eta}} = r_I^{\frac{1}{2\eta}} e^{i\frac{\theta_I}{2\eta}} \\ &\equiv \tilde{r}_I e^{i\tilde{\theta}_I} \sim t^{-1},\end{aligned} \tag{6.17}$$

where $\tilde{r}_I = r_I^{\frac{1}{2\eta}} \sim t^{-1}$, and $\tilde{\theta}_I = \theta_I/(2\eta)$ is dimensionless.

From Equation 6.15, $G_{IJ}(t,t') = G_{IJ}(|z-z'|) = G_{IJ}(|t^\eta - t'^\eta|)$, which means $G_{IJ}(t,t')$ is symmetric function of t,t', and only depends on the difference of t,t'.

§ 6.4 Data Analysis and Model Calibration

§ 6.4.1 Historical data

We study daily stock return data for 50 companies listed on the NYSE, and we obtain the data from the Wharton Research Data Services (WRDS). We choose the companies which represent a wide variety of sectors and those which have a long history of time series. These

50 stocks are first sorted by the size of market capitalization. Table 6.1 shows the name of 50 stocks.

1∼10	11∼20	21∼30	31∼40	41∼50
Exxon Mobil	Pfizer	Travelers	Cummins	Bob Evans Farm
Microsoft	HP	Costco wholesale	Dun & Bradstreet	Overseas Shipping
Johnson & Johnson	Verizon	FedEx	CNA Financial	AAR Corp
P & G	Pepsi	Archer	Supervalu	OfficeMax
IBM	Bridgford Food	Dow Chemical	Telephont & Data	Hadera Paper
AT & T	Schlumberger	Motorola	Con Way	CDI Corp
Apple	United Tech	Kroger	Temple-Inland	Standard Motor
GE	3M	Cardinal Health	Kennametal	Computer Task
Toyota	Lockheed Martin	Paccar	Frontier Oil	Maine & Maritimes
Coca cola	Caterpillar	Sprint Nextel	Microsemi	Kids Ent

Table 6.1: 50 stocks sorted by market capitalization. 1∼10,Large capitalization; 21∼30, Medium capitalization; 41∼50, Small capitalization.

Each stock provides 5753 daily rate of returns from 16-03-1986 to 31-12-2008. All the results in this Chapter is based on data before 04-Sep-2007, since the financial crisis in 2008 made that period data unrepresentative. t is set to zero on 04-Sep-2007. t' is positive, and time lag is $\tau = t' - t = t'$. Consequently, $\Delta_{II}(z, z')$ in Equation 6.18 is simplified to

$$\Delta_{II}(z, z') = \frac{1}{2(a_I^2 - b_I^2)} \left(\frac{e^{-|b_I||z'|}}{b_I} - \frac{e^{-|a_I||z'|}}{a_I} \right). \tag{6.18}$$

The rate of return $X_I(t)$ was denoised by DB8 wavelet denoising, and details are discussed in Section § 6.4.6.

§ 6.4.2 Goodness of fit

R^2 is used to measure goodness of fit.

A data set has observed values y_i, and each has an associated predicted value f_i. The variability of data is measured through sum of squares. Sum of squares due to error (SSE) measures the total deviation of the response values from the fit to the response values.

$$SSE = \sum_i (y_i - f_i)^2. \tag{6.19}$$

Total sum of squares (SST) is

$$SST = \sum_i (y_i - \bar{y})^2. \tag{6.20}$$

R^2 is defined as

$$R^2 = 1 - \frac{SSE}{SST}. \tag{6.21}$$

R^2 can take any value between 0 and 1, with a value closer to 1 indicating that a greater proportion of variance is accounted for by the model.

§ 6.4.3 Time scheme

A fundamental assumption in the empirical analysis is to treat expectation values of the various financial instruments as being equal to the time average value of these instruments, taken over the time series of the past stock prices. This assumption is the ergodic hypothesis of statistical physics. Under this assumption, the empirical correlator $C_{IJ}(t,t')$ is given by covariance of the returns, and the averaging is over previous n days:

$$\begin{aligned} C_{IJ}(t,t') &= E\left[\varphi_I(t)\varphi_J(t')\right] &(6.22)\\ &= \frac{1}{n}\sum_{k=0}^{n-1}\varphi_I(t-k)\varphi_J(t'-k). &(6.23)\end{aligned}$$

Nevertheless, we expect the stock prices long time ago should not have the same effect as latest data on current correlator $C_{IJ}(t,t')$. A common solution is to multiply a decaying exponential function $\exp(-\gamma k)$, which leads to a gradually truncation of data after $t = 1/\gamma$. Therefore $C_{IJ}(t,t')$ can be rewritten as

$$C_{IJ}(t,t') = \gamma\sum_{k=0}^{\infty} e^{-\gamma k}\varphi_I(t-k)\varphi_J(t'-k). \tag{6.24}$$

Long time schemes use more data for averaging. Due to the averaging, the empirical correlator is more smooth, which reflects the long term property of the equities. Figure 6.1 shows correlator for γ^{-1} is 260 and 5200 trading days.

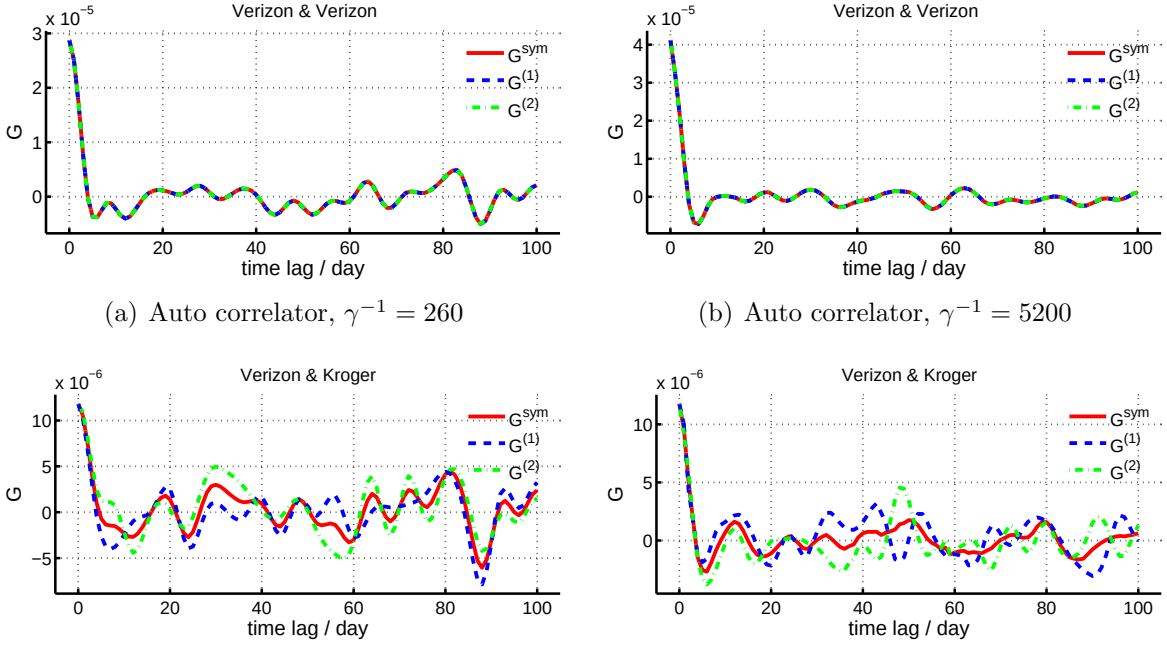

(a) Auto correlator, $\gamma^{-1} = 260$

(b) Auto correlator, $\gamma^{-1} = 5200$

(c) Cross correlator, $\gamma^{-1} = 260$

(d) Cross correlator, $\gamma^{-1} = 5200$

Figure 6.1: Correlator with different schemes. Denoised by DB8, level=2.

When γ^{-1} increase, the equal time correlator increase, and correlator with large time lag converge to zero. As a result, $\tilde{r}$ will increase since amplitude of $C_{IJ}(t, t')$ rises; and $\tilde{\theta}$ decreases, because the oscillation fades out. Figure 6.2 shows this change of $\tilde{r}$ and $\tilde{\theta}$ of as time scheme changes. From Figure 6.2(c), when $\gamma^{-1} > 150$, the single equity fit R^2 is over 0.95.

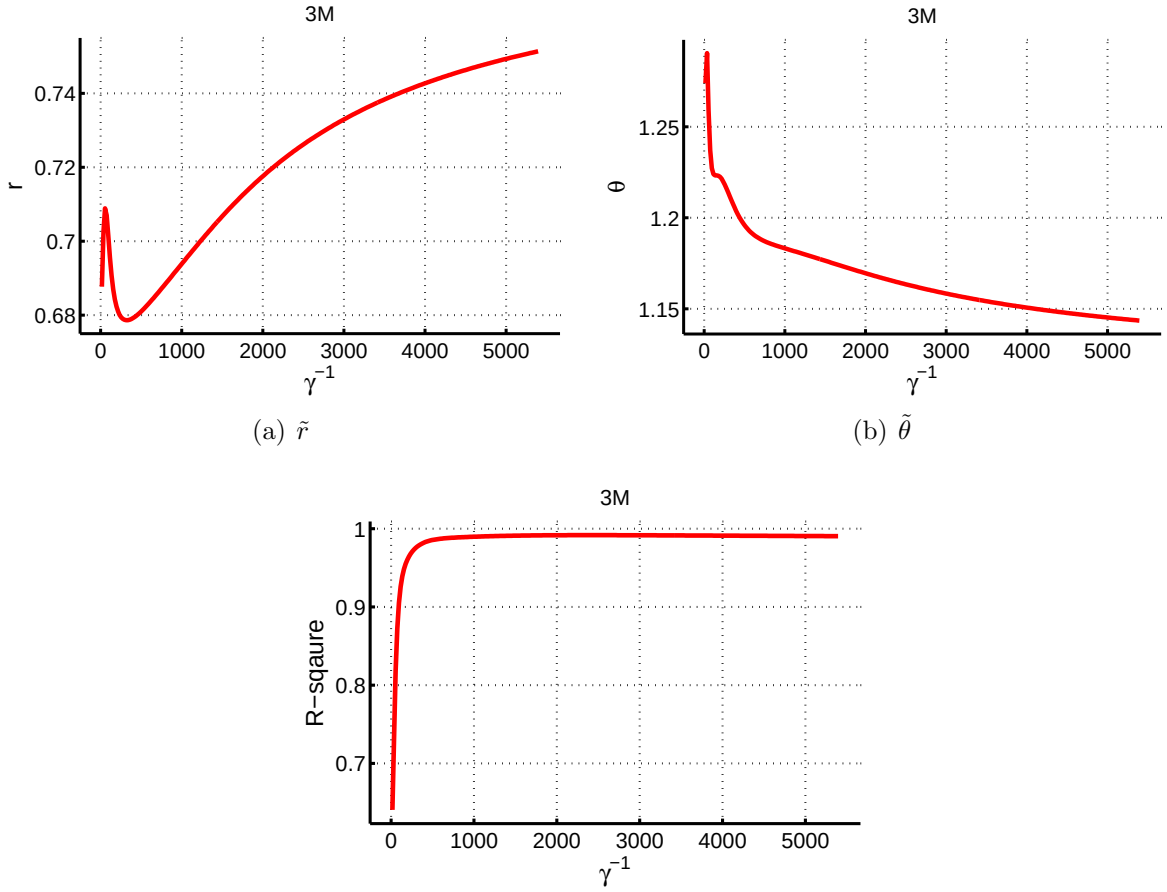

(a) $\tilde{r}$ (b) $\tilde{\theta}$

(c) R^2

Figure 6.2: $\tilde{r}, \tilde{\theta}$, R^2, as a function of γ^{-1}. Denoised by DB8, level2.

We choose two trading years' data to study a specific period correlator of equities. Since typical trading year is around 260 trading days, we set γ^{-1} to 520.

§ 6.4.4 Symmetry property of empirical correlator

Two stocks have similar influence on each other, but the effects are not equivalent for all time. This is more obvious when considering a large capitalization equity and a small capitalization equity. For example, ABC is a small IT company; when Google stock rise a lot, then ABC might increase; furthermore, when ABC goes up, Google may not be affected. Therefore, from an empirical view, $C_{IJ}(t, t')$ is not symmetric with respect to I, J. From the definition of empirical correlator $C_{IJ}(t, t')$ in Equation 6.24, it is obvious that $C_{IJ}(t, t')$ has a full symmetry for I, J and t, t' - that is, when changing I to J, and simultaneously changing

t to t', $C_{IJ}(t,t')$ remains the same, i.e.,

$$C_{IJ}(t,t') = C_{JI}(t',t) = E\left[\varphi_I(t)\varphi_J(t')\right]. \tag{6.25}$$

On the other hand, for the model, with reference to the definition of propagator $G_{IJ}(t,t')$ in Equation 6.9, $G_{IJ}(t,t')$ has full symmetry with I,J and t,t'; besides, Equations 6.12 and 6.18 show that $G_{IJ}(t,t')$ only depends on $|t-t'|$, which means $G_{IJ}(t,t')$ is symmetric with t and t'. Therefore, considering the full symmetry, $G_{IJ}(t,t')$ should also be symmetric with I,J. The empirical result does not support this symmetry - $C_{IJ}(t,t')$ is not symmetric with I,J. Hence, we decompose $C_{IJ}(t,t')$, $t \le t'$ to two symmetric parts: $C^{(1)}_{IJ}(t,t')$, the upper triangle of $C_{IJ}(t,t')$ and its transpose; and $C^{(2)}_{IJ}(t,t')$, the lower triangle of $C_{IJ}(t,t')$ and its transpose; Figure 6.3 demonstrates this operation.

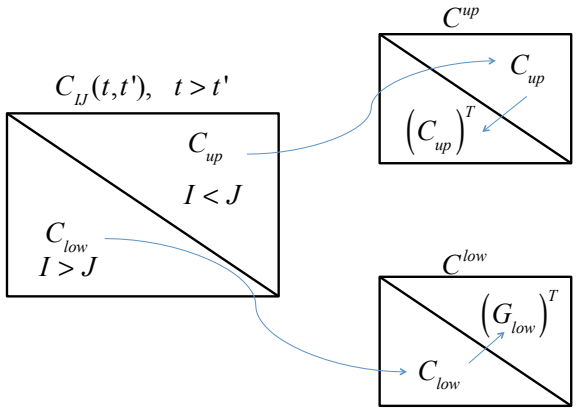

Figure 6.3: Asymmetric $C_{IJ}(t,t')$ is decomposed to symmetric C^{up} and C^{low}.

Similarly for same t,t', $C_{IJ}(t',t)$ is decomposed to $C^{(3)}_{IJ}(t',t)$ and $C^{(4)}_{IJ}(t',t)$.

$$C^{(1)}_{IJ}(t,t') = \begin{cases} C_{IJ}(t,t'), & \text{when } I < J, \\ C_{JI}(t,t'), & \text{when } I > J \end{cases} \tag{6.26}$$

$$C^{(2)}_{IJ}(t,t') = \begin{cases} C_{JI}(t,t'), & \text{when } I < J, \\ C_{IJ}(t,t'), & \text{when } I > J \end{cases} \tag{6.27}$$

$$C^{(3)}_{IJ}(t',t) = \begin{cases} C_{IJ}(t',t), & \text{when } I < J, \\ C_{JI}(t',t), & \text{when } I > J \end{cases} \tag{6.28}$$

$$C^{(4)}_{IJ}(t',t) = \begin{cases} C_{JI}(t',t), & \text{when } I < J, \\ C_{IJ}(t',t), & \text{when } I > J. \end{cases} \tag{6.29}$$

According to the full symmetry property of $C_{IJ}(t,t')$,

$$C_{IJ}^{(1)}(t,t') = C_{IJ}^{(4)}(t,t') \equiv C_{IJ}^{up}(t,t'), \tag{6.30}$$
$$C_{IJ}^{(2)}(t,t') = C_{IJ}^{(3)}(t,t') \equiv C_{IJ}^{low}(t,t'). \tag{6.31}$$

Consequently, only $C_{IJ}^{up}(t,t')$ and $C_{IJ}^{low}(t,t')$ are independent. Now that $C_{IJ}^{up}(t,t')$ and $C_{IJ}^{low}(t,t')$ are defined symmetric, we can fit them separately by the propagator $G_{IJ}(t,t')$ of our model. The following Equation combines the two results to $C_{IJ}^{ul}(t,t')$ to fit the original correlator $C_{IJ}(t,t')$.

$$C_{IJ}^{ul}(t',t) = \begin{cases} C_{JI}^{up}(t',t), & \text{when } I < J, \\ \frac{1}{2}\left[C_{JI}^{up}(t',t) + C_{IJ}^{low}(t',t)\right], & \text{when } I = J, \\ C_{IJ}^{low}(t',t), & \text{when } I > J. \end{cases} \tag{6.32}$$

Otherwise, since $C_{IJ}(t,t')$ and $C_{JI}(t,t')_{IJ}(t,t')$ are similar, we can define $C_{IJ}^{sym}(t,t')$ as the average of this two correlators, then one fit can be done for the whole matrix $C_{IJ}^{sym}(t,t')$. The empirical results shown these two methods have similar errors.

§ 6.4.5 Calibration of parameters

With reference to the form of $G_{IJ}(t,t')$ in Equation 6.12, we must first invert D and D^T and move them to the left hand side. However, D is unknown initially. To resolve this problem, we write

$$G_{IJ}(t,t') = \left(DU\Delta(z')U^T D^T\right)_{IJ} \tag{6.33}$$
$$= \left(DUf_0 h(z')U^T D^T\right)_{IJ}, \tag{6.34}$$

where $\Delta(z') = f_0 h(z')$ and $h(z')$ is diagonal with $h(0) = I$. From Equation 6.18 we have $\Delta(0) = f_0 h(0)$, and the diagonal matrix f_0 is given by

$$(f_0)_I = \Delta_{II}(0) = \frac{1}{2(a_I^2 - b_I^2)}\left(\frac{1}{b_I} - \frac{1}{a_I}\right). \tag{6.35}$$

Furthermore, since $UU^T = 1$ we write

$$\begin{aligned} G(t,t') &= DUf_0^{1/2}U^T Uh(z)U^T Uf_0^{1/2}U^T D^T \\ &= gUh(z')U^T g^T, \qquad (6.36) \\ \text{where} \quad g &= DUf_0^{1/2}U^T. \qquad (6.37) \end{aligned}$$

Note that we can obtain g from the equal time propagator since

$$G(0) = gg^T. \qquad (6.38)$$

As a result, we have

$$g^{-1}G(t,t')g^{-T} = Uh(z)U^T, \qquad (6.39)$$

and we can diagonalize the left hand side to obtain $h(z)$.

g that satisfied Equation 6.38 are not unique. An unique $g = L$ exists according Cholesky decomposition. But Different decomposition varies an orthogonal matrix V that $g' = gV^{-1}$. g' also satisfies this requirement, i.e. $g'g'^T = gV{-}1V^{-T}g^T = G(0)$. Then

$$\begin{aligned} g'^{-1}G(t,t')g'^{-T} &= Vg^{-1}G(t,t')g^{-T}VT \\ &= VUh(z)U^T V^T \\ &= Wh(z')W^T, \qquad (6.40) \end{aligned}$$

where $W = VU$. It is easy to verify that W is also a orthogonal matrix - $WW^T = VU(VU)^T = 1$. So when g changes to g', and U changes to another orthogonal matrix W, $h(z)$ remains the same. Besides, since $g'W = gV^{-1}VU = gU$, from Equation 6.36, G(t,t') also does not change. Therefore, decomposition of g from Equation 6.38 does not affect empirical result. We choose a simple g that $g = g^T$. Because $G(0)$ is symmetric, $g_{IJ} = \sqrt{G_{IJ}(0)}$.

Given g, we can diagonalize $h(z)$ from Equation 6.39. The left hand side of Equation 6.39 depends on $|t - t'|$, it is a series square matrices, and there is no constant unique U to diagonalize all of these matrices. We find a series $U(|t - t'|)$, which diagonalizes each square matrix; and then among all these U, we choose the one which gives the smallest norm of the nondiagonal pieces. Furthermore, we ignore the nondiagnal terms caused by choosing one U, and let $h(z)$ equal to the diagonal elements. This estimation introduces about 0.02 - 0.2 error in R^2. For a single equity, the error is zero; and for 50 equities, this will cause around 0.15 deduction in R^2, and will lead to relatively large errors.

We fit $h(z)$ by minimizing the mean square errors, obtaining the values for $\tilde{r}_I, \tilde{\theta}_I, \eta$, $I = 1, 2, \cdots, N$. The total degree of freedom for fitting is $2N + 1$. Considering that each element of α_I, λ_I and $h_I(z)$ only depends on single equity I, we first calibrate all the parameters to get η for all equites, and the appropriate value for α and λ. Fixing η, another calibration of α_I and λ_I was done to obtain a better fit for each $h_I(z)$.

We can obtain a_I and b_I according to the definition of $\tilde{r}_I, \tilde{\theta}_I$ in Equation 6.16 and 6.17.

Since g, U and f_0 is known, the matrix D is given by Equation 6.37

$$D = gUf_0^{-1/2}U^T. \tag{6.41}$$

Finally, the propagator can be obtained by Equation 6.36.

§ 6.4.6 Denoising

It is a stylized fact that before denoising, the returns at different time seem to have no correlation, as shown in Figure 6.4(a) and 6.4(b).

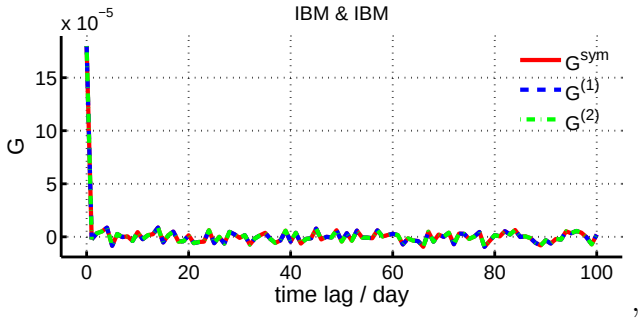

(a) Auto correlator, original

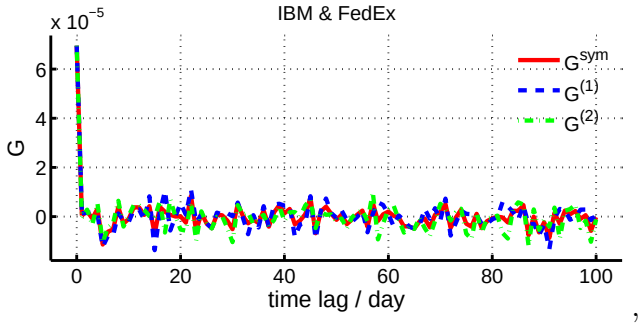

(b) Cross correlator, original

Figure 6.4: $C_{IJ}(t, t')$ for IBM and Fedex. $\gamma^{-1} = 540$.

However, after denoising, the empirical correlator $C_{IJ}(t,t')$ of any two stocks have similar oscillation: when time lag is zero, that is, two set of stocks data are in the same period, they have maximal correlation; and when time lag become larger, two stocks tend to decorrelate. Nevertheless, the correlation does not directly decay to zero, but becomes negative, which means the two stocks are over decorrelated, and the magnitude is smaller than the first positive correlation. Afterwards, the correlation arises above zero again, and oscillates like noise along axis. Figure 6.5 show four typical denoised $C_{IJ}(t,t')$ graphs for IBM and Fedex. For daily data, the first two oscillating processes take about 15 days, and afterwards, the correlation is like noise. Thus our calibration is also for time lag less than 15 days.

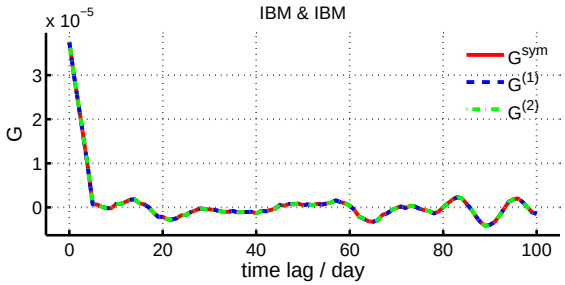

(a) Auto correlator, by moving average, span=5

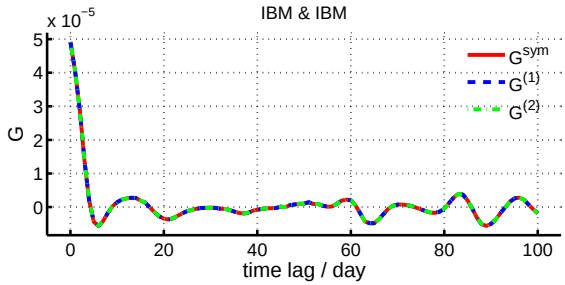

(b) Auto correlator, by DB8, level=2

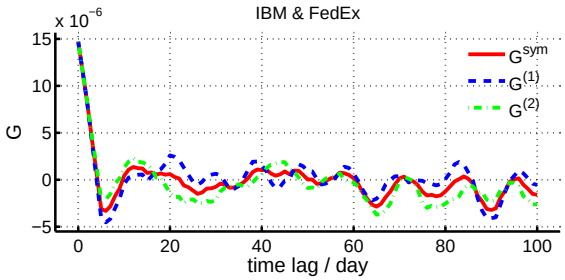

(c) Cross correlator, by moving average, span=5

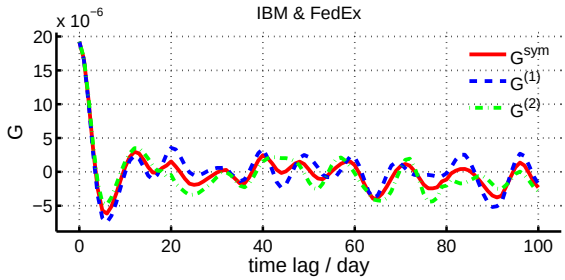

(d) Cross correlator, by DB8, level=2

Figure 6.5: Correlator by different denoising methods. $\gamma^{-1} = 540$.

We chose two methods for denoising: one is moving average smoothing, and the other is Daubechies 8 (DB8) wavelet denoising. For moving average, the averaging is from 5 data points, i.e. span=5; for DB8, denoising level is level 2. When span or level increase, both moving average and DB8 tend to give larger oscillations after 15 days. Figure 6.6 shows 100 trading days' raw rate of return data and denoised data of IBM. Figure 6.5 shows auto correlator, and cross correlator by two methods. Compared with moving average, DB8 can give more smooth curves.

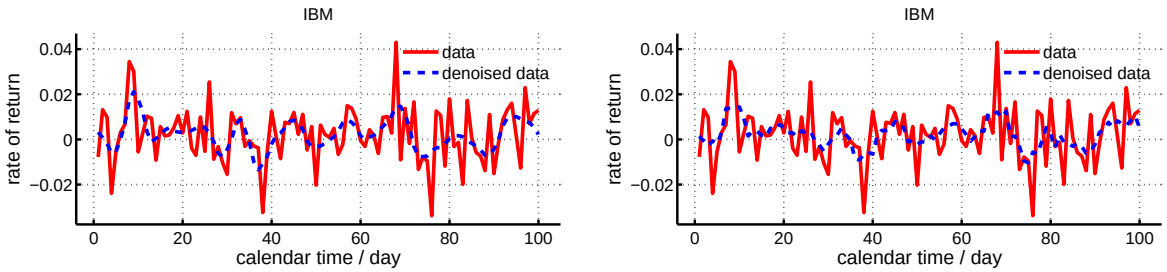

(a) by moving average, span=5 (b) by DB8, level=2

Figure 6.6: Rate of return of IBM denoised by different methods, from 13-Apr-2007 to 04-Sep-2007, 100 trading days.

The signal-to-noise ratio (SNR)is defined as:

$$SNR = \frac{A_{\text{signal}}}{A_{\text{noise}}}, \tag{6.42}$$

where A is amplitude.

Table 6.2 shows SNR of IBM, Fedex and mean SNR of all 50 stocks denoised by the two methods. All the historical 5753 days' data are used to calculate SNR. From this result, DB8 wavelet denoising preserves more signal. Therefore, we choose DB8 wavelet level 2 denoising.

SNR	IBM	Fedex	mean
Moving average	0.2290	0.2501	0.1456
DB8 wavelet	0.3827	0.3611	0.4565

Table 6.2: Signal-to-noise ratio (SNR) of (a)moving average method, span=5; (b)DB8 wavelet denoising, level=2.

To show that the cross correlator is an intrinsic property and not due to the denoising of equities, we generate ten series of white noise data, and denoise the data by DB8 wavelet method, and then calculate the correlator. Figure 6.7(a) shows that after denoising, white noise data does have similar auto correlator with equity data; but the cross correlator in Figure 6.7(b) are quite irregular, and different from equity. This test shows that the shape of equity on cross correlator does have oscillation property, that is not due to denoising.

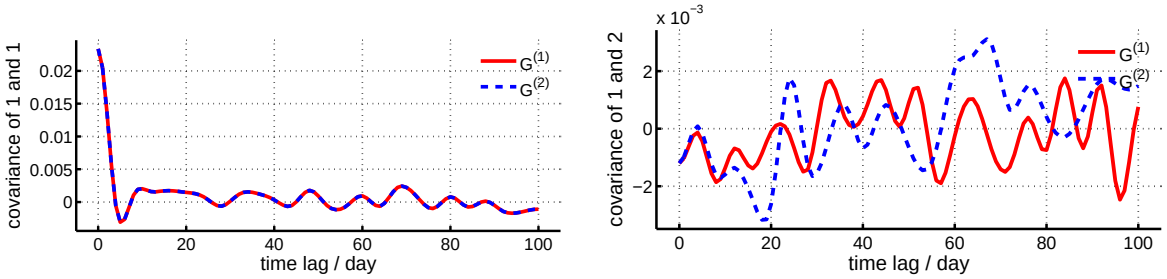

(a) Auto correlator (b) Cross correlator

Figure 6.7: Auto correlator and cross correlator of white noise. $\gamma^{-1} = 540$; denoised by DB8 level=2.

§ 6.5 Empirical results

§ 6.5.1 Single equity fit

Since the equity model can be used on any quantity of stocks, 50 equity data is first separately fitted. Single equity has the most smooth shape, and does not need to be diagonalized, so the correlator $C_{IJ}(t,t')$ can be fitted quite well. R^2 of fitting $C_{IJ}(t,t')$ is from 0.9558 to 0.9981, with an average value of 0.9868. η is from 0.7739 to 1.0000, with an average value of 0.9841. The value of η, R^2, $\tilde{r}, \tilde{\theta}$, α and λ are shown in Figure 6.8.

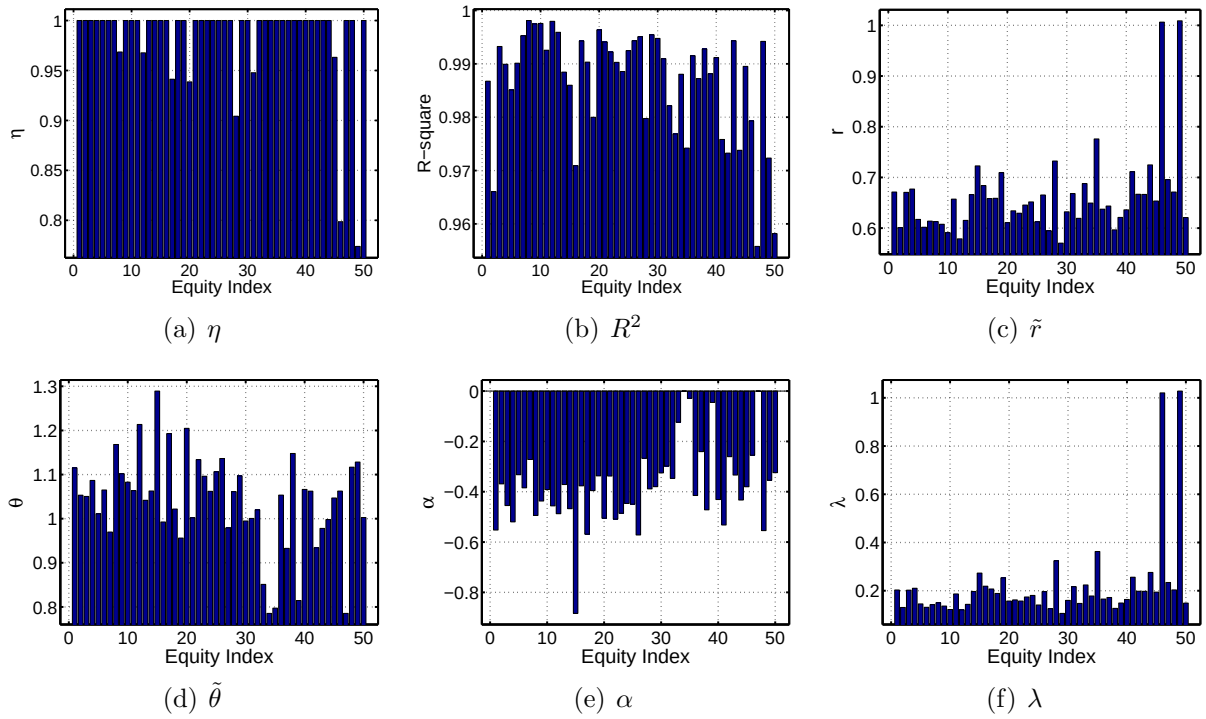

(a) η (b) R^2 (c) $\tilde{r}$

(d) $\tilde{\theta}$ (e) α (f) λ

Figure 6.8: Results of single equity; $\gamma^{-1} = 540$; Denoised by DB8, level 2.

§ 6.5.2 Calibration of η

Three different categories of data (large capitalization, medium capitalization, small capitalization) was first used to calibrate this model, and the value of η are shown in Table 6.3. R^2 of diagonalization is listed in Table 6.4; R^2 of data fitting of the model is also stated in Table 6.5 and 6.6.

η	C^{sym}	C^{up}	C^{low}
Large capitalization	1.0000	1.0000	1.0000
Medium capitalization	0.9981	1.0000	0.9724
Small capitalization	1.0000	0.9667	0.8985
50 all	0.9619	0.9410	0.9212

Table 6.3: η of different capitalization and combined capitalization.

R^2	C^{sym}	C^{up}	C^{low}
Large capitalization	0.9819	0.9722	0.9618
Medium capitalization	0.9752	0.9582	0.9668
Small capitalization	0.9537	0.9140	0.9315
50 all	0.9175	0.8560	0.8723

Table 6.4: Diagonalization error of different capitalization and combined capitalization.

R^2	C^{sym}	C^{up}	C^{low}
Large capitalization	0.9686	0.9655	0.9532
Medium capitalization	0.9715	0.9479	0.9615
Small capitalization	0.9369	0.8471	0.9064
50 all	0.9144	0.8474	0.8658

Table 6.5: Fitting error compared with symmetrical C^{sym}, C^{up} and C^{low} of different capitalization and combined capitalization.

R^2	C^{sym}	C^{up}	C^{low}
Large capitalization	0.9491	0.9459	0.9446
Medium capitalization	0.9369	0.9141	0.9228
Small capitalization	0.8839	0.8346	0.8537
50 all	0.8338	0.8066	0.8124

Table 6.6: Fitting error of compared with unsymmetrical G^E of different capitalization and combined capitalization.

The values of η were around 0.95. For large and medium capitalization, the R^2 of C^{sym} was above 0.97, respectively. For small capitalization and all capitalization (total 50 stocks data), the R^2 was relatively smaller. This is due to the fact that the stocks of large and medium capitalization are strongly correlated and the trend of the correlation is quite obvious. The correlation for the stocks of small capitalization is relatively small, and fitting R^2 is around 0.85. For 50 stocks, the error also comes from the simultaneous diagonalization of 15 50×50 matrixes.

Two graphs of the fit of this Gaussian model for all 50 capitalization are given in Figure 6.9. Figure 6.9(b) has the largest R^2 value, and Figure 6.9(a) is the worst fit with an $R^2 = -6.4045$. The bad fit is because the shape of Maine & Maritimes and Coca cola correlator is positive, and does not follow the regular features. This irregular shape is very rare, which can be reflected from very low R^2 compared with all fitting results.

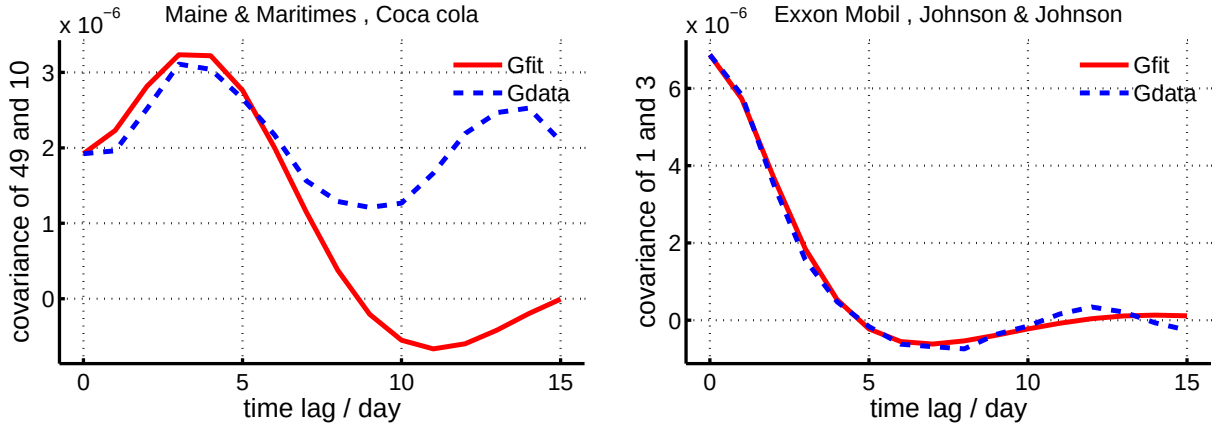

(a) Maine & Maritimes and Coca cola, R^2=-6.4045 (b) Exxon Mobil and Johnson & Johnson, R^2=0.9936

Figure 6.9: Comparison of unequal time correlator from empirical correlator C and the Gaussian model propagator G.

§ 6.5.3 Results with fixed η

The diagonal elements λ_I, α_I for stocks of different market capitalization are shown in Figure 6.10, 6.11 respectively. The figures of λ_I for large, medium, small, and all 50 capitalization are all around 0 0.5. U and D are shown in Figure 6.12 and 6.13.

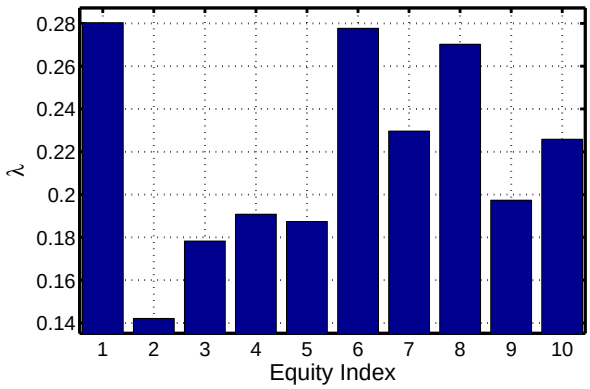

(a) 10 stocks of large capitalization

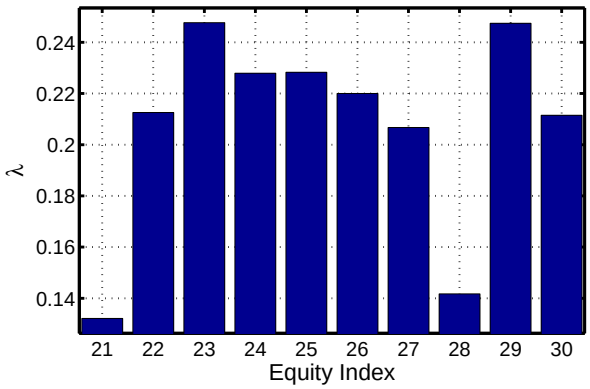

(b) 10 stocks(B) of medium capitalization

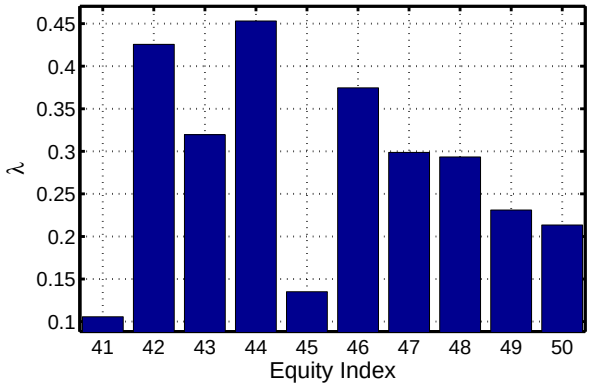

(c) 10 stocks of small capitalization

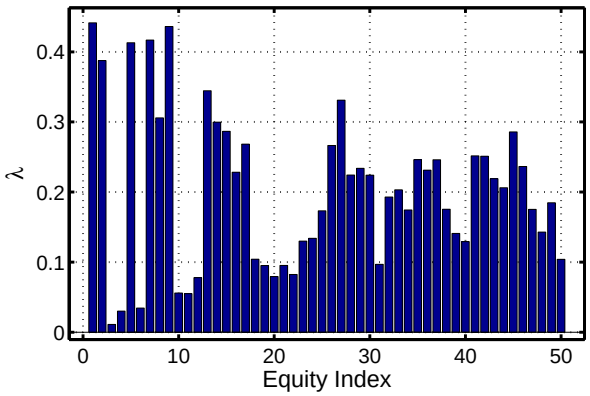

(d) all 50 stocks

Figure 6.10: λ_I for equities.

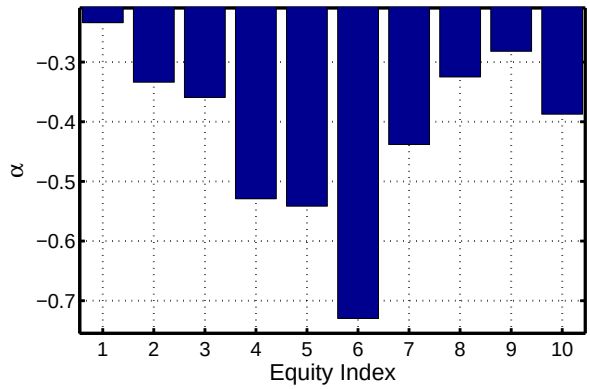

(a) 10 stocks of large capitalization

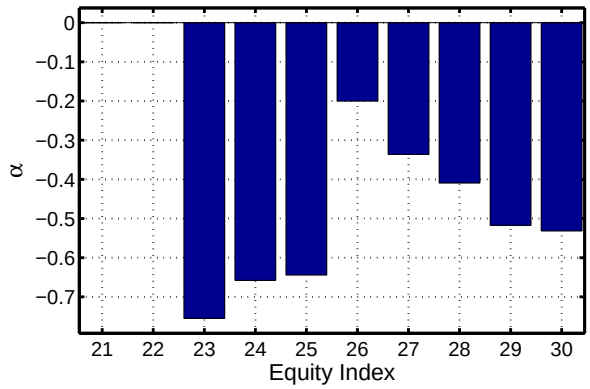

(b) 10 stocks(B) of medium capitalization

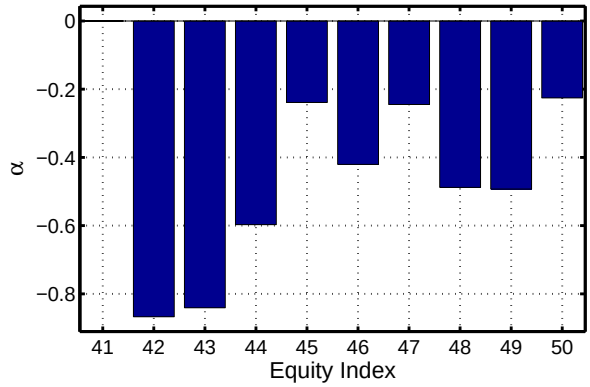

(c) 10 stocks of small capitalization

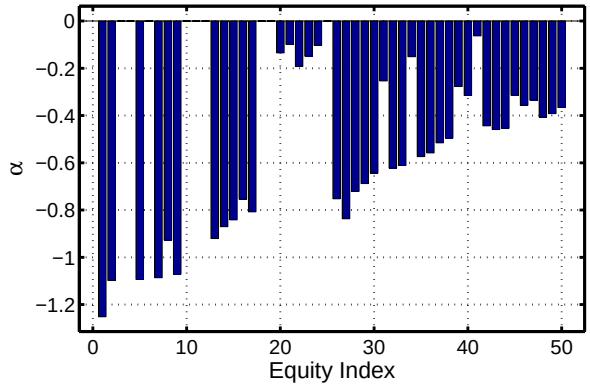

(d) all 50 stocks

Figure 6.11: α_I for equities.

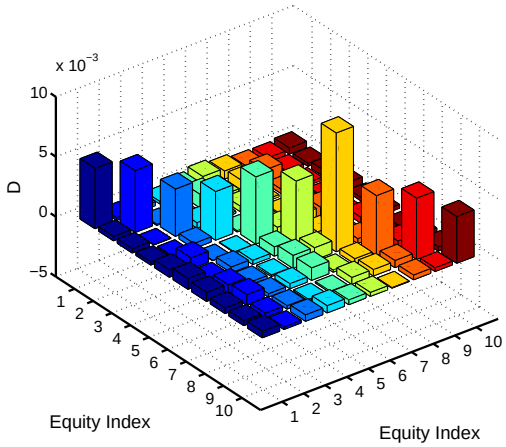

(a) 10 stocks of large capitalization

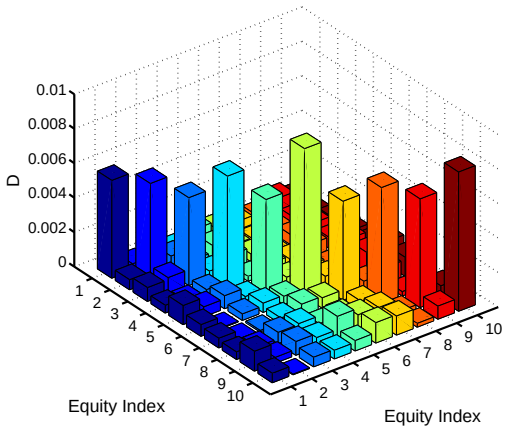

(b) 10 stocks of medium capitalization

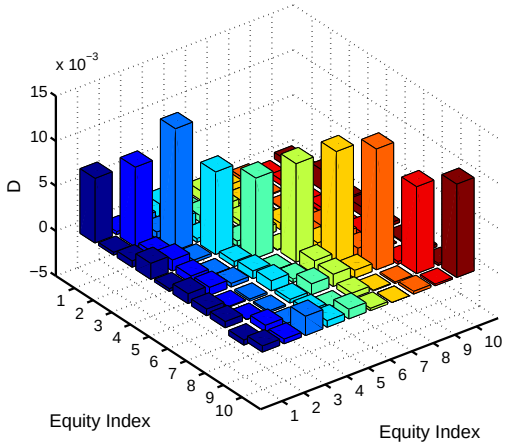

(c) 10 stocks of small capitalization

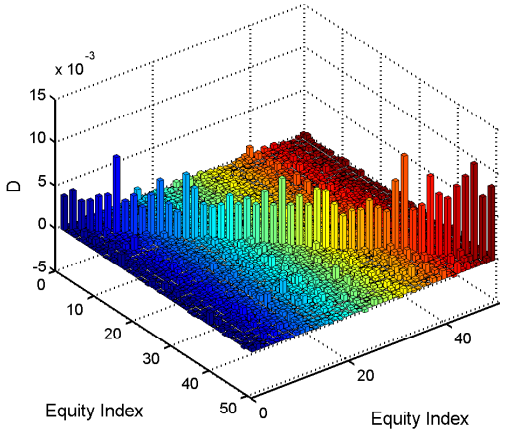

(d) all 50 stocks

Figure 6.12: Matrix D for equites.

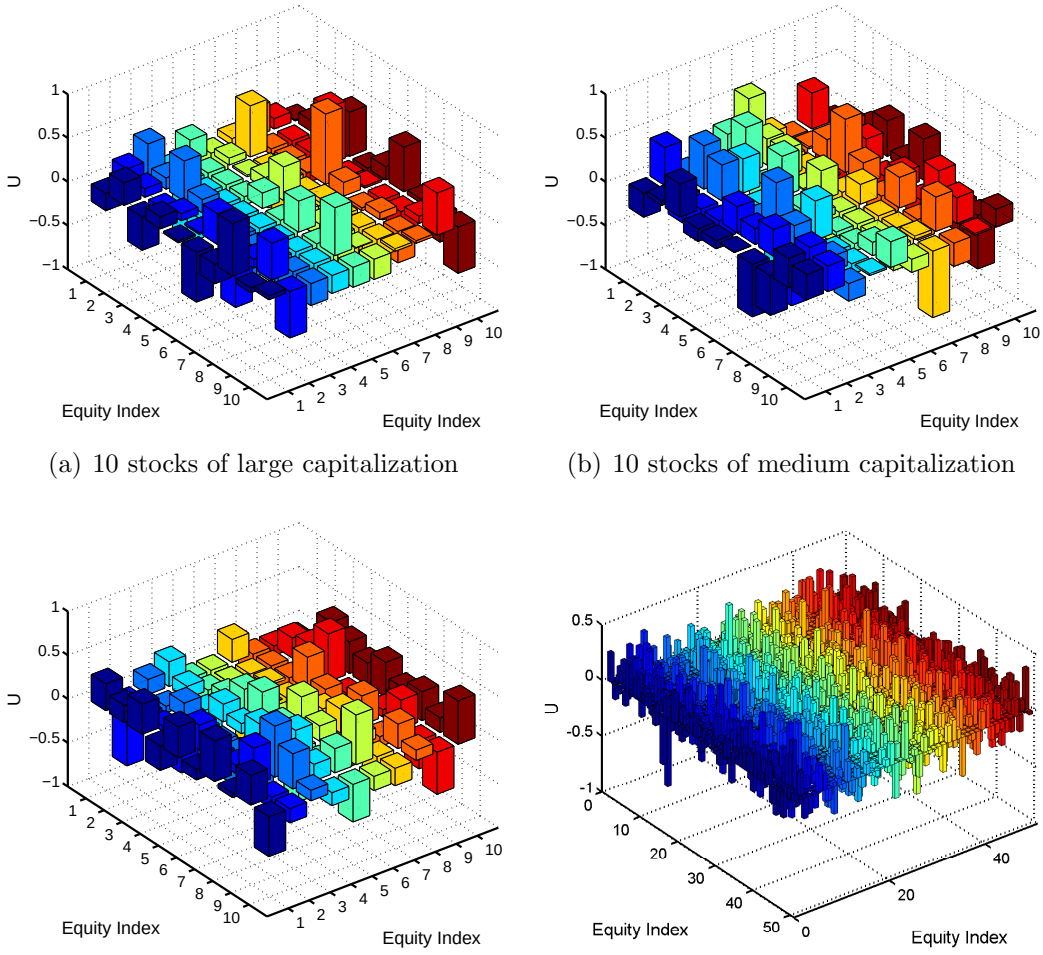

(a) 10 stocks of large capitalization

(b) 10 stocks of medium capitalization

(c) 10 stocks of small capitalization

(d) all 50 stocks

Figure 6.13: Matrix U for equities.

§ 6.6 Conclusion

This study has explored a dynamical modeling of portfolio. An unequal time Gaussian model was developed to calibrate the stock market data. The nontrivial fourth order derivative Lagrangian was defined and the unequal time propagator was derived from the Lagrangian. Current stock market data was used to calibrate the model.

The detailed modeling of portfolio evolution by the Gaussian model has revealed that two different stocks at different times have a strong correlation. For the unequal time correlator, the value of correlation function decayed like an exponential function. It was found that the correlation of return of undenoised data is noise like. Instead, the correlation of the denoised

rate of return has some interesting structure which can be modeled. The unequal time correlation function (propagator) was calibrated from the stock market data. The results show that the fit of this unequal time Gaussian model with data is quite good, with R^2 over 0.9 for about 10 stocks data. Based on these results, it appears that the Gaussian model has more flexibility in describing the behavior of unequal time correlation, because the Lagrange equation has a forth order time derivative. It was also found that the fit of this model is quite good for single equity, and especially large capitalization stocks market. An important feature of this Gaussian model is that it is generally applicable to many other markets, such as foreign currencies exchange rate , commodities, where the asset of the market is quite liquid and the individual asset of unequal time is strongly correlated.

Being a preliminary study, this work needs more investigation in future studies. This model gives a new way to capture information from unequal time correlation of different stocks, and the complex structure of unequal time propagator can be described by a few parameters. However, the current study only gives a theoretical tools for analyzing the market data, and the empirical application of this model needs to be studied. Future research should be attempted to find the evolution of optimum portfolio in the future time. Moreover, further formulas and algorithms to price the options should be done by using the dynamical Gaussian model.

Bibliography

[1] L. Bachelier, P. A. Samuelson, M. Davis, and A. Etheridge. *Louis Bachelier's Theory of Speculation: The Origins of Modern Finance*.

[2] B. E. Baaquie. *Quantum Finance*. Cambridge University Press, UK, 2004.

[3] wikipedia. Interest rate derivative. *www.wikipedia.org*.

[4] Arthur O'Sullivan and Steven M. Sheffrin. *Economics: Principles in action*. Pearson Prentice Hall, Upper Saddle River, New Jersey 07458, 2003.

[5] B. E. Baaquie. *Interest Rates and Coupon Bonds in Quantum Finance*. Cambridge University Press, UK, 2009.

[6] R. A. Jarrow. *Modelling Fixed Income Securities and Interest Rate Options*. McGraw-Hill, USA, 1995.

[7] J. C. Hull. *Options, Futures, and Other Derivatives*. Prentice Hall, New Jersey, 2006.

[8] F. Black and M. Scholes. The pricing of options and corporate liabilities. *Journal of Political Economy*, 1973.

[9] Robert C. Merton. Theory of rational option pricing. *Bell Journal of Economics and Management Science*, 4(1):141–183, 1973.

[10] O.Vesicek. An equilibrium characterisation of the term structure. *Journal of Financial Economics*, 5, 1977.

[11] J.C. Cox, J.E. Ingersoll, and S.A. Ross. A theory of the term structure of interest rates. *Econometrica*, 53, 1985.

[12] T.S.Y. Ho and S.B. Lee. Term structure movements and pricing interest rate contingent claims. *Journal of Finance*, 41, 1986.

[13] J.C. Hull and A. White. Pricing interest-rate derivative securities. *The Review of Financial Studies*, 3(4):573–592, 1990.

[14] F.Black, E.Derman, and W.Toy. A one-factor model of interest rates and its application to treasury bond options. *Financial Analysts Journal*, 1990.

[15] F.Black and P.Karasinski. Bond and option pricing when short rates are lognormal. *Financial Analysts Journal*, 1991.

[16] F. A. Longstaff and E. S. Schwartz. Interest rate volatility and the term structure: A two factor general equilibrium model. *Journal of Finance*, 47, 1992.

[17] L. Chen. Stochastic mean and stochastic volatility-a three-factor model of the term structure of interest rates and its application to the pricing of interest rate derivatives. *Financial Markets, Institutions, and Instruments*, 5, 1996.

[18] R. Jarrow D. Heath and A. Morton. Bond pricing and the term structure of interest rates: A new methodology for contingent claim valuation. *Econometrica*, 60, 1992.

[19] J. Cohen and R. Jarrow. *Markov Modeling in the Heath, Jarrow, and Heath Term Structure Framework*. Cornell University, Ithaca, 2000.

[20] D.Kennedy. The term structure of interest rates as a gaussian randim field. *Mathematical Finance*, 4, 1994.

[21] P. Goldstein. The term structure of interest rates as a random field. *Journal of Financial Studies*, 13(2):365, 2000.

[22] P. Santa-Clara and D.Sornette. The dynamics of the forward interest rate curve with stochastic string shocks. *Journal of Financial Studies*, 14(1):149, 2001.

[23] B. E. Baaquie. Quantum field theory of treasury bonds. *Physical Review E*, 64(016121), 2001.

[24] D Gatarek A. Brace and M. Musiela. The market model of interest rate dynamics. *Mathematical Finance*, 7, 1996.

[25] B. E. Baaquie and J.P.Bouchaud. Stiff interest rate model and psychological future time. *Wilmott Magazine*, 2004.

[26] B. E. Baaquie. Interest rates in quantum finance: The Wilson expansion and Hamiltonian. *Physical Review E*, 80(4):046119, 2009.

[27] B. E. Baaquie. Quantum finance hamiltonian for coupon bond european and barrier options. *Physical Review E*, 77(036106), 2008.

[28] J. P. Bouchaud and A. Matacz. Explaining the forward interest rate term structure. *International Journal of Theoretical and Applied Finance*, 3(381), 2000.

[29] P. J. Knez, R. Litterman, and J. Scheinkman. Exploration into factors explaining money market returns. *Journal of Finance*, 49(5):1861–1882, 1994.

[30] R.-R. Chen and L. Scott. Maximum likelihood estimation for a multifactor equilibrium model of term structure of interest rate. *Journal of Fixed Income*, 3(3):14–31, 1993.

[31] R. Litterman and J. Scheinkman. Common factors affecting bond returns. *Journal of Fixed Income*, 1:54–61, 1991.

[32] M. K. Singh. Estimation of multifactor Cox, Ingersoll, and Ross term structure model: Evidence on volatility structure and parameter stability. *Journal of Fixed Income*, 5(2): 8–28, 1995.

[33] P. Ritchken and L. Sankarasubramanian. The importance of forward rate volatility structures in pricng interest rate-sensitive claims. *Journal of Derivatives*, 3(1):25–41, 1995.

[34] K. Inui and M. Kijima. A markovian framework in multi-factor Heath-Jarrow-Morton models. *Journal of Financial and Quantitative Analysis*, 33(3):423–440, 1998.

[35] F. de Jong and P. Santa-Clara. The dynamics of the forward interest rate curve: A formulation with state variables. *Journal of Financial and Quantitative Analysis*, 34(1): 131–157, 1999.

[36] C. Chiarella and O. K. Kwon. Forward rate dependent markovian transformations of the Heath-Jarrow-Morton term structure model. *Finance and Stochastics*, 5(2):237–257, 2001.

[37] C. Chiarella and O. K. Kwon. Finite dimensional affine realisations of HJM models in terms of forward rates and yields. *Review of Derivatives Research*, 6(2):129–155, 2003.

[38] Carl Chiarella, Hing Hung, and Thuy-Duong Tô. The volatility structure of the fixed income market under the HJM framework: A nonlinear filtering approach. *Computational Statistics & Data Analysis*, 53(6):2075–2088, 2009.

[39] F. Jamshidian. Libor and swap market models and measures. *Finance and Stochastics*, 1(14):293–330, 1997.

[40] R. Rebonato and M. Joshi. A joint empirical and theoretical investigation of the modes of deformation of swaption matrices: Implications for model choice. *International Journal of Theoretical and Applied Finance*, 5(7):667–694, 2002.

[41] Dariusz Gatarek, Przemyslaw Bachert, and Robert Maksymiuk. *The LIBOR Market Model in Practice*.

[42] D. Brigo and F. Mercurio. *Interest Rate Models – Theory and Practice*. Springer, Germany, 2007.

[43] B. E. Baaquie and Cao Yang. Empirical analysis of quantum finance interest rate models. *Physica A*, 388(13):2666–2681, 1 July 2009.

[44] L. Anderson and J. Andresean. Volatility skews and extensions of the libor market model. *Applied Mathematical Finance*, 7(1):1–32, 2000.

[45] A. Amin. Multi-factor cross currency libor market models: Implementation, calibration and examples. *Working Paper*, 2003.

[46] B. E. Baaquie and Tang Pan. Simulation of coupon bond european and barrier options in quantum finance. *submitted for publication*, 2010.

[47] B. E. Baaquie. Interest rates in quantum finance: Caps, swaptions and bond options. *Physica A*, 389, 2010.

[48] Press William H., Teukolsky Saul A., Vetterling William T., and Flannery Brian P. *Numerical Recipes: The Art of Scientific Computing*.

[49] C. Albanese and O. Chen. Pricing equity default swaps. *RISK*, 18, 2005.

[50] L. Campi, S Polbennikov, and A. Sbuelz. Systematic equity-based credit risk: A cev model with jump to default. *Journal of Economic Dynamics & Control*, 33(1):93–108, 2009.

[51] D. Davydov and V. Linetsky. Pricing and hedging path-dependent options under the cev process. *Management Science*, 47(7):949–965, 2001.

[52] J. (1975) Cox. Notes on option pricingI: Constant elasticity of variance diffusions. *Working paper, Stanford University (reprinted in* Journal of Portfolio Management, 22, 1996.

[53] J. Cox and S. Ross. The valuation of options for alternative stochastic processes. *Journal of Financial Economics*, 3, 1976.

[54] JPMorgan. *Equity Default Swaps. European equity derivatives.* JPMorgan, London, 2003.

[55] D. Emanuel and J. MacBeth. Further results on the constant elasticity of variance call option pricing model. *J. Financial and Quant. Anal.*, 17, 1982.

[56] B. E. Baaquie and M. A. Khan. Portfolio evolution driven by a two dimensional stochastic (quantum) field. *working paper*, 2009.